HUMAN CALCITONIN: AN INVESTIGATION OF AMYLOID FORMATION AND INHIBITION

by

Richard Lantz

A Dissertation Submitted to the Faculty of

The Charles E. Schmidt College of Science

in Partial Fulfillment of the Requirements for the Degree of

Doctor of Philosophy

Florida Atlantic University

Boca Raton, FL

August 2020

HUMAN CALCITONIN: AN INVESTIGATION OF AMYLOID FORMATION AND INHIBITION

by

Richard Lantz

This dissertation was prepared under the direction of the candidate's dissertation advisor, Dr. Deguo Du, Department of Chemistry and Biochemistry, and has been approved by the members of his supervisory committee. It was submitted to the faculty of the Charles E. Schmidt College of Science and was accepted in partial fulfillment of the requirements for the degree of Doctor of Philosophy.

SUPERVISORY COMMITTEE:

Deguo Du (Jun 30, 2020 08:32 EDT)

Deguo Du, Ph.D.
Dissertation Advisor

Lyndon West (Jul 2, 2020 10:28 EDT)

Lyndon West, Ph.D.

Andrew Terentis (Jul 2, 2020 10:44 EDT)

Andrew C. Terentis, Ph.D.

YUnqing Kang (Jul 2, 2020 10:47 EDT)

Yunqing Kang, Ph.D.

Predrag Cudic, Ph.D.
Chair, Department of Chemistry and Biochemistry

Ata Sarajedini, Ph.D.
Dean, Charles E. Schmidt College of Science

Robert W. Stackman Jr., Ph.D.
Dean, Graduate College

July 2, 2020
Date

ACKNOWLEDGEMENTS

First, I would like to thank Dr. Deguo Du for his unwavering support and mentorship throughout my studies as a graduate student. Your commitment to your work and your compassion for your fellow graduate students is something I admire and look up to. You strive to bring out the best scientist in us and is always there when we need guidance. I would also like to thank my committee members: Dr. Andrew C. Terentis, Dr. Lyndon West, and Dr. Yunquing Kang. I am forever thankful for their support and guidance with my journey through graduate school. I also want to thank Dr. Patricia Snyder for her mentorship and guidance. I want to thank Haiyang (Ocean) Liu and Esmail Elbassal for showing me the ropes when I first entered the lab. I want to thank Dr. Ewa Wojcikiewicz for her suggestions and use of the AFM instrument. I also need to thank all of my lab members: Thomas W. Kent, Jennifer Luks, Clifford Morris, Deepika Regmi, Majedul Mousoum, Fengyun Shen, and Brian Busbee. You are all awesome and I wish you the best. I want to thank Patrick Cosme and Bobby Duersch for their for support and advice. I also want to thank Javier Rivera and Dr. Floyd Russel for all of their support. I am very grateful to Florida Atlantic University and to the Department of Chemistry & Biochemistry for my time as both an undergraduate and graduate student. Our school has grown so much over my time here and I look forward to what our fellow Owls will do in the future. I also want to thank the National Institute of Health and the Alzheimer's Association for their generous funding and support to the Dr. Du group.

ABSTRACT

Author: Richard Lantz

Title: Human Calcitonin: An Investigation of Amyloid Formation and Inhibition

Institution: Florida Atlantic University

Dissertation Advisor: Dr. Deguo Du

Degree: Doctor of Philosophy

Year: 2020

Human calcitonin (hCT) is a peptide hormone that is produced by the thyroid gland where it regulates blood calcium and stimulates bone formation. However, increased concentrations can cause hCT to aggregate into amyloid fibrils where they can cause cellular toxicity. In this dissertation, we investigated the role of the N-terminal intramolecular disulfide bond, the effects cholesterol derivatives, the inhibitory effects of a group of polyphenolic molecules, and membrane interactions on hCT amyloid formation. To better understand hCT amyloid formation, we investigated the role of the N-terminal intramolecular disulfide bond has on the aggregation kinetics of hCT. Our results demonstrated that the presence of the disulfide bond is key to the formation of the oligomeric nucleus that is needed for amyloid formation. We also investigated the role of cholesterol, cholesterol sulfate, and 3β-[N-(dimethylaminoethane)carbamoyl]-cholesterol (DC-cholesterol) in moderating hCT fibril formation. We showed that cholesterol does not significantly affect hCT fibrillization while high concentrations of cholesterol sulfate has

a moderate inhibiting effect. However, DC-cholesterol strongly inhibits hCT fibril formation in a concentration-dependent manner suggesting the role of electrostatic and hydrogen bonding interactions have in moderating the interactivity between hCT and the surface of DC-cholesterol vesicles. We also probed the inhibitory effects of a group of polyphenolic molecules on hCT fibril formation. Our results showed that molecules containing vicinal hydroxyl groups on the phenyl ring effectively inhibits hCT fibril formation though a plausible covalent linkage between the oxidized polyphenol and hCT. This covalent linkage would obstruct the critical electrostatic and aromatic interactions needed for hCT fibril formation. Finally, we examined the effects of liposome concentration, size, and curvature on the kinetics of hCT amyloid formation by using zwitterionic palmitoyl-2-oleoyl-glycero-3-phosphocholine (POPC) and negatively charged palmitoyl-2-oleoyl-phosphatidylglycerol (POPG) liposomes. Both inhibited hCT amyloid formation in a dose-dependent manner through a number of interactions with the vesicle surface such as electrostatic, hydrophobic, and hydrogen bonding. When the size of the POPC liposomes was reduced, hCT amyloid inhibition was even more pronounced possibly due to higher curvature and the exposure of water-accessible hydrophobic regions for hCT to bind to in the liposome bilayer.

DEDICATION

I dedicate this dissertation to my family and friends. To my fiancée and future wife Natalie, for her love and support throughout the years. You have always been there for me through the good, the bad, and the ugly times. I could have not done this without you and I love you so much. I can't wait to see what the future brings for us sweetie. To my dad, as he has always been there for me. We have been through some really tough times together and I admire the man that you are. I am so grateful to have you as a father. To all of my dear friends: David, Billy, Eva, Logan, Jojo, Bobby, Reinier, Ashley, Camilo, Gabi, Matias, Inshawn, Brad, Vinny, Jordan, Lauren, Izzy, Sam, Sammy, and Brandon. You all have had an impact on my life and I love you so much. To Vicky, I will always love you as if you were my daughter. To my high school chemistry teacher, Craig Schuett. You are the very reason I made a career out of chemistry and it really shows how much of an impact a teacher can have on a student's life. To my late mom as her perseverance, fight, and will to live was second to none. Every time I encounter a hardship, I think about you and I push through as hard as I can. Lastly, to the promise I made to her: to be happy, to do the things I want to do, and to lead a successful life. I feel that I am fulfilling that promise and I will continue to do so.

HUMAN CALCITONIN: AN INVESTIGATION OF AMYLOID FORMATION AND INHIBITION

LIST OF TABLES

LIST OF FIGURES

ABBREVIATIONS

3-HBA	3-Hydroxybenzoic Acid
3,4-HBA	3,4-Hydroxybenzoic Acid
3,5-HBA	3,5-Hydroxybenzoic Acid
5-HF	5-Hydroxyflavone
6-HF	6-Hydroxyflavone
7-HF	7-Hydroxyflavone
Aβ	Beta Amyloid
AFM	Atomic Force Microscopy
Asp	Aspartic Acid
Baic	Baicalein
bCT	Bovine Calcitonin
CD	Circular Dichroism
CMC	Critical Micelle Concentration
CT	Calcitonin
Cys	Cysteine
DC-cholesterol	3β-[N-(dimethylaminoethane)carbamoyl]-cholesterol
DLS	Dynamic Light Scattering
DMSO	Dimethyl Sulfoxide
DTNB	5,5`-dithiobis-(2-nitrobenzoic) Acid
ECG	Epicatechin Gallate

EGC	Epigallocatechin
EGCG	Epigallocatechin-3-Gallate
GA	Gallic Acid
Gly	Glycine
hCT	Human Calcitonin
HFIP	Hexafluoroisopropanol
His	Histidine
IAPP	Islet Amyloid Polypeptide
Leu	Leucine
Lut	Luteolin
Lys	Lysine
MALDI	Matrix Assisted Laser Desorption Ionization
Myr	Myricetin
Nar	Naringenin
NMR	Nuclear Magnetic Resonance
PAP	Prostatic Acid Phosphatase
PdI	Polydiversity Index
Phe	Phenylalanine
POPC	1-palmitoyl-2-oleoyl-glycero-3-phosphocholine
POPG	1-palmitoyl-2-oleoyl-glycero-3-phosphoglycerol
Pyro	Pyrogallol
RA	Rosmarinic Acid
RP-HPLC	Reversed Phase High-Performance Liquid Chromatography

sCT	Salmon Calcitonin
t_{50}	Aggregation Half-Time
TCEP	Tris(2-carboxyethyl)phosphine
TEM	Transmission Electron Microscopy
Thr	Threonine
ThT	Thioflavin-T
Tyr	Tyrosine
Quer	Quercetin

CHAPTER I: INTRODUCTION

1.1 Peptide Architecture

To understand human calcitonin (hCT) amyloid formation, it is important to be familiar with the fundamental concepts of peptide structure. Peptides and proteins are composed of amino acids which contain an amine functional group, a carboxyl functional group, and a side chain. The carboxyl group of one amino acid can form a chemical bond with the amine group of another amino acid to form a covalent peptide bond. This and a number of non-covalent interactions can form complex peptide structures needed for biological function. These structures are classified into four main levels: primary, secondary, tertiary, and quaternary. The sequence of the amino acids in a polypeptide chain is known as the primary structure. By convention, the amine group of the N-terminus is deemed the "beginning" of the peptide sequence and the carboxyl group of the C-terminus is taken to be the "end" of the peptide sequence. Secondary structure is the three-dimensional arrangement of local sections in the polypeptide. These arrangements form by hydrogen bonding interactions between the amino hydrogen and the carbonyl oxygen of the peptide backbone. Tertiary structure refers to the folding of the overall polypeptide chain. Non-covalent interactions such as hydrophobic, salt bridge formation between charged residues, disulfide bonds, and hydrogen bonding may be involved as well. Quaternary structure is the three-dimensional structure of multiple polypeptide chains (subunits) that operate as a single functional unit. These subunits interact with other

subunits through much of the same interactions as seen in the formation of the tertiary structure of polypeptides.

1.2 Peptide Folding, Misfolding, and Amyloid Formation

It is known that peptides can fold as fast as a few microseconds.[1] In 1969, Cyrus Levinthal proposed that if protein folding occurred through random interactions, it would take a longer amount of time than the age of the universe to reach its natively folded structure.[2] Therefore, protein folding must occur through an efficient mechanism involving sequential steps leading to a native structure with the lowest configurational energy.[3] A number of folding models have been proposed over the years. In particular, the folding funnel hypothesis, proposed by José Onuchic, is a widely accepted model for explaining protein folding.[4] The funnel is a 2D representation of the energy landscape of a folding polypeptide chain. In this model, a large number of unordered, highest energy, structures are found at the top of the funnel and the bottom contains the lowest energy native structure.[4-5] However, this funnel is not smooth and contains local energy minima of varying depths. These minima can be populated with intermediates that will eventually lead to the native structure or they become trapped and cannot overcome the energy barrier due to nonoptimal interactions.[5-6] These trapped structures will lead to partially folded or misfolded proteins.

However, this model only describes the folding behavior of a single polypeptide chain.[7] Therefore, an expanded folding funnel is used to account for protein aggregation. In this expanded model, the folding polypeptide chains become kinetically trapped in these local energy minima.[7] This could be due to many physiological factors such as changes in pH, temperature, protein concentration, errors in posttranslational modification, oxidative

damage, etc.[7] The partially folded or misfolded structures can then associate with each other through intermolecular interactions such as hydrophobic, hydrogen bonding, and electrostatic. This will ultimately generate either off-pathway metastable amorphous aggregates or highly ordered and insoluble amyloid fibrils. The formation of amyloid fibrils is particularly significant because these structures are known to be involved in the pathology of more than 40 devastating diseases such as Alzheimer's, Parkinson's, and type II diabetes.[8]

1.3 Human Calcitonin and Amyloidogenesis

In the 1950s, it was thought that the parathyroids controlled the concentration of blood calcium by releasing parathormone during hypocalcemia to elevate calcium levels and then is inhibited during hypercalcemia to reduce calcium levels.[9] However, in 1962, Copp et al. found that this mechanism was too simplistic when observing the reduction of blood calcium in fasted and anesthetized canines by the parathormone hormone alone.[9] Instead, they discovered a new hormone, calcitonin (CT), that was responsible for reducing elevated concentrations of blood calcium.[9] Later, it was unearthed that CT is produced by the C-cells of the thyroid gland, promotes bone formation through inhibiting osteoclast activity, and may play a role in gastrointestinal function.[10-13] In 1968, human calcitonin's (hCT) complete amino acid sequence was elucidated by Riniker and colleagues.[14] Over the years, several other specie variants of CT have been sequenced including salmon, bovine, porcine, and murine CTs.[15-18] Even though the sequences between these species can vary, all of them contain 32 amino acids with an N-terminal disulfide bond bridge between residues 1 and 7. In addition, all of these sequences have the ability to aggregate and form amyloid fibrils.[11, 19-22] The formation of these highly ordered amyloid fibrils and/or its

intermediates has been shown to be toxic to cells in many different diseases including CT.[21, 23-25]

Plasma hCT is normally less than 50 pg/mL in healthy individuals.[26] However, in medullary carcinoma of the thyroid, elevated levels of CT can be found in the blood and this can cause the formation of amyloid deposits in and around the thyroid gland.[27-28] In addition, CT has been used in the treatment of bone disorders such as hypercalcemia, osteoporosis, and Paget's disease.[29-30] However, any use of hCT has been discontinued due to its high aggregation propensity and formation of amyloid fibrils.[29, 31] Instead, the isoform salmon calcitonin (sCT) is utilized because of its substantially reduced aggregation propensity and increased bioavailability compared to hCT.[12, 31-32] Nonetheless, even though the aggregation rate is reduced, sCT still aggregates and this has a negative impact on the bioavailability of the drug.[11] Also, the use of sCT carries a series of unwanted side effects such as anorexia, vomiting, and can interfere with the immune system.[33-36] Therefore, it would be of great interest to find ways of preventing hCT amyloid formation to utilize it as a therapeutic agent.

1.4 General Mechanism of Amyloid Formation

Amyloid fibrils were first discovered in the mid-19th century while observing iodine stained deposits in the liver during an autopsy.[37] Later, it was discovered, through X-ray diffraction, that these fibrils contain β-strands oriented perpendicular to the fibril axis in what is known as a cross-β structure.[38] Despite the differences in amino acid sequence, this structure is prevalent in all amyloidogenic peptides. The formation of these fibrils generally follow what is known as a nucleated polymerization process.[39] As shown in Figure 1, the process of amyloid formation can be tracked with the addition of an

amyloid binding fluorescent dye and a sigmoid-shaped curve will emerge as aggregation and amyloid formation proceeds. This sigmoid-shaped curve can be broken down into three distinct stages: nucleation, elongation, and equilibrium (plateau).[40] In the nucleation stage, unfolded monomers begin to associate with each other reversibly. Eventually, monomer association reaches a critical threshold where a heterogenous oligomeric nucleus emerges. The formation of this critical nucleus is known to be a rate limiting step in the process.[41-42] However, when this nucleus is formed, it provides a "seed" for subsequent monomers to irreversibly bind to the ends of the thermodynamically unstable nucleus and elongate along the fibril axis.[37, 41] Further formation of these "seeds" accelerate the rate of the fibrillization reaction until mature fibrils emerge and an equilibrium or plateau of amyloid formation is reached.

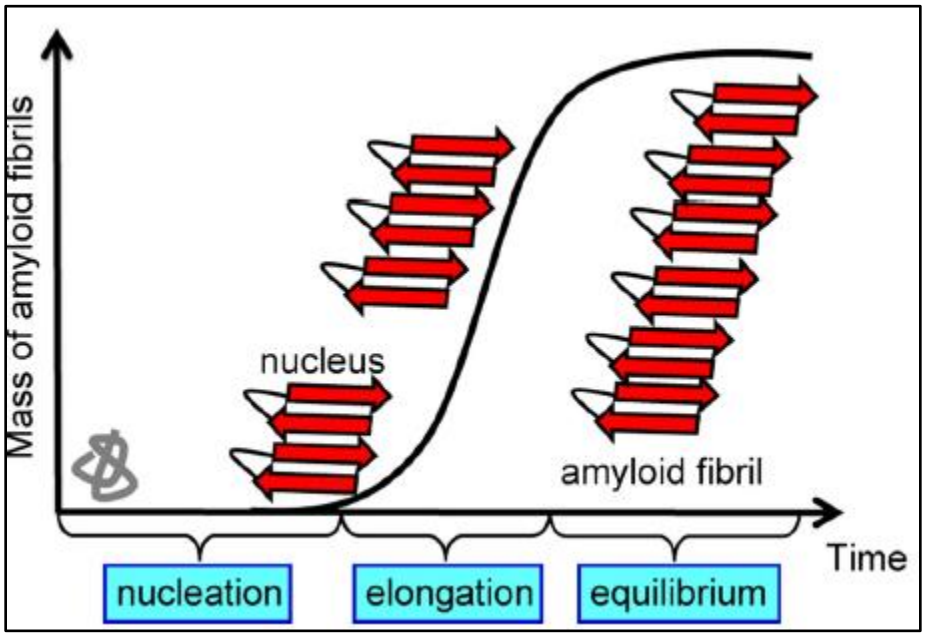

Figure 1. Representative illustration of the kinetics of amyloid fibril formation that follows the nucleation-dependent polymerization mechanism. The three phases, i.e. nucleation, elongation, and equilibrium, are labeled. Adapted from ref. [40].

1.4.1 Mechanism of hCT Amyloid Formation

Arvinte et al. was one of the first groups to study the structure and mechanism of hCT amyloid formation.[19] Arvinte observed that hCT forms well-ordered amyloid fibrils through transmission electron microscopy (TEM) and that as the concentration of hCT increases, a decrease in the nucleation time is also seen.[19] These characteristics are common in other amyloids.[24, 43-44] In addition, it was proposed that hCT follows a two-step nucleated polymerization process.[19, 45-46] As shown in Figure 2 below, the first step involves monomers associating with each other to form bundles composed of partial α-helical content that is located between Gly10 and Phe22.[46] These bundles then go through a conversion where the α-helical structures are simultaneously converted into oligomeric β-sheet structures.[19, 45-46] In the second step, monomers associate with the pre-formed oligomers and is converted into β-sheets to elongate and form mature amyloid fibrils.[19, 45-46] Even though these mature fibrils contain both α-helical and β-sheet components, studies show that CT fibril configuration mostly relies on the existence of the β-sheet structure.[19, 46-48]

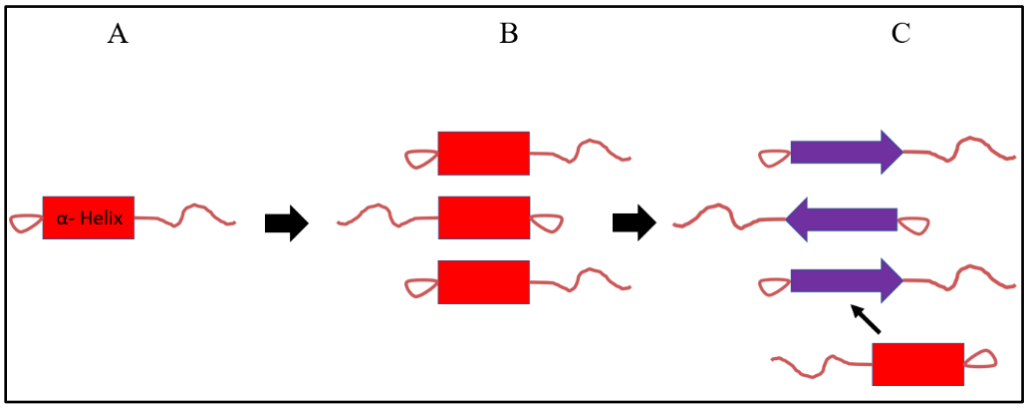

Figure 2. Two-step nucleated polymerization process of hCT. (A) Monomer. (B) α-helix bundle. (C) β-sheet.

1.4.2 Factors Affecting hCT Amyloid Formation

The formation and structure of these hCT amyloid fibrils are affected by several major factors. hCT contains three charged amino acids: Aspartic acid (Asp15), Lysine (Lys18), and Histidine (His20). Two of these charged residues are involved in the central pentapeptide fragment, $D_{15}FNKF_{19}$, which has been shown to be essential for fibril formation in hCT.[49] Saito et al. reported structural deviations in the observed fibrils when the pH of the environment was changed.[46-47] At a pH of 7.5, solid-state nuclear magnetic resonance (NMR) spectroscopy of site-specific labeled ^{13}C indicated that hCT fibrils formed an antiparallel β-sheet and were short in length as indicated by TEM.[46-47] However, at an acidic pH of 3.3, long and twisted fibrils formed with a mixture of antiparallel and parallel β-sheets.[46-47] They also noted that the second step of the nucleation process was faster at neutral than acidic pH.[47] This difference was due to the observed favorable electrostatic interaction between Asp15 and Lys18.[47] At physiological pH, these residues are charged and are able to interact with each other in alternating strands. However, when the pH is changed to 3.3, Asp15 no longer contains a negative charge and there is now a positive charge on Lys18 and His20, which also face the same side in the β-strand.[50] This leads to electrostatic repulsion between these two positively charged residues and interferes with the formation of the fibril, leading to a mixture of parallel and antiparallel β-sheets.[50]

Another major factor that affects the formation and structure of hCT fibrils is aromatic (π-π) interactions. The essential central hCT pentapeptide fragment, $D_{15}FNKF_{19}$, also contains two aromatic amino acids, Phe16 and Phe19. Naito et al. showed in solid-state ^{13}C NMR experiments that the phenyl rings of Phe16 and Phe19 of alternating strands could align with each other to stabilize the antiparallel β-sheet by π-π interactions.[51-52] In

addition, when the aromatic amino acids Tyr12, Phe16, and Phe19 were replaced by Leucine (Leu), there is a significant instability of the fibrils along with a reduction in the fibrillization rate.[52] Therefore, aromatic interactions, especially between Phe16 and Phe19, are important in the formation and structure of hCT fibrils. It also should be noted that sCT lacks these aromatic residues and is known to form fibrils at a considerably slower rate than hCT.[53 54]

In addition, the formation of amyloid fibrils of calcitonin may be affected by the N-terminal disulfide bond. The N-terminal sequence that includes the disulfide bond is highly preserved in all known calcitonin sequences.[11, 46, 55] Epand et al. observed that when sCT lacks the N-terminal region containing the disulfide bond, there is little helical structure acquired compared to unmodified sCT.[55] Furthermore, Kamihira et al. observed that the reduced form (hCT-SH), which lacks the disulfide bond, does not show turbidity even after two months compared to hCT with the disulfide bond which showed turbidity after 2 hours.[46] They also observed through solid-state ^{13}C NMR that the fibrils formed from the reduced form of hCT had a slightly different conformation compared to hCT with the disulfide bond.[46] They then postulated that even though the N-terminal disulfide bond is not directly involved in the β-sheet structure of the fibrils, it may still play an important role in the stabilization and maturation of the fibrils.[46]

1.5 Membranes, Cholesterol, and Toxicity

Among the many biomolecules that are found in the physiological surroundings, recent research suggests that cellular membranes play a major role in moderating CT aggregation and subsequent cellular toxicity.[21, 56-57] Cholesterol is a critical component of cellular membranes where it aids in receptor function, fluidity and permeability.[58-61] With

regards to bovine calcitonin, phospholipid vesicles containing cholesterol boosted the amount of β-sheet content and consequently increased amyloid production. Furthermore, the removal of cholesterol content from the membranes attenuated the toxicity to cells.[21] In addition to cholesterol, it has also been implicated that CT has an affinity to bind to membranes containing GM1 gangliosides.[11, 21, 62-64] GM1 gangliosides have been reported to aid in crucial biological functions such as ion transport, neuronal differentiation, neuroprotective signaling, and immune system function.[65] Due to GM1 containing a negatively charged sialic acid residue, electrostatic interactions between salmon CT and GM1 has been reported to cause spherical fibril aggregates to occur on the surface of liposomes.[57] These interactions have been reported to be enhanced by the presence of cholesterol.[57] Similarly, phospholipid vesicles containing GM1 enhanced β-sheet content and amyloid content of bCT.[21]

It has also been documented that CT can form pore-like structures in membranes and cause ion leakage.[59, 62, 64, 66] Such deformations can disrupt cell ion homeostasis and cause cell dysfunction and death. This phenomenon is believed to be directly responsible for diseases such as Alzheimer's and type II diabetes.[67] Meleleo and Sblano reported that cholesterol promotes hCT incorporation and channel formation in membranes.[59] This channel formation has also been observed with sCT favorably binding to membranes containing lipid rafts composed of cholesterol and GM1.[62] This binding resulted in annular oligomer formation and the genesis of ion-permeable channels in the membrane.[62] It was later discovered that this CT oligomer formation has been shown to be the culprit of channel development and subsequent ion leakage and neurotoxicity.[64] The generation of

these toxic oligomers in amyloid diseases has been increasingly evidenced that they play a primary role in amyloid-induced cytotoxicity.[68-70]

1.6 Inhibition of CT Aggregation

Unlike the therapeutically used sCT, hCT is not associated with any negative side effects or immune related responses.[71] However, there are no pharmaceutical drugs that inhibit hCT amyloid production making it impossible to be used as a therapeutic for bone related disorders. Nevertheless, the search for finding effective inhibitors of CT is ongoing. Ye et al. discovered that heme can reversibly bind with hCT and block the essential β-sheet formation needed to form amyloid fibrils.[31] In addition, they showed that the heme-hCT complex still exhibits bioactivity.[31] To date, this is the only study where both hCT amyloid formation is inhibited and yet it still has bioavailability. There have been several mutation studies where specific amino acids are substituted in order to inhibit amyloid fibril formation.[52-53, 72-74] Andreotti et al. hypothesized that sCT forms a stable helix early on through Leu-Leu interactions and this helix prevents the formation of aggregates.[73] Because of the difference in sequence homology, hCT lacks stability in the helix, contains aromatic residues that promote amyloid formation, and is consequently more prone to amyloid formation.[53, 75-76] Accordingly, they substituted hCT residues at five specific positions for the corresponding residues in sCT and showed that this new mutated hCT formed a more stable helix and mimicked the aggregation-resistant behavior of sCT.[53] Similarly, three amyloid promoting aromatic amino acids in hCT were substituted for the helix stabilizing Leu residues found in the same positions in sCT.[52] These substitutions created a more stable helix, prevented the π-π interactions needed for β-sheet formation, and led to a decrease in fibrillization rate by 2-3 orders of magnitude.[52] The strategy

targeting the amyloid inducing aromatic amino acids in hCT has also been utilized through the use of substitution by unnatural amino acids as well.[54, 74]

Besides substitution, aromatic amino acids have been targeted by small molecules to inhibit hCT amyloid formation as well. Shang et al. used cucurbit[n]uril, a macrocycle that has been evidenced to inhibit other amyloids, to form complexes with the aromatic residues of hCT to inhibit fibril formation.[77-78] In addition, the class of polyphenols have also been utilized and proven effective to inhibit amyloid formation.[79-80] Resveratrol and rosmarinic acid both have been shown to inhibit amyloid formation.[81-84] Magnolol and honokiol have been reported to inhibit hCT fibril formation through possible aromatic interactions but the mechanism still remains unclear.[85] In addition, Epigallocatechin-3-gallate (EGCG), the most abundant polyphenol found in green tea, has been shown to inhibit hCT and other amyloidogenic peptides as well.[48, 80, 86] However, the mechanism of how EGCG and other polyphenols inhibit amyloid formation is currently under debate. Huang et al. reported EGCG was able to prevent the initial association of hCT by interacting with the aromatic side chains of the peptide.[48] This hCT-EGCG interaction blocks the π-π interactions between the hCT aromatic residues and prevent fibril formation.[48] However, it has also been evidenced that EGCG can auto-oxidize and form quinones.[87] Quinones can react with the SH groups of cysteine and with the side chains of lysine, histidine and arginine.[88] This mechanism has been identified with prostatic acid phosphatase where oxidized EGCG can form a Schiff base with lysine and prevent amyloid fibril formation.[89] However, hydrogen bonding interactions have been identified to play a role in amyloid inhibition as well.[89-91]

1.7 Techniques Useful to the Characterization, Quantification, and Inhibition of hCT

The ideal way to probe hCT amyloid formation and inhibition thereof would be to directly observe *in vivo*. However, trying to achieve this is very difficult and instead, hCT studies are largely done *in vitro*. Many of these studies employ different techniques to investigate hCT amyloid formation and inhibition. hCT has been used as an amyloidogentic model due to its propensity to aggregate and form a kinetics profile that is similar to other amyloids. In order to track and study the kinetics profile of hCT fibril formation, one cannot just directly observe the physical changes due to the changes being too small and/or too fast. Instead, one needs a sensitive extrinsic reporter like the fluorescent dye, thioflavin-T (ThT), to track the changes in the local environment and the conformation of the peptide leading up to fibril formation.[92] However, these extrinsic reporters have limitations in tracking these changes such as not recognizing oligomers and giving false positives.[92] Therefore, visual techniques such as TEM or atomic force microscopy (AFM) are used to confirm the products formed in the kinetics. Also, circular dichroism (CD) spectroscopy is often used to track the secondary structure of the peptide. Other techniques such as dynamic light scattering (DLS) can be used to characterize peptides and determine liposome sizes.

1.7.1 Fluorescence Spectroscopy

Fluorescence spectroscopy is one the most widely used techniques to probe peptide folding due to its ease of use and high sensitivity.[93] hCT contains four intrinsic fluorophores including Tyr and Phe. These fluorophores can be used to track the local conformational changes of proteins.[93] However, hCT contains three Phe residues so this can make it difficult to track the local conformational changes at each residue. Therefore, using extrinsic fluorophores would be advantageous as they can be used to track the kinetics and

aggregation of peptides. ThT, originally used to stain amyloid deposits in tissues, is one of the most utilized dyes for the identification and quantification of amyloid fibrils as well as the fibrillization kinetics of the amyloid with small molecules.[92] On its own, ThT is only weakly fluorescent, but when bound to β-sheet rich amyloid fibrils, there is a 10-fold increase in fluorescence.[92] However, the exact mechanism of how ThT binds to amyloid fibrils is still under debate. It is known that the benzylamine and benzathiole rings of ThT are able to freely rotate in solution and are quenched by the rapid rotation upon fluoresence.[94-95] However, when these rings are immobilized, there is an increase in the quantum yield leading to the enhancement of the fluorescence. It has been suggested that this immobilization happens when ThT binds to the surface of the channels made by cross-β structures that run parallel to the axis of the amyloid fibril.[95] This allows for the tracking of hCT kinetics and the formation of amyloid fibrils. However, one needs to be cautious as this method is not sensitive towards the detection of transient structures, may give false positives, and will lose fluorescence if the aggregated peptide precipitates out of solution. Therefore, other methods for detecting fibril formation or inhibition needs to be utilized in conjunction with the use of ThT and fluorescence spectroscopy.

1.7.2 Circular Dichroism Spectroscopy

CD spectroscopy is a widely used method for detecting the conformation of peptides and proteins.[96] This technique utilizes left and right handed circularly polarized light that interacts with a chromophore that exhibits chirality.[96] If this left and right handed radiation is absorbed to different extents, then a CD signal will be observed.[96] Depending on the wavelength being observed, one can study the peptide backbone, the side chains of aromatic amino acids, and disulfide bonds. A common use of this technique is to determine

secondary structure composition from the peptide backbone (240 nm and below). The α-helix, random coil, β-sheet, and β-turn secondary structures can all be easily distinguished from this method.[96] In addition, this technique has been applied for determining the conformation of amyloid fibrils by the conversion to the β-sheet structure.[33, 97-98] This technique can also be used to determine tertiary structure (260-320 nm) and conformational changes by way of binding of ligands to peptides.[96] However, CD spectroscopy is limited due to the use of algorithms that rely on databases containing already known structures and just because the peptide contains a β-sheet structure does not mean it contains fibrils. Also, if the peptide precipitates out of solution, a CD signal can no longer be observed.[99] Therefore, other methods in addition to CD spectroscopy needs to be used to confirm the formation of amyloid fibrils.

1.7.3 Atomic Force Microscopy

AFM is one of the most widely used single-molecule methods to directly study the structural and morphological properties of amyloid fibrils and the fibrillization process.[100-102] These structures can be seen in three dimensions with a high atomic resolution.[103] In addition, AFM allows the direct visualization of protofibrils, oligomers, and other transient species during the aggregation process.[104] Generally, biomolecules such as amyloids are adsorbed onto freshly cleaved mica which offers a flat and even surface to scan.[100, 105] Then, AFM utilizes a fine probe that is attached to a flexible cantilever to scan over the surface of the sample.[103] A laser beam, that is positioned on the cantilever, is deflected as the cantilever scans the sample and the change in height is detected by a photodiode, position-sensitive detector.[103] This technique lets us detect the fine details in amyloid morphology. As shown in our work, we are able to clearly detect the morphology of hCT fibril and

oligomer formation. In addition, it is able to detect the lack of fibril formation and therefore show inhibition of hCT by small molecules.

1.7.4 Dynamic Light Scattering

DLS is a widely used technique for measuring particle sizes, zeta potentials, and molecular weights of different particles in solution.[106] This method is based on the principle of a beam of light interacting with a particle that exhibits Brownian motion and scatters.[106] The fluctuations of light intensity is measured and this allows the size of the particle to be measured by the use of the Stokes-Einstein equation.[106] This technique can be used to measure the size of amyloid aggregates and liposomes.[107-108] In addition, the zeta potential of different molecules such as charged cholesterol can be measured as well. Zeta potential is the potential measured at the slipping plane of a particle under an electric field.[106] In other words, this technique can measure the surface charge of particles in a solution. This method can be particularly useful when studying the interaction of charged molecules with amyloidogenic peptides.

1.8 Dissertation Outline

In Chapter II, our work began with probing the effect of the intramolecular disulfide bond to gain a better insight into the aggregation kinetics of hCT. Our results indicated that the disulfide bond is critical in forming the nucleus that is needed for hCT fibril formation. In addition, we examined the effects of cholesterol, cholesterol sulfate, and 3β-[N-(dimethylaminoethane)carbamoyl]-cholesterol (DC-cholesterol) on hCT amyloid formation. Our results showed that cholesterol itself does not affect hCT amyloid formation and cholesterol sulfate has a moderate inhibiting effect at high concentrations. However, DC-cholesterol shows strong inhibition of hCT fibril formation in a dose-dependent

manner. Additional experiments, at different pH conditions, implicates the critical influence electrostatic and hydrogen bonding interactions have in moderating the interactions between hCT and the surface of DC-cholesterol vesicles. In addition, these interactions can lead to a better understanding of the inhibiting function of DC-cholesterol on hCT amyloid formation.

In Chapter III, we explored a number of polyphenolic molecules for inhibition of hCT amyloid formation. Our results showed that the gallate moiety in epigallocatechin-3-gallate (EGCG), a well-known amyloid inhibitor, is not crucial for its inhibiting activity of hCT fibril formation. However, our results showed that compounds containing vicinal hydroxyl groups on the phenyl ring such as in myricetin, quercetin, and baicalein are effective inhibitors of hCT amyloid formation. In addition, our results indicate a possible mechanistic role vicinal hydroxyl groups have in attenuating hCT amyloidogenesis. This may include the oxidation of the vicinal hydroxyl groups to form a quinone which can subsequently form a Schiff base with the lysine or histidine residues contained in hCT. This interaction could disrupt the critical electrostatic and aromatic interactions that are needed in hCT fibril formation. In addition, interactions such as hydrogen bonding and aromatic stacking may also be involved which all may act together in inhibiting hCT amyloid formation.

In Chapter IV, we examined how liposome concentration, size and curvature affected the kinetics of hCT fibril formation. Our results showed that both 200 nm zwitterionic 1-palmitoyl-2-oleoyl-glycero-3-phosphocholine (POPC) and 200 nm negatively charged 1-palmitoyl-2-oleoyl-phosphatidylglycerol (POPG) liposomes exhibited inhibitory effects on the aggregation of hCT in a concentration-dependent

manner. However, POPC was shown to be a stronger inhibitor than POPG. Also, in the presence of low concentrations of POPC liposomes, there was an enhancement in fibril formation whereas POPG did not exhibit this phenomena. We hypothesize that hCT can interact with POPC and POPG through a combination of electrostatic and hydrophobic interactions. The negatively charged POPG liposomes can cause hCT to insert itself deep into the bilayer where fibril formation is avoided. With POPC, we speculate that hCT loosely interacts with the surface of the liposomes where this can cause nucleation points to occur that leads to increased fibrillization. As the concentration of liposomes increase, this would lead to increased monomer interacting with the liposomes and would reduce the effective monomer concentration in solution leading to inhibition. In addition, the interactions between hCT and the liposomes may lead to lipid structures that exhibit high curvature and more water-exposed hydrophobic regions in the bilayer. When the size of the POPC liposomes were reduced, inhibition was more pronounced, indicating size and vesicle curvature does have an effect on hCT fibril formation. This study allows us to have a better understanding of how hCT interacts with cellular membranes and could lead to the development of novel inhibitors that could be used in treating bone-related disorders.

CHAPTER II: EFFECTS OF DISULFIDE BOND AND CHOLESTEROL DERIVATIVES ON HUMAN CALCITONIN AMYLOID FORMATION

This chapter was adapted from the following publication

> Lantz, R., Busbee, B., Wojcikiewicz, E. P., and Du, D. (2020) Effects of Disulfide Bond and Cholesterol Derivatives on Human Calcitonin Amyloid Formation. *Biopolymers* 111, e23343

2.1 Introduction

Human calcitonin (hCT) is a 32-residue peptide hormone that is produced by the parafollicular cells (C-cells) in the thyroid where it regulates blood calcium levels and promotes bone formation.[10, 33] It has been well recognized that hCT tends to aggregate when elevated levels of the peptide are either produced naturally or injected for therapeutic treatment.[27-28] The hCT amyloid fibrils have been reported to exert cellular toxicity.[21] The formation of amyloid deposits of hCT has also been suggested to be associated with medullary carcinoma of the thyroid.[27, 109] Because of its high aggregation propensity, the clinical therapies of using hCT for treating bone disorders such as hypercalcemia, osteoporosis or Paget's disease, have been discontinued.[29, 31] Instead, salmon calcitonin (sCT), a calcitonin derivative, is applied for therapeutic treatment because of its substantially reduced aggregation propensity in comparison to hCT.[12, 31-32]

Aggregation of a variety of amyloidogenic proteins usually undergoes a nucleated polymerization process.[39] Fibrillization of hCT has also been manifested to proceed via a two-step mechanism that includes the early association of monomers to form nuclei composed of partial α-helical structures and the subsequent conformational conversion into

β-sheet structures.[19, 45-46] The addition of monomers onto the formed β-sheet structures leads to the growth of nucleus to form amyloid fibrils.[19, 45-46] Based on the solid-state NMR studies, Kamihira et al. revealed that both the central region (Phe16-Thr21) and the C-terminal region of hCT undergo conformational transitions to form β-sheets during fibril formation in acidic solution.[46] The N-terminal region of hCT, in contrast, contains a specific loop structure via the disulfide bond formed between Cys1 and Cys7 as shown in figure 3A below. Remarkably, this N-terminal disulfide bond is highly conserved in all known calcitonin sequences.[46, 55] Epand et al. reported that when sCT lacks the N-terminus region where the disulfide bond is located, there is little helical structure attained compared to unmodified sCT.[55] Furthermore, although the N-terminal loop region is not directly involved in the β-sheet structure in amyloid fibrils, the disulfide bond in this region has been suggested to play an important role in stabilizing and maturing the hCT amyloid fibrils.[46] However, the mechanistic influence of the disulfide bond formation in mediating the kinetic details of hCT aggregation has not been well clarified. In this study, we investigate the amyloidogenic characteristics of both unoxidized and oxidized hCT at physiological conditions using the thioflavin-T (ThT) assay and atomic force microscopy (AFM), to provide new insights into the mechanical role of the disulfide bond in the formation of hCT amyloid fibrils.

The physiological environment wherein hCT amyloids are formed *in vivo* are filled with extensive amounts of biomolecules and biostructures. Among these, a growing body of recent research suggests the importance of cellular membranes in mediating calcitonin self-assembly and consequent cellular toxicity.[21, 56-57] Cholesterol, a neutral hydrophobic sterol molecule (Figure 3B) with a concentration of ~200 mg/dL in human plasma,[110] is an

important component of the cellular membrane where it helps regulate fluidity, permeability and receptor function.[59-61] Wang et al. reported that amyloids of bovine calcitonin (bCT) bind more strongly to phospholipid vesicles containing cholesterol.[21] It has also been evidenced that as cholesterol and ganglioside content decreased in cell membranes, the less toxic bCT and sCT were to cells.[21, 56] Furthermore, it has been reported that electrostatic interactions between sCT and GM1 (a ganglioside component of cellular membranes) which are stabilized by cholesterol cause spherical amyloid aggregation to occur on the surface of liposomes.[57] In addition, hCT is capable to form channels within the membrane and cause ion leakage,[62, 64, 66] and this hCT-induced membrane pore formation is enhanced by the presence of cholesterol.[59] Therefore, cholesterol may play a crucial role in modulating calcitonin amyloid formation and cellular toxicity *in vivo*. However, while most of the previous studies have mainly focused on cholesterol as the component of cellular membranes, to our knowledge, the mechanistic role of cholesterol itself in modulating amyloid formation of calcitonin remains little addressed.

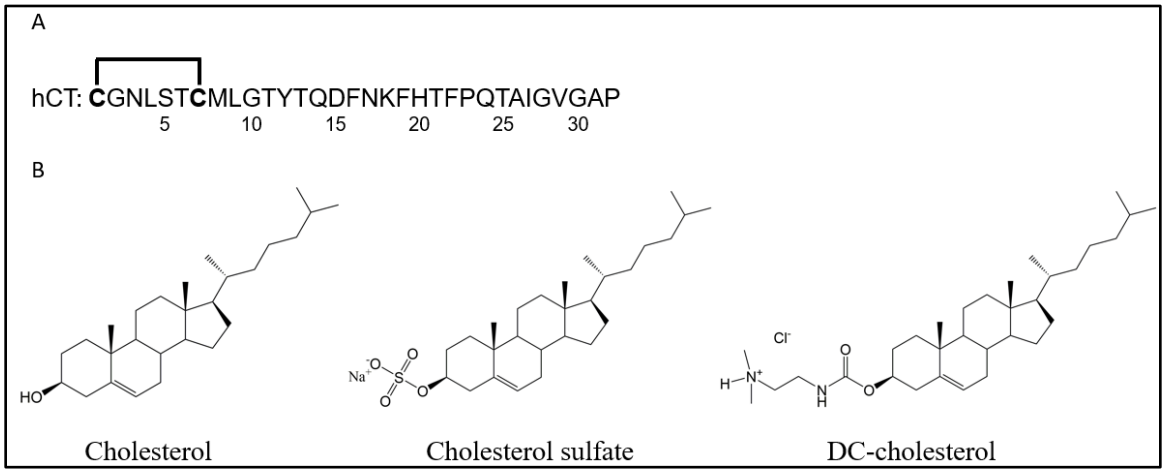

Figure 3. (A) Sequence of hCT. The formation of the disulfide bond between Cys1 and Cys7 is shown. (B) Structures of cholesterol and its two derivatives.

Cholesterol is susceptible to be modified into a series of derivatives, some of which commonly exist in eukaryotes. Among these, cholesterol sulfate (Figure 3B) is one of the most important known sterol sulfates and has emerged as a significant lipid constituent in a variety of human tissues,[111] with a concentration of ~110-170 μg/mL in human plasma.[112-113] Cholesterol sulfate is involved in signal transduction and shows elevated levels with hypothyroidis.[111] Women with autoimmune primary hypothyroidism also show a deficiency in calcitonin.[114] Understanding the effect of this cholesterol derivative on calcitonin amyloidogenesis may provide new insight into the potential correlation of calcitonin and cholesterol sulfate in this disease. Cholesterol sulfate contains a negatively charged sulfate moiety with a pK_a of ~3.3, which makes it ionized under physiological conditions and more amphiphilic than cholesterol (Figure 3B).[115] On the other hand, another cholesterol derivative, 3β-[N-(dimethylaminoethane)carbamoyl]-cholesterol (DC-cholesterol) contains a positively charged dimethylethylenediamine group attached to the cholesterol moiety (Figure 13B). DC-cholesterol has been used in the preparation of liposomes for the drug delivery of sCT in rats.[116] Because of the presence of additional charged moieties on cholesterol sulfate and DC-cholesterol molecules, these cholesterol derivatives may provide a novel perspective in investigating the effect of steroid-based molecules in modulating hCT amyloidogenesis. Dissecting the impact of these molecules on hCT fibrillization will give more insight into the roles of the interactions, e.g., electrostatic, hydrophobic, and hydrogen bonding, in directing interactions of hCT and steroid molecules and the subsequent hCT aggregation. Therefore, in this study, we also investigate and compare the effects of cholesterol and the two charged derivatives on hCT amyloid formation.

2.2 Materials and Methods

2.2.1 Materials

All chemical reagents were purchased from commercial suppliers and used without further purification. Tris(2-carboxyethyl)phosphine (TCEP), cholesterol, cholesterol sulfate, and DC-cholesterol were purchased from Sigma Aldrich. Stock solutions of DC-cholesterol and cholesterol sulfate were prepared by dissolving compound powder in dimethyl sulfoxide (DMSO), and the stock solution of cholesterol was prepared by dissolving in a mixture of hexane/chloroform/ethanol 11:5:4 v/v/v.[117]

2.2.1 Synthesis and Preparation of Oxidized hCT

The hCT peptide was synthesized on a PS3 solid phase peptide synthesizer (Protein Technologies Inc., Woburn, MA) using the standard Fmoc strategy. The crude peptide was purified by reversed phase high-performance liquid chromatography (RP-HPLC) using a C18 reverse phase column, characterized by matrix-assisted laser desorption ionization (MALDI) mass spectrometry and lyophilized. The unoxidized peptide was stored at -80 °C until further use. To form the disulfide bond between Cys1 and Cys7, the air oxidation was run overnight of dilute hCT (pH 8.1) in 6 M urea to prevent fibrillization.[48, 118] An Ellman test was used to confirm disulfide bond formation after oxidation.[119] The oxidized peptide was further purified by HPLC and lyophilized. To ensure the peptide was monomerized, the unoxidized and oxidized peptides were dissolved in hexafluoroisopropanol (HFIP), sonicated for 5 min and incubated for 1 h. The peptide solution was then separated into ~50 µL aliquots in centrifuge tubes, leaving the caps open with a stream of air to evaporate off the HFIP. The sample was further stored in a vacuum desiccator overnight to ensure complete evaporation of HFIP. The resulting film was stored at -80 °C until further use.

Peptide solutions were prepared by resolubilizing in sodium phosphate buffer (pH 7.4) and the concentration was determined by UV absorbance at 275 nm (ε = 1531 cm^{-1} M^{-1}).[120]

2.2.2 Aggregation Kinetics by ThT Fluorescence

To monitor the aggregation kinetics, 5 μM of oxidized hCT or unoxidized hCT was prepared in phosphate buffer (5 mM Na phosphate, pH 7.4) containing 20 μM ThT. 100 μL of solution was transferred to wells in a 96-well microplate (Costar black, clear bottom). The plate was sealed with a microplate cover, parafilmed and loaded into a Gemini SpectraMax EM fluorescence plate reader (Molecular Devices, Sunnyvale, CA) where it was incubated at 25 °C. The fluorescence of ThT was measured every 10 min after shaking for 5 s with an excitation wavelength of 440 nm and an emission of 480 nm. All fluorescence kinetics data are reported as a means of triplicate results.

To measure the aggregation kinetics with additional cholesterol and the derivatives, cholesterol sulfate and DC-cholesterol were dissolved in DMSO and cholesterol was dissolved in hexane:chloroform:ethanol 11:5:4 v/v/v to prepare 5 mM stock solutions, respectively. Further dilutions were applied to make stock solutions with different concentrations. A particular amount of stock solutions was then added to oxidized hCT (final concentration of 5 μM) in phosphate buffer (5 mM Na phosphate, pH 7.4) containing 20 μM ThT. To be consistent, all the solutions contained the same volume of DMSO or hexane:chloroform:ethanol. The solutions were then pipetted into the wells of the plate (100 μL/well) for the kinetic assay. For the kinetic assays at high pH, 5 μM of oxidized hCT was prepared in 5 mM carbonate buffer (pH 10.2).

2.2.3 Circular Dichroism

50 μM of oxidized hCT was incubated with phosphate buffer (5 mM Na phosphate, pH 7.4) quiescently at 25 °C. At desired time points, 200 μL of the incubated solution was transferred into a 1 mm path length quartz sample cuvette. The CD spectra were collected on a J-810 spectropolarimeter (JASCO). The average of 4 scans was collected.

2.2.4 Atomic Force Microscopy

To measure AFM imaging, aliquots (15-20 μL) of the hCT samples either taken from the aggregation kinetics assay or incubated quiescently after predetermined periods of time were adsorbed onto the surface of freshly cleaved mica (5 x 5 mm). The samples were dried overnight, and AFM images were acquired in tapping mode using the Asylum Research MFP 3D AFM system with MikroMasch NSC15/Al BS cantilevers.

2.2.5 Vesicle Size Measurement Using Dynamic Light Scattering

500 μL aliquots of different concentrations of cholesterol and its derivatives in either phosphate buffer (5 mM Na phosphate, pH 7.4) or 5 mM carbonate buffer (pH 10.2) with 5% DMSO or hexane:chloroform:ethanol 11:5:4 v/v/v were incubated at 25 °C for 24 h, quiescently. The samples were stirred and 100 μL of each DC-cholesterol solution were transferred to a 1 cm cuvette. Size measurements were performed on a Zetasizer Nano ZS instrument (Malvern Instruments, UK) with disposable cuvettes. The average diameters of the vesicles were calculated as the mean of three measurements with 11-19 runs per measurement.

2.3 Results and Discussion

2.3.1 Disulfide Bond Formation in hCT Facilitates the Kinetics of hCT Amyloidogenesis

In order to form the intramolecular disulfide bond, the hCT peptide was air oxidized in a dilute concentration to prevent intermolecular disulfide bonds from forming.[48, 121] The disulfide bond formation was confirmed by the Ellman reaction.[119] Free thiol groups can be detected through colorimetric analysis by an exchange reaction with 5,5`-dithiobis-(2-nitrobenzoic) acid (DTNB).[119, 122] The free thiol side chain of cysteine residues in the hCT sample without air oxidation (hereafter referred to as unoxidized hCT) reacts with DTNB and shows an absorbance peak at 412 nm as shown in Figure 4A below. The oxidized hCT shows no absorbance at this region, affirming the formation of the disulfide bond (Figure 4A). In addition, the oxidized hCT was characterized by MALDI with the reported mass of 3417.53 Da, further validating the formation of the intramolecular disulfide bond, instead of instead of an intermolecular disulfide bond (Figure 4B).

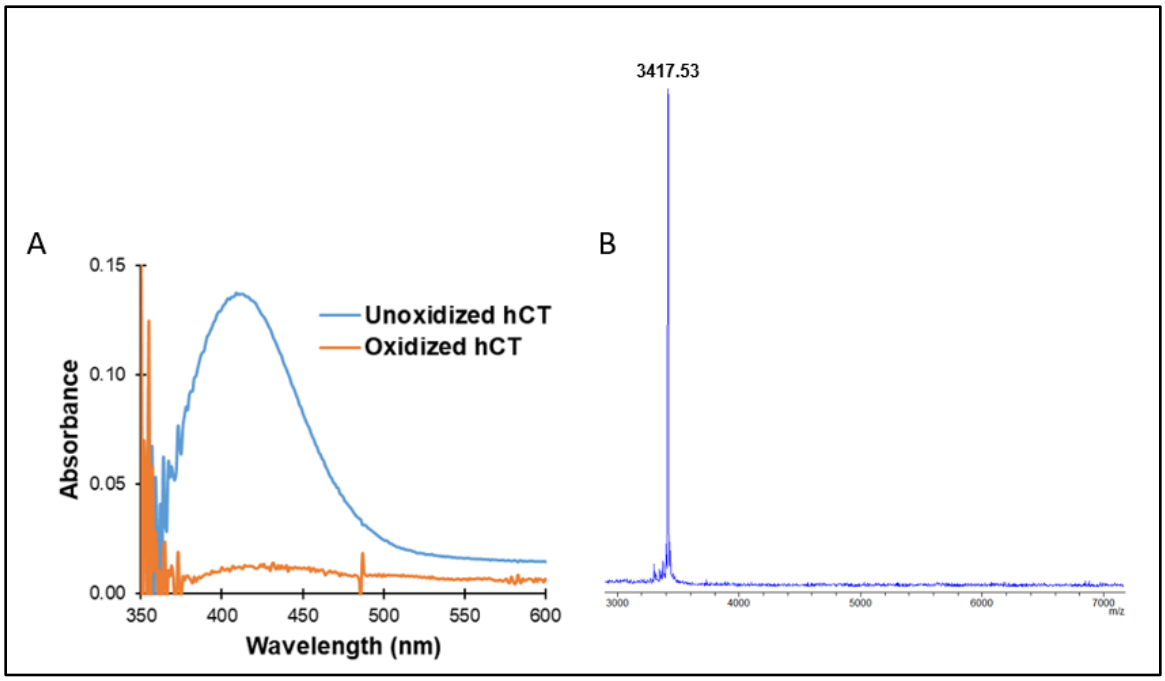

Figure 4. (A) UV-Vis absorbance of the unoxidized and oxidized hCT after reacting with DTNB. (B) MALDI spectrum of oxidized hCT. The calculated molecular weight of oxidized hCT is 3417.85 Da.

The aggregation kinetics of hCT (5 µM) in phosphate buffer (5 mM Na phosphate, pH 7.4) was monitored by ThT, a widely used fluorescent dye that can specifically bind to the amyloid fibril structure leading to an increase in the fluorescence intensity in the vicinity of 480 nm.[95, 123-124] As shown in Figure 5A below, the aggregation kinetics of oxidized hCT exhibits a fast increase immediately after the start of the measurement until reaching the maximum of the fluorescence intensity at about 10 h. This result is consistent

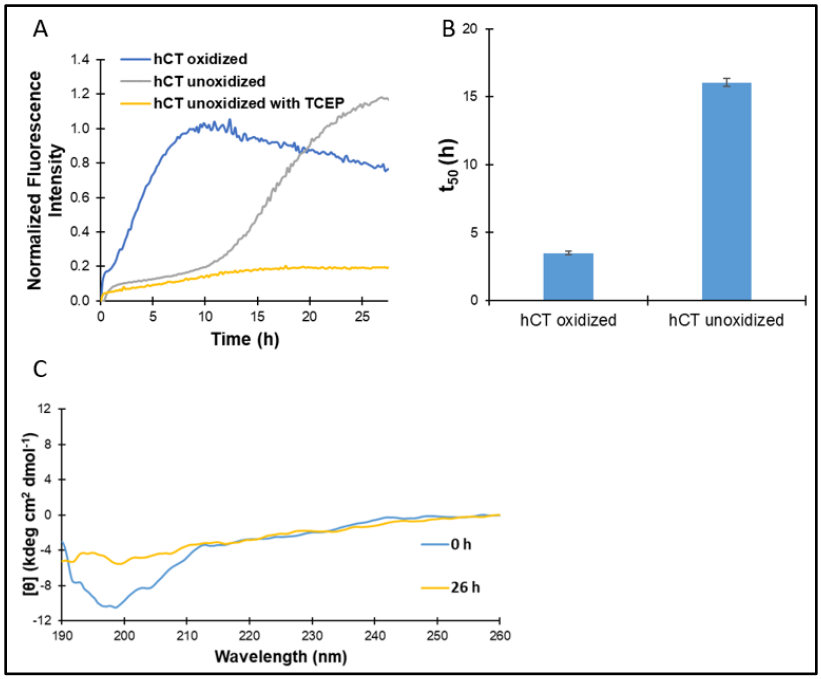

Figure 5. (A) ThT aggregation kinetics of oxidized hCT, unoxidized hCT, and unoxidized hCT with 1 mM TCEP. The peptides (5 µM) were incubated in phosphate buffer (5 mM Na phosphate, pH 7.4) at 25 °C. (B) Aggregation half-time (t50) of hCT. Data are reported as means ± the standard deviation of triplicate results. (C) CD spectra of oxidized hCT (50 µM) in phosphate buffer (5 mM Na phosphate, pH 7.4) at 25 °C. The spectra are the average of 4 scans.

with previous reports indicating a rapid rate of hCT amyloid formation.[31, 53] Notably, after reaching the maximum, the fluorescence intensity slowly decreases over time. The CD

spectrum of the fresh oxidized hCT sample initially shows a minimum peak at 198 nm, indicating a random coil structure (Figure 5C). As time progresses, the intensity of this peak diminishes (Figure 5C). Our result is consistent with the study of Kawashima et al. who also reported the loss of CD signal of hCT after aggregation, likely attributed to the precipitation of hCT aggregates over the course of incubation.[99] This may also account for the decrease of ThT fluorescence intensity observed in the aggregation kinetics result (Figure 5A).

The aggregation kinetics of unoxidized hCT shows a more typical sigmoidal process in comparison to the oxidized species (Figure 5A). A lag phase of approximately 10 h, which is associated with the formation of crucial oligomeric nuclei, is followed by a growth phase linked to the formation and propagation of amyloid fibrils. The aggregation half-time (t_{50}), which is defined as the time at which the ThT fluorescence reaches half of the maximum intensity, is ~16 h for unoxidized hCT (Figure 5B). The t_{50} value of unoxidized hCT is 4.5 times as much as that of the oxidized species (Figure 5B). These results demonstrate that the rate of amyloid formation of unoxidized hCT is significantly slower than that of the oxidized peptide. Considering the lack of the disulfide bond in the unoxidized hCT in comparison to the oxidized sample, our kinetic results implicate the remarkable effect of the disulfide bond on aggregation kinetics of hCT.

To further validate the crucial role of the disulfide bond in hCT aggregation, we studied the aggregation of unoxidized hCT in the presence of TCEP (1 mM). TCEP is a reducing agent widely employed for breaking disulfide bonds in proteins.[125] Here, TCEP is used to prevent disulfide bond formation of hCT throughout the kinetics experiment. The aggregation kinetics show a more subdued progression of ThT fluorescence intensity

increase (Figure 5A). The fluorescence intensity of the unoxidized hCT peptide with TCEP is significantly lower than that of oxidized hCT and unoxidized hCT over the whole experimental period. These results further confirm that completely inhibiting disulfide bond formation can effectively prevent the peptide from forming amyloid fibril structures.

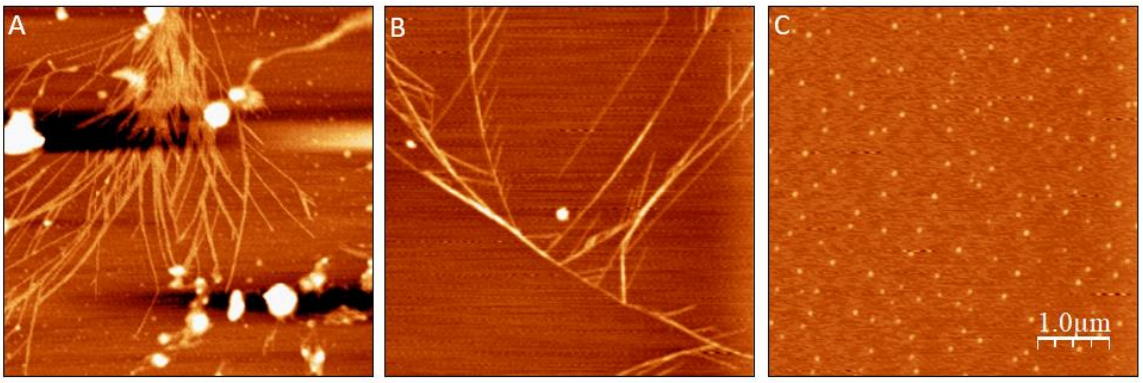

Figure 6. Tapping mode AFM images of (A) oxidized hCT, (B) unoxidized hCT, and unoxidized hCT with 1 mM TCEP (C). The peptide samples were incubated in phosphate buffer (5 mM Na phosphate, pH 7.4) at 25 °C for 24 h before imaging.

The morphology of aggregates of oxidized hCT, unoxidized hCT, and unoxidized hCT with TCEP was also assessed using AFM imaging. The AFM imaging samples were aliquoted from the ThT aggregation kinetics assay that had been incubating at 25 °C for 24 h prior to imaging. As depicted in Figure 6A above, oxidized hCT aggregated and formed long and stacked fibrillar structures. The initially unoxidized hCT also exhibited the formation of amyloid fibrils after incubation (Figure 6B). When the unoxidized hCT was co-incubated with TCEP, no mature fibrils were observed; instead, only spherical oligomeric structures were identified (Figure 6C). This AFM imaging result is consistent with the ThT aggregation kinetics result showing weak ThT fluorescence response in the presence of TCEP due to a lack of amyloid fibril content.[31, 126] It is speculated that these spherical oligomers formed by hCT without the disulfide bond are off-pathway intermediates trapped with considerable meta-stability and incapable of carrying out the

conformational conversion to grow into fibrillar structures. In the absence of TCEP, the progressive oxidation of the initially unoxidized hCT over the course of the experimental period is expected to facilitate the nucleation reaction upon disulfide bond formation, leading to a delayed fibrillization process compared to the initially oxidized peptide (Figure 5A-B).

2.3.2 Effect of Cholesterol on hCT Aggregation

Cholesterol and its derivatives can self-associate and form vesicles above their critical micelle concentration (CMC) values. The CMC values of cholesterol, cholesterol sulfate, and DC-cholesterol are approximately 31 nM, 12.6 nM, and 14 nM, respectively.[115, 127] Since the physiological concentrations of cholesterol and cholesterol sulfate are much higher than their CMC values, we examined the effect of the choleterol vesicles formed at concentrations above the CMC value on the aggregation of the oxidized hCT. As shown in Figure 7A below, the presence of cholesterol (2.5-25 μM) does not show a noticeable influence on the aggregation kinetics of oxidized hCT. The formation of amyloid fibrils of oxidized hCT co-incubated with cholesterol for 24 h was also confirmed by AFM imaging (Figure 7B). These results show that the vesicles formed by pure cholesterol does not significantly modulate the characteristics of hCT amyloidogenesis, indicating weak (if there is any) interactions of the peptide and the cholesterol vesicle structure. In cells, besides being an abundant lipid in secretory vesicles, cholesterol is also an important component of the plasma membrane. Some lipids in the membrane, e.g., GM1, have been recognized to have a cholesterol-dependent influence on the formation of protein amyloid fibrils.[21, 62, 128-130] Fantini et al. reported that cholesterol facilitates a conformational change of GM1 in the membrane which makes it more favorable to interact

with amyloid-β peptide.[117] Although our results show that cholesterol vesicles do not influence hCT aggregation dramatically, it cannot be ruled out that cholesterol might play an indirect role in manipulating hCT aggregation *in vivo* by cooperating with other lipid membrane components in a concerted manner.

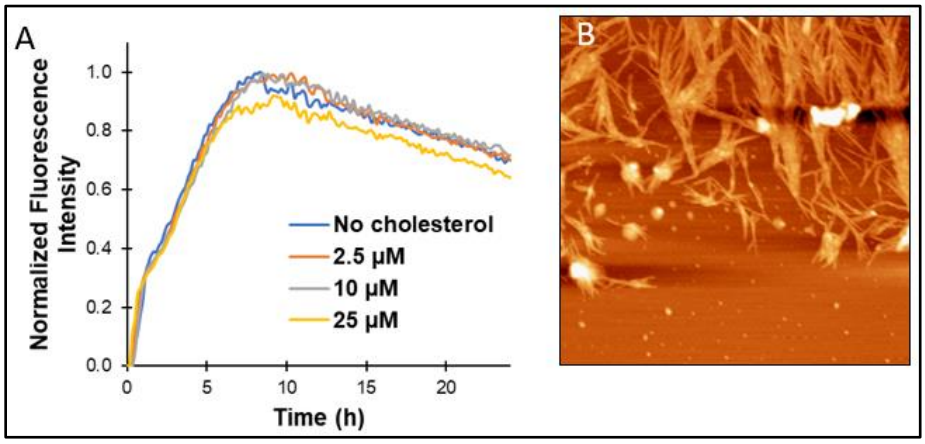

Figure 7. (A) Effect of cholesterol on aggregation kinetics of oxidized hCT (5 μM) in phosphate buffer (5 mM Na phosphate, pH 7.4) at 25 °C. (B) Tapping mode AFM image of oxidized hCT (5 μM) in the presence of 25 μM cholesterol. The sample was incubated for 24 h at 25 °C before imaging.

2.3.3 Effect of the Cholesterol Derivatives on hCT Aggregation

The effects of the two cholesterol derivatives on oxidized hCT amyloidogenesis were also studied using both ThT fluorescence and AFM imaging. For cholesterol sulfate, our kinetic results show that the addition of relatively low concentrations of this cholesterol derivative does not change the aggregation rate significantly as shown in Figure 8A below. However, in the presence of 25 μM cholesterol sulfate, the aggregation of oxidized hCT is delayed (Figure 8A). AFM imaging reveals that amyloid fibrils still readily formed after 24 h incubation of oxidized hCT with 25 μM cholesterol sulfate (Figure 8B). These results indicate that higher concentrations of cholesterol sulfate can moderately inhibit amyloid fibril formation of oxidized hCT. Vesicles formed by amphipathic phospholipids normally contain a structure with the hydrophilic head group facing the surrounding aqueous solvent,

sequestering the hydrophobic tail regions in the vesicle center. Although the characteristic steroid structure of cholesterol sulfate makes it less favorable to form ordered gel- or liquid crystalline-like vesicle structures, considering the amphipathic nature of cholesterol

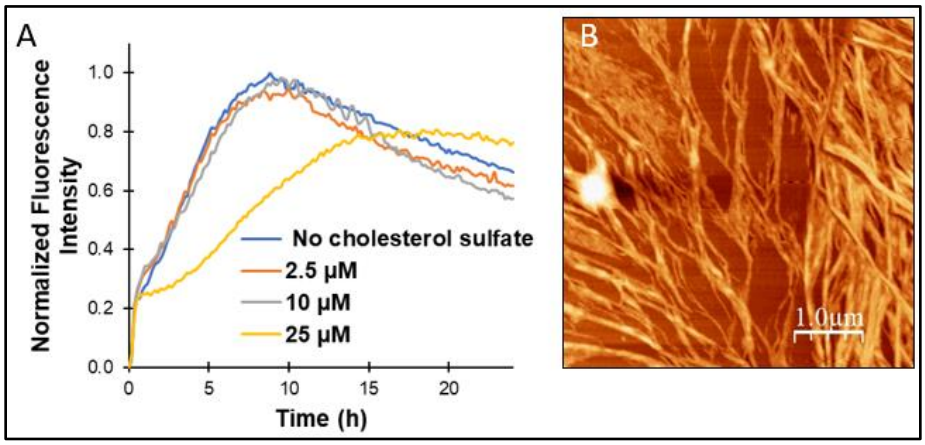

Figure 8. (A) Effect of cholesterol sulfate on aggregation kinetics of oxidized hCT (5 μM) in phosphate buffer (5 mM Na phosphate, pH 7.4). (B) Tapping mode AFM image of oxidized hCT (5 μM) in the presence of 25 μM cholesterol sulfate. The sample was incubated for 24 h at 25 °C before imaging.

sulfate, a considerable amount of negatively charged sulfate ion moieties may still likely to be exposed to face the solvent on the surface of the vesicles.[115] It has been reported that hCT interacts with negatively charged vesicles such as 1-palmitoyl-2-oleoyl-*sn*-glycero-3-phosphoglycerol (POPG) liposomes through electrostatic interactions.[131-132] Here, the negatively charged sulfate moiety at the surface of the cholesterol sulfate vesicles may favorably interact with the positively charged residues of hCT, e.g., Lys18 and partially protonated His20, through electrostatic interactions. It has been reported that the intermolecular electrostatic interactions between the positively charged Lys18 and His20 residues and negatively charged Asp15 can facilitate assembly of hCT in an antiparallel pattern.[46] Altering these interactions affects the fibril elongation rate of hCT.[50] Such electrostatic interactions between Asp15 and Lys18/His20 would be competitively

disrupted by the presence of cholesterol sulfate vesicles. In addition, a favorable π-π stacking interaction between the aromatic residues Phe16 and Phe19 from the adjacent intermolecular strands are also crucial in facilitating amyloid structure formation.[52] Because of their proximity to Lys18 and His20, the π-π stacking interaction may also be interrupted due to the interplay of the positively charged residues of oxidized hCT and the sulfate moiety of the cholesterol sulfate vesicles. Taken together, favorable local electrostatic interactions between the cholesterol sulfate vesicles and oxidized hCT may result in the retardation of hCT fibril formation.

In contrast to cholesterol and cholesterol sulfate, DC-cholesterol shows a much stronger inhibitory effect on the aggregation of hCT. As shown in Figure 9A and 9B below, the presence of DC-cholesterol decreases the maximum fluorescence intensity and dramatically retards the aggregation rate of oxidized hCT in a dose-dependent manner, suggesting its ability to inhibit fibril formation. For example, the maximum fluorescence intensity in hCT aggregation kinetics with 15 μM of DC-cholesterol is only about half of that without DC-cholesterol. The t_{50} value in the presence of 15 μM DC-cholesterol is ~39.5 h, over 10 times larger than that without DC-cholesterol (t_{50} of ~3.3 h) (Figure 9B). The addition of DC-cholesterol with concentrations of 20 μM or higher eliminates the ThT fluorescence, suggesting a strong inhibition activity at these concentrations. It is noteworthy that when DC-cholesterol concentrations are 10 μM or higher, there is a fast increase in ThT intensity within 2 h of incubation which decreases quickly afterward. This may indicate that the early formed aggregation intermediate structures of hCT could also interact with DC-cholesterol and be sequestered by the vesicles.

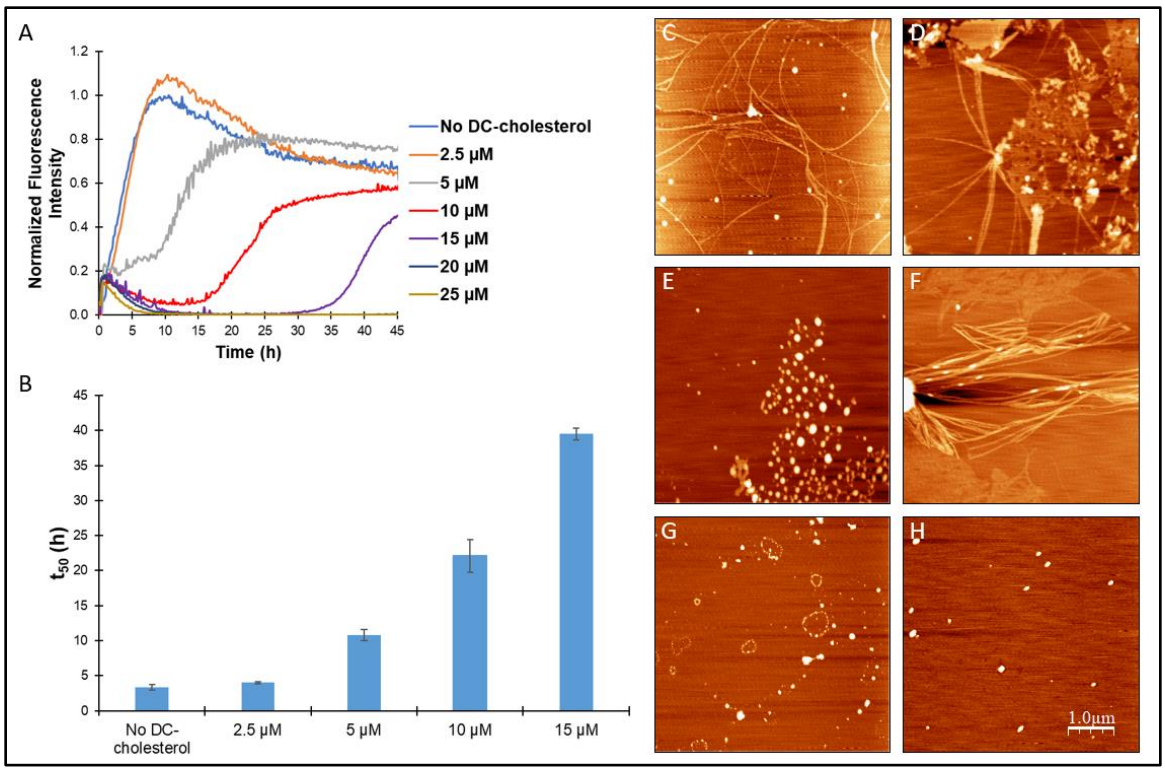

Figure 9. (A) Effect of DC-cholesterol on aggregation kinetics of oxidized hCT (5 µM) in phosphate buffer (5 mM Na phosphate, pH 7.4) at 25 °C. (B) Aggregation half-time (t50) of oxidized hCT in the presence or absence of DC-cholesterol. Data are reported as means ± the standard deviation of triplicate results. (C-H) Tapping mode AFM images of oxidized hCT aggregates (5 µM) in the presence of 2.5 µM (C,D), 15 µM (E,F), or 25 µM (G,H) DC-cholesterol. The samples were incubated quiescently at 25 °C in phosphate buffer (5 mM Na phosphate, pH 7.4) and the images were acquired after 14 h (C, E, G) or 28 h (D, F, H) of incubation.

The inhibitory activity of DC-cholesterol on fibrillogenesis of oxidized hCT was also examined by AFM imaging. In the presence of 2.5 µM DC-cholesterol, the formation of the fibrillar structures is evident after 14 h of incubation (Figure 9C, 9D). When 15 µM DC-cholesterol was added, only amorphous oligomeric aggregates were seen after 14 h of incubation (Figure 9E). The fibrillar structures were observed after 28 h of incubation (Figure 9F). With a higher concentration of 25 µM DC-cholesterol, no fibrils were observed even after 28 h of incubation, with only some spherical intermediate structures presented in the images (Figure 9H). These imaging results are in agreement with the ThT

kinetics results, signifying the inhibitory effect of DC-cholesterol on fibril formation of oxidized hCT.

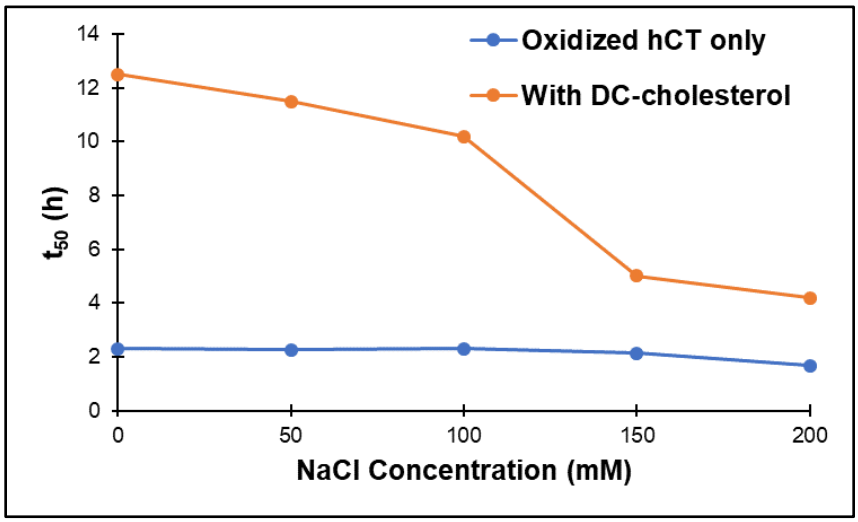

Figure 10. Effect of NaCl on the aggregation half-time (t50) of oxidized hCT (5 μM) in the presence or absence of 5 μM DC-cholesterol with 5 mM phosphate buffer (pH 7.4) at 25 °C. All data reported are a means of triplicate results.

Electrostatic interactions between amyloidogenic proteins and the membrane surface have been commonly considered as critical interactions in the modulating activities of lipid structures on protein aggregation.[131-133] Considering that one of the major structural differences between DC-cholesterol and cholesterol sulfate is their distinct charge moieties, our results may suggest the potential effects of electrostatic interactions in mediating the interplay between the vesicles and the peptide. It has been reported that the DC-cholesterol vesicles contain a positively charged surface at physiological pH,[115] allowing favorable electrostatic interactions with the negatively charged Asp15 in the hCT sequence. To evaluate the role of the electrostatic interactions in the inhibiting activities of DC-cholesterol on hCT aggregation, we studied the effect of DC-cholesterol on hCT aggregation with the addition of different amount of NaCl to increase the ionic strength of solution. As shown in Figure 10 above, the addition of NaCl salt does not significantly

influence the aggregation kinetics of hCT alone. However, the inhibiting activity of DC-cholesterol decreases with increasing concentration of NaCl (Figure 10), suggesting the importance of electrostatic interactions in the interaction of hCT and DC-cholesterol and the inhibiting activity of DC-cholesterol on hCT fibrillogenesis.

To further clarify the inhibitory function of DC-cholesterol on aggregation of oxidized hCT, we conducted hCT aggregation kinetics studies at a high pH of 10.2. The positively charged tertiary amine group of DC-cholesterol has a pKa value of 7.8.[134] At pH 10.2, this tertiary amine group should be mostly deprotonated. This would to a large extent eliminate potential electrostatic interactions between DC-cholesterol and the oxidized hCT peptide. The kinetic results show that the oxidized hCT (5 μM) aggregates with a slightly faster rate at pH 10.2 (t_{50} of ~2 h, Figure 11) compared to that at pH 7.4 (t_{50} of ~3.4 h, Figure 9). Kamihira et al. previously reported that the rate of hCT amyloid fibril formation is slower at acidic pH than at physiological pH.[46] At acidic pH, Lys18 and His20 both contain positive charges on their side chains and face the same side in the β-strand.[50] This would cause strong electrostatic repulsions between the monomeric peptide molecules and thus interfere with their assembly.[50] At physiological pH, only less than 10% of the His20 residue still retains a positive charge on its side chain and therefore the unfavorable electrostatic repulsions will be attenuated. At pH 10.2, the side chain of His20 is completely neutralized, and the side chain of Lys18 is also partially deprotonated. This would further eliminate intermolecular electrostatic repulsions, leading to a faster aggregation rate. Interestingly, the presence of DC-cholesterol under this higher pH condition still shows a remarkable inhibiting activity on amyloid formation of hCT in a concentration-dependent manner. For instance, the addition of 2.5 μM of DC-cholesterol decreases the maximum

ThT fluorescence intensity and delays fibril formation (Figure 11A below), with a t_{50} of ~20 h which is significantly larger than the control peptide without DC-cholesterol (Figure 11B). The presence of 10 µM DC-cholesterol shows stronger inhibiting activity (Figure 11). When 25 µM DC-cholesterol is added, there is no observable ThT fluorescence at the ending time point of the kinetics experiment, suggesting a complete inhibition of hCT fibrillization. In the presence of DC-cholesterol, a fast increasing phase within approximately 2 h followed by decreasing intensity is also observed here, likely due to the inhibition of the elongation of hCT aggregate intermediates which could be further sequestered by the DC-cholesterol vesicles.

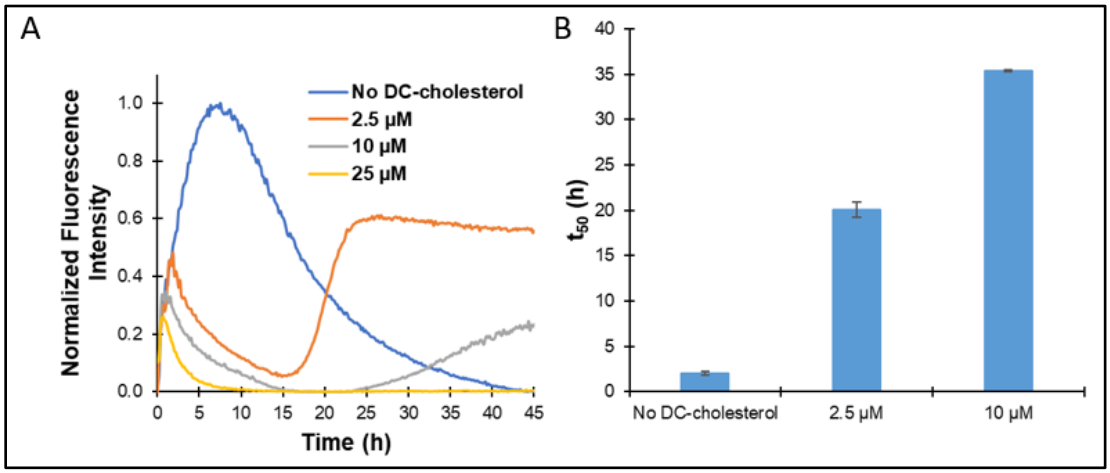

Figure 11. (A) Effect of DC-cholesterol on aggregation kinetics of oxidized hCT (5 µM) in 5 mM carbonate buffer (pH 10.2) at 25 °C. (B) Aggregation half-time (t50) of oxidized hCT in the presence or absence of DC-cholesterol at pH 10.2. Data are reported as means ± the standard deviation of triplicate results.

Our results at high pH show that DC-cholesterol is still an effective inhibitor of hCT aggregation even when the positive charge on the tertiary amine of DC-cholesterol is neutralized. This suggests that electrostatic interactions appear not to be the only major force that determines the inhibiting function of DC-cholesterol vesicles on hCT fibrillization. It has been well recognized that the intermolecular hydrogen bonding

network is critical in the formation and stabilization of the characteristic cross-β-sheet structure in protein amyloid fibrils.[47, 135] Note that DC-cholesterol contains a carbamoyl group that is able to form hydrogen bonds.[136] Therefore, DC-cholesterol may interact with hCT through hydrogen bonding between the carbamoyl group in DC-cholesterol and the backbone and/or side chains of the peptide, thus interfering with amyloid formation. Moreover, at higher pH, the neutralized tertiary amine in DC-cholesterol may also interact

	pH	Concentration (μM)	Diameter (nm)
Cholesterol	7.4	2.5 10 25	78 ± 15 85 ± 1 61 ± 7
	10.2	2.5 10 25	242 ± 5 231 ± 9 223 ± 11
Cholesterol Sulfate	7.4	2.5 10 25	116 ± 9 162 ± 7 404 ± 10
	10.2	2.5 10 25	200 ± 16 263 ± 22 416 ± 21
DC-cholesterol	7.4	2.5 10 25	270 ± 43 249 ± 15 190 ± 3
	10.2	2.5 10 25	117 ± 3 98 ± 3 100 ± 0.8

Table 1. Size of the vesicles of cholesterol and its derivatives formed at different concentrations and pH values. The sizes were determined by dynamic light scattering.

with the peptide as a hydrogen bond acceptor. Consequently, an acceptor-donor-acceptor hydrogen bond pattern would form between the tertiary amine and the carbamoyl group of DC-cholesterol. It has been reported that a group of molecules with a similar hydrogen bond pattern can form favorable multipoint hydrogen bonding interactions with Aβ peptide and inhibit fibril formation of Aβ.[137-138] In addition, although the interaction details of DC-cholesterol and hCT at molecular level are not available, it is conceivable that van der Waals interactions may also be a factor of the interplay between hCT and DC-cholesterol,

contributing to the inhibiting activity of hCT amyloidogenesis. Furthermore, it has been evidenced that the size and curvature properties of the liposome vesicles are crucial factors in determining the binding of the vesicles and amyloidogenic proteins.[108, 139] Elbassal et al. reported that the DC-cholesterol vesicle diameter decreases as the concentration increases.[115] Our results show a similar concentration-dependent DC-cholesterol vesicle size change at physiological pH as shown in Table 1 above. At a high pH of 10.2, the size of DC-cholesterol vesicles formed at different concentrations becomes less variant, with a diameter of approximately 100-120 nm (Table 1). Since the diameter of DC-cholesterol vesicles formed at pH of 10.2 is about half of the smallest vesicle size formed at physiological pH, this structural difference should be taken into consideration when comparing the inhibiting activity of DC-cholesterol under different pH environments. Nonetheless, the binding of the hCT peptide on the surface of a large amount of these small vesicles will significantly reduce the concentration of monomeric hCT in solution. This would possibly lead to retardance or complete inhibition of critical nucleus formation, as well as fibril growth and elongation. In addition, the size of cholesterol and cholesterol sulfate vesicles are also sensitive to pH (Table 1). The aggregation kinetics results showed that cholesterol and cholesterol sulfate exhibit little effect on the aggregation of oxidized hCT at pH 10.2 (Figure 12 below), similar to that at pH 7.4, suggesting the weak sensitivity of their influence on hCT amyloid formation to the particle size and pH conditions.

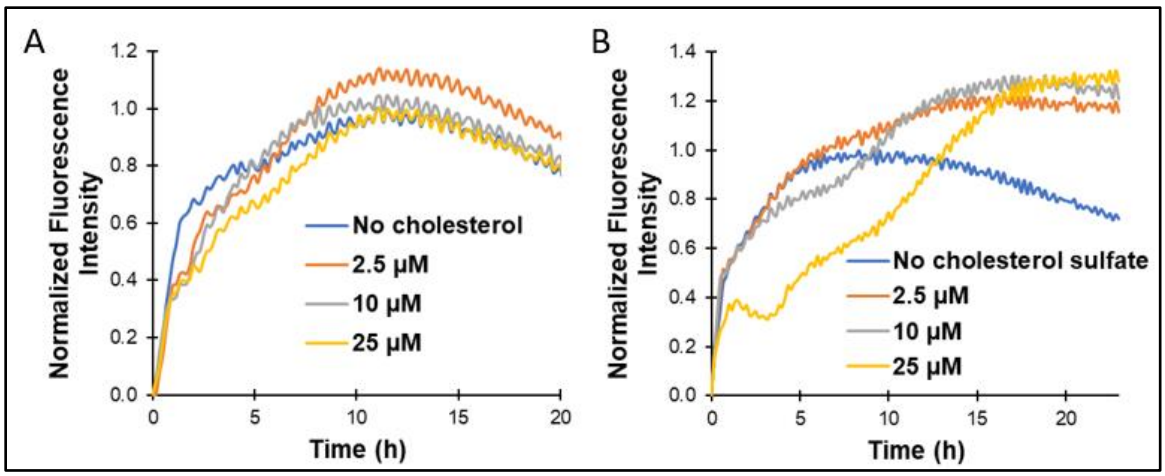

Figure 12. (A) Effect of cholesterol on aggregation kinetics of oxidized hCT (5 µM) in 5 mM carbonate buffer (pH 10.2) at 25 °C. (B) Effect of cholesterol sulfate on aggregation kinetics of oxidized hCT (5 µM) in 5 mM carbonate buffer (pH 10.2) at 25 °C.

2.4 Conclusions

In conclusion, we report the mechanistic effect of the disulfide bond formed at the N-terminal region of hCT in modulating the aggregation characteristics of hCT. Our results indicate that the presence of the disulfide bond in the peptide plays a crucial role in forming the critical nucleus needed for fibril formation. Furthermore, we report for the first time the effects of cholesterol, cholesterol sulfate and DC-cholesterol on the amyloid formation of oxidized hCT. Our results demonstrate that cholesterol does not affect fibrillogenesis of oxidized hCT dramatically, whereas high concentrations of cholesterol sulfate show a moderate inhibiting activity on the aggregation of hCT. Moreover, our results show that DC-cholesterol strongly inhibits the amyloidogenesis of oxidized hCT at both physiological and basic pH conditions. These studies imply the importance of electrostatic and hydrogen bonding interactions, possibly in combination with van der Waals forces, in mediating the interplay of hCT and DC-cholesterol vesicles and the inhibiting function of DC-cholesterol on hCT fibrillization. These findings provide new insights into the mechanistic effects of cholesterol and the derivatives on hCT amyloid formation. Our

studies may also illuminate the future design of novel steroid-based molecular structures for inhibiting hCT aggregation.

CHAPTER III: FLAVONOIDS WITH VICINAL HYDROXYL GROUPS INHIBIT HUMAN CALCITONIN AMYLOID FORMATION

This chapter was adapted from the following publication

> Lantz, R., Busbee, B., Wojcikiewicz, E. P., and Du, D. (2020) Flavonoids with Vicinal Hydroxyl Groups Inhibit Human Calcitonin Amyloid Formation. *Chem. Eur. J.* 10.1002/chem.202002027

3.1 Introduction

Human calcitonin (hCT) is a 32-residue polypeptide hormone produced by the parafollicular cells of the thyroid gland.[11] It plays a regulatory role in calcium-phosphorus metabolism and skeletal bone formation.[10-11] Therefore, hCT injections were once used as a therapeutic treatment for bone-related disorders such as osteoporosis, hypercalcemia, and Paget's disease.[29] However, hCT has a tendency to self-associate and form amyloid fibrils which may cause cellular toxicity.[19, 21] The elevated production and subsequent amyloid deposition of hCT has been found to be associated with medullary thyroid carcinoma.[11] Due to its high aggregation propensity, hCT injections are no longer used as a therapeutic treatment for bone disorders.[29, 31] Instead, a different species of calcitonin, salmon calcitonin (sCT) is utilized because of its considerably lower tendency to form amyloid fibrils.[12, 31-32] Unfortunately, the use of sCT is accompanied by potential side effects such as vomiting, anorexia, and unwanted immune responses.[33-36] It has been reported that hCT exhibits a higher potency of preventing osteoclast bone resorption than sCT when hCT fibrillation is avoided, making it a superior treatment for bone-related disorders.[140] Hence, developing effective inhibition strategies against hCT amyloidogenesis is of considerable

importance for treating hCT fibrillization related diseases and the therapeutic applications of hCT as an effective drug for bone-related disorders.

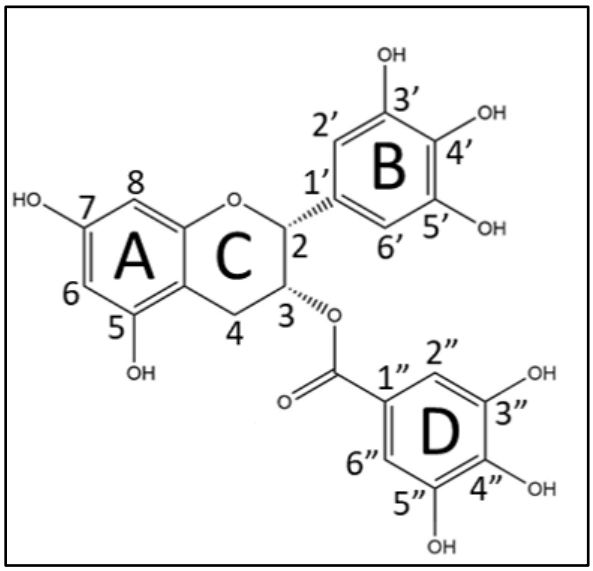

Figure 13. Structure of EGCG with carbons labeled.

A large number of small molecules have been reported as inhibitors of the amyloid formation of aggregation-prone proteins.[141-143] One class of these molecular inhibitors is polyphenols which contain multiple phenol units and are known to often carry antioxidant and anticancer activities.[144] Polyphenols are found to be abundant in a wide variety of fruits, vegetables, and beverages including wine and tea. A variety of polyphenols have been found to inhibit fibril formation of amyloidogenic proteins such as α-synuclein, amyloid-β (Aβ), prion, tau, and islet amyloid polypeptide (IAPP).[145] So far, however, there have been very few polyphenol-based molecules reported as inhibitors of hCT aggregation.[48, 85, 146] Among these is epigallocatechin-3-gallate (EGCG), a polyphenol that belongs to the flavonoid family and makes up 50-80% of all the polyphenols in green tea.[147] The abundance of polyphenols in green tea has been suggested to be associated with many health benefits including neuroprotective, antioxidant, anti-inflammatory, and anti-

carcinogenic effects.[148] EGCG has been found to be capable of preventing fibril formation of a variety of amyloidogenic proteins including hCT.[48, 86, 89-90, 149] However, the inhibiting mechanism of EGCG in protein amyloid formation is not fully clear. EGCG's base structure contains three phenyl rings (A, B, and D) and a heterocyclic ring (C) (Figure 13 above). The B-ring contains a vicinal trihydroxyl structure and the D-ring is composed of a gallic acid moiety with a vicinal trihydroxyl structure. It is known that these trihydroxyl groups of EGCG can auto-oxidize to form quinones under neutral or alkaline pH.[149] The formed quinone structures may further react with free SH groups in cysteine, or form

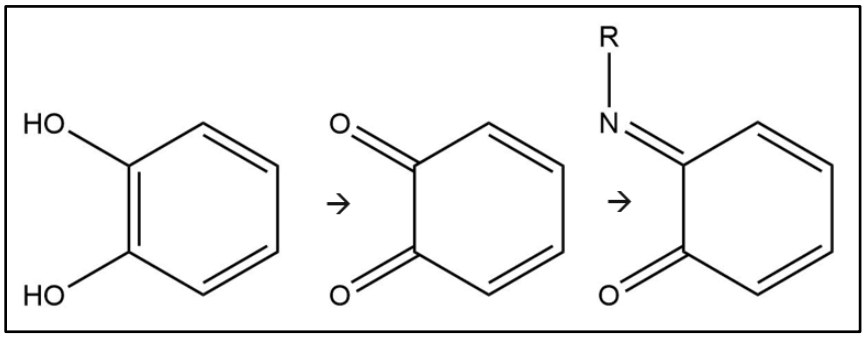

Figure 14. Schematic representation of the formation of quinone and the subsequent Schiff base formation between quinone and selected amino acids such as lysine or arginine.

covalent bonds with lysine, histidine, or arginine residues to produce adducts like Schiff base (Figure 14 above).[89, 149-150] It has been suggested that the oxidized EGCG is able to covalently bind with amyloidogenic proteins such as lysozyme which results in amyloid inhibition.[151] However, this is still under debate as it has also been reported that Schiff base formation may occur but may not be necessary for amyloid inhibition activity.[89, 149] Alternatively, it has also been suggested that hydrogen bonding and/or aromatic interactions may be actively involved in the amyloid inhibiting function of EGCG.[89, 91] Regarding hCT, it has been reported that EGCG may inhibit hCT fibrillization by interacting with the aromatic residues Tyr12, Phe16, and Phe22 which are known to be

crucial in the formation and stabilization of the fibrillar structure of hCT.[48, 52] Identifying the molecular mechanism of EGCG and other polyphenols in inhibiting hCT amyloid formation will illuminate novel strategies for the development of effective inhibitors of hCT amyloid formation. In this study, we investigated the hCT amyloid inhibition activities of a group of polyphenols, most with flavonoid skeletons, and assessed the structural features of the effective polyphenol inhibitors that may be crucial for the amyloid inhibiting function.

3.2 Materials and Methods

3.2.1 Materials

All chemical reagents were purchased from commercial suppliers and used without further purification. Epigallocatechin-3-gallate (EGCG), epigallocatechin (EGC), epicatechin gallate (ECG), pyrogallol (Pyro), gallic acid (GA), 3-hydroxybenzoic acid (3-HBA), 3,4-hydroxybenzoic acid (3,4-HBA), 3,5-hydroxybenzoic acid (3,5-HBA), flavone (Fla), 5-hydroxyflavone (5-HF), 6-hydroxyflavone (6-HF), 7-hydroxyflavone (7-HF), naringenin (Nar), quercetin (Quer), myricetin (Myr), luteolin (Lut), baicalein (Baic), rosmarinic acid (RA), and resveratrol (Resv) were purchased from Sigma Aldrich. 3-HBA, 3,4-HBA, and 3,5-HBA were prepared by dissolving the compound powder in water. All other compounds were dissolved in dimethyl sulfoxide (DMSO).

3.2.2 Synthesis and Preparation of hCT

The hCT peptide was synthesized on a PS3 solid-phase peptide synthesizer (Protein Technologies Inc., Woburn, MA) using the appropriate Fmoc protected amino acids. The hCT peptide was cleaved from the resin, purified by reversed phase high-performance liquid chromatography (RP-HPLC) utilizing a C18 column, and lyophilized until further

use. The molecular weight of the peptide was confirmed with matrix-assisted laser desorption ionization (MALDI) mass spectrometry. Air oxidation was used to form the hCT disulfide bond as previously described.[58] Briefly, hCT was dissolved under dilute conditions in 6 M urea (pH 8.1) to prevent fibrillization.[48, 118] The solution was incubated overnight with air bubbling to form the disulfide bond between Cys1 and Cys7. An Ellman test was utilized to confirm disulfide bond formation and MALDI mass spectrometry was performed to ensure that no intermolecular disulfide bond formation occurred.[119] The oxidized hCT peptide was further purified by HPLC and subsequently lyophilized to form dry white powder. The peptide was then dissolved in hexafluoroisopropanol (HFIP), sonicated for 5 min, and quiescently incubated on ice for 1 h to ensure monomerization. The HFIP-peptide solution was pipetted into centrifuge tubes each containing ~50 µL of the solution. The caps were left open and a stream of air was used to evaporate off the HFIP. To ensure the evaporation of the HFIP, the samples were stored in a vacuum desiccator overnight. The resulting clear crystals/film was stored at -80 °C until further use. For all of the assays, oxidized and monomerized hCT peptide solutions were prepared by dissolving in 5 mM sodium phosphate buffer (pH 7.4) and the concentration was determined by UV absorbance at 275 nm ($\varepsilon = 1531\ cm^{-1}\ M^{-1}$).[120]

3.2.3 Aggregation Kinetics by ThT Fluorescence

The aggregation kinetics of hCT, without or with additional small molecules, was prepared with 5 µM oxidized hCT, 5 mM sodium phosphate buffer (pH 7.4) and 20 µM ThT dye. 3-HBA, 3,4-HBA, and 3,5-HBA were dissolved in water and all of the other compounds were dissolved in DMSO to prepare 10 mM stock solutions, respectively. Additional dilutions were applied to make stock solutions with different concentrations. A

particular amount of stock solutions was then added to the peptide solution to make a solution with 5 μM hCT, 20 μM ThT and 5 mM sodium phosphate buffer (pH 7.4). For the assays that contained DMSO, all of the solutions contained the same volume of DMSO to ensure consistency. 100 μL of solution was pipetted into each well of a 96-well microplate (Costar black, clear-bottom). The microplate was capped with a cover and sealed with para-film. The plate was then loaded into a Gemini SpectraMax EM fluorescence plate reader (Molecular Devices, Sunnyvale, California). The ThT fluorescence was measured every 10 min after shaking for 5 sec with an excitation wavelength of 440 nm and an emission of 480 nm at 25 °C for 22-24 h. All fluorescence kinetics data are reported as a means of triplicate results.

3.2.4 Atomic Force Microscopy

15-20 μL of hCT without or with the small molecules were taken directly from the aggregation kinetics assay (after incubating for 22-24 h) and were adsorbed onto the surface of freshly cleaved mica (5 × 5 mm). The samples were covered and left to dry overnight. AFM imaging of the samples was acquired in tapping mode using the Asylum Research MFP-3D-BIO AFM system with MikroMasch NSC15/Al BS cantilevers.

3.3 Results and Discussion

3.3.1 Inhibitory Effect of EGCG Analogues on hCT Amyloidogenesis

The aggregation kinetics of hCT (5 μM) with differing concentrations of EGCG in phosphate buffer (5 mM sodium phosphate, pH 7.4) was monitored using the fluorescence of thioflavin T (ThT). ThT selectively binds to the amyloid fibrillar structure, leading to an increase in the fluorescence intensity in the vicinity of 480 nm.[95, 123-124] As shown in Figure 15A below, the aggregation kinetics of hCT shows a fast increase in fluorescence intensity

until it reaches maximum intensity at ~9 h. This result is in accordance with previous reports indicating rapid hCT amyloid formation.[31, 53, 58] Notably, after reaching the

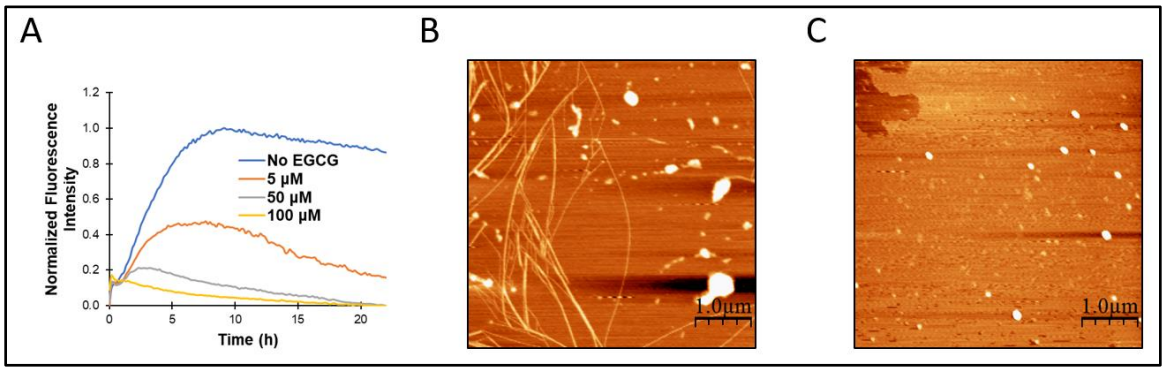

Figure 15. (A) Effect of EGCG on aggregation kinetics of hCT (5 μM) followed by ThT fluorescence in sodium phosphate buffer (5 mM, pH 7.4) at 25 °C. (B and C) Tapping mode AFM images of hCT (5μM) in the absence (B) or the presence (C) of 100 μM EGCG. The samples were incubated for 22-24 h at 25 °C before imaging.

maximum, the fluorescence intensity slowly declines over time. This is consistent with other reports where the decrease of the signal is likely attributed to the precipitation of hCT aggregates over the incubation period.[58, 99] When 5 μM EGCG is added, there is a ~50% decrease in the maximum ThT fluorescence intensity compared to that of hCT only (Figure 15A). In the presence of 50 μM EGCG, the maximum fluorescence intensity is reduced by ~80%. Treatment with 100 μM EGCG results in negligible ThT fluorescence over the period of measurement, indicating a strong inhibition of hCT fibril formation. The morphology of the aggregates of hCT without or with EGCG was further assessed by atomic force microscopy (AFM) imaging. As shown in Figure 15B, hCT aggregated and formed long, thin and stacked fibrillar configurations. When hCT was incubated with 100 μM EGCG, no fibrillar structures were observed (Figure 15C). Instead, only some spherical oligomeric aggregates were seen. Overall, these results are consistent with previous

findings that EGCG is an effective inhibitor of hCT amyloid fibril formation.[48]

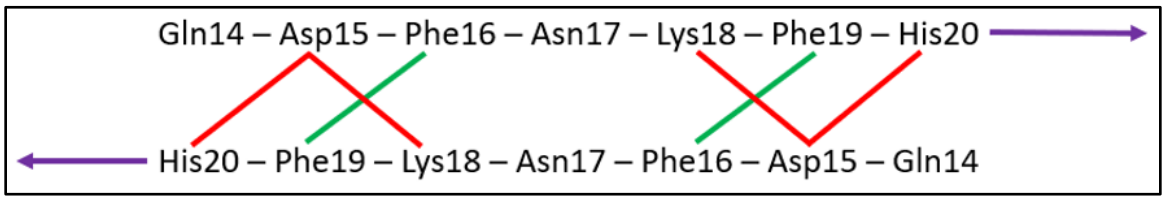

Figure 16. Plausible interstrand aromatic (green line) and electrostatic (red line) interactions between the adjacent monomeric strands in the antiparallel β-sheet structure of hCT amyloids.

A recent 2D nuclear magnetic resonance (NMR) study of Huang et al. showed that EGCG binds largely to the central and C-terminus regions of the hCT peptide.[48] Their results suggest the formation of favorable π-π stacking interactions between the aromatic rings of EGCG and the side chains of the aromatic residues in hCT.[48] It has been reported that intermolecular interactions between the aromatic residues, e.g., Phe16 and Phe19 (Figure 16 above) from the adjacent strands in the antiparallel β-sheet structure of hCT amyloids, play an important role in fibril formation of hCT, and disrupting such interactions can significantly affect the formation and stability of the aggregated structures.[52, 75] On the other hand, EGCG has also been indicated to undergo auto-oxidation to form superoxides and quinones.[152-153] Palhano et al. demonstrated that EGCG is fully oxidized after an incubation period of 6 h in pH 7.4 phosphate buffer at 25 °C.[149] Oxidized EGCG may covalently bind to the peptide via Schiff base formation and/or reaction with sulfhydryl groups in cysteine residues.[88, 149, 154] hCT contains cysteine residues at positions 1 and 7. However, the peptide used in this study was oxidized to form an intramolecular disulfide bond between Cys1 and Cys7, and there is no free SH group available in hCT to react with the oxidized EGCG structure. Nevertheless, hCT contains Lys18 and His20 residues in the central region of the sequence which may form covalent adducts such as

Schiff base with EGCG. These residues have been reported to be critical in the formation and stabilization of hCT amyloid fibrils by forming electrostatic interactions with the Asp15 residue on the adjacent monomeric chain in the β-sheet structure of hCT fibrils (Figure 16).[46, 50] In addition, these residues are in close proximity to the Phe16 and Phe19 aromatic residues. If the covalent linkage were to form on the lysine or histidine residues, it might potentially interfere with both the electrostatic and aromatic interactions that are critical for fibril formation. To identify the covalent linkage of EGCG and hCT peptide, the hCT (5 μM) sample incubated with 100 μM EGCG overnight was examined using matrix assisted laser desorption ionization (MALDI). The results do not show an observable mass signal corresponding to the covalent adduct of hCT and the oxidized EGCG (data not shown). Palhano et al. previously reported that the products between Aβ40 and EGCG likely form high molecular weight cross-linked aggregates that could not be volatilized with MALDI.[149] Therefore, our current results could not rule out the possibility of covalent bond formation that may be responsible for the amyloid inhibiting function of EGCG. Furthermore, it has been suggested that EGCG can form nonspecific interactions with the backbone and/or side chains of α-synuclein, IAPP, and Aβ via hydrogen bonding.[86, 90-91] Shaham-Niv et al. reported that EGCG can also affect both early and later stages of metabolite fibril self-assembly through inhibitor-metabolite interactions possibly including hydrogen bonding interaction.[155] In this regard, nonspecific hydrogen bonding interactions between EGCG and hCT may also contribute to the inhibiting function of EGCG on hCT fibrillization.

In order to investigate the structural features that are crucial for the inhibition function of EGCG, we studied two flavanol analogues of EGCG, epicatechin gallate (ECG)

and epigallocatechin (EGC). ECG does not contain a trihydroxyl group on the B-ring, and instead possesses a catechol moiety (3',4'-OH on the B-ring, Figure 17A). EGC lacks the

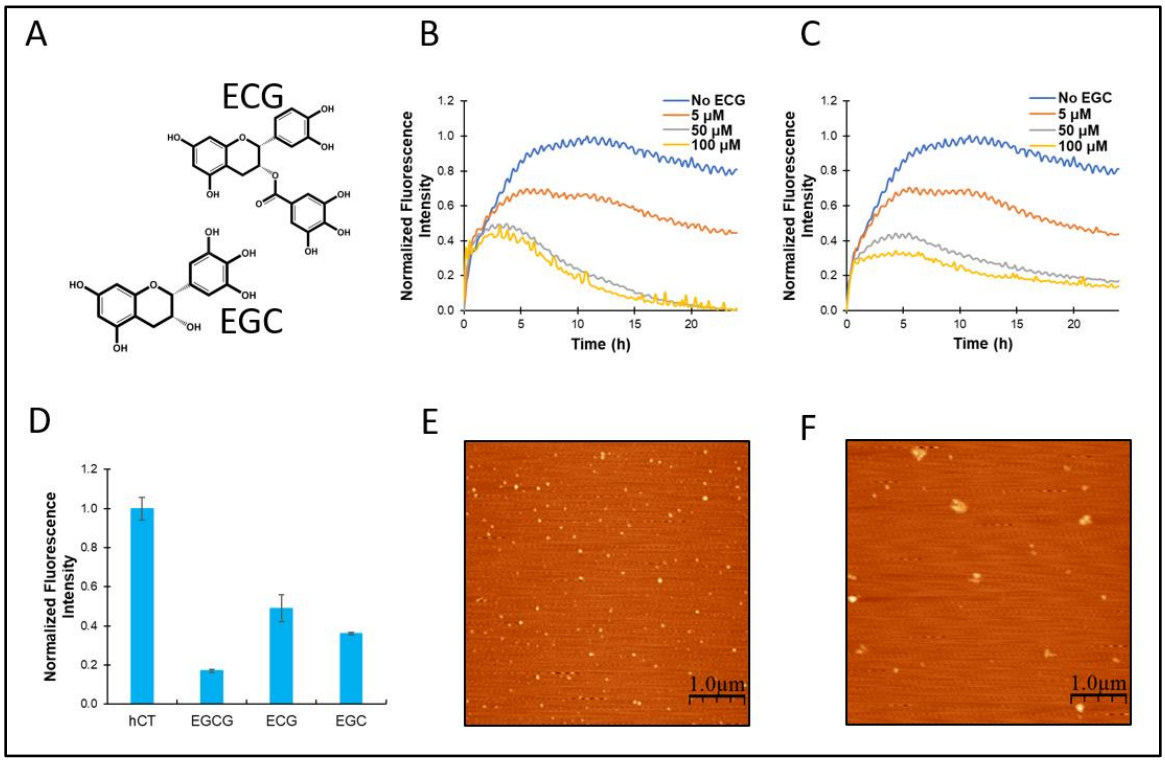

Figure 17. (A) Chemical structures of ECG and EGC. (B-C) Effect of ECG (B) or EGC (C) on the aggregation kinetics of hCT (5 μM) followed by ThT fluorescence in sodium phosphate buffer (5 mM, pH 7.4) at 25 °C. (G) Normalized maximum ThT fluorescence intensity in the aggregation of hCT in the absence or the presence of 100 μM EGCG, ECG, or EGC. Data are reported as means ± standard deviation (SD) of triplicate results. (E-F) Tapping mode AFM images of hCT (5 μM) in the presence of 100 μM ECG (E) or 100 μM EGC (F). The samples were incubated in sodium phosphate buffer (5 mM, pH 7.4) at 25 °C for 24 h before imaging.

gallate moiety compared to EGCG (Figure 17A). Both compounds are also found in green tea but in less abundance than EGCG.[88] ECG has been found to be a potent amyloid inhibitor for Aβ while a less potent inhibitor for IAPP compared to EGCG.[90, 156] In contrast, EGC is much less effective in inhibiting aggregation of IAPP and Aβ, implying that the gallate moiety is critical in the inhibition of these amyloids.[90, 156] Our results show that the addition of ECG or EGC leads to the decrease of the maximum ThT fluorescence intensity

in hCT aggregation in a dose-dependent manner (Figures 17B and 17C), suggesting that both are able to inhibit fibril formation of hCT. Nevertheless, the decrease in ThT fluorescence with ECG or EGC is not as dramatic as that with EGCG (Figure 17D). When hCT is incubated with 100 μM EGCG, the maximum fluorescence intensity falls by ~83%. When 100 μM ECG or EGC is applied, the fluorescence intensity falls by ~50% for ECG and ~65% for EGC, respectively. These results are consistent with the report of Cao and Raleigh that ECG and EGC are less effective inhibitors of IAPP compared to EGCG.[90] In addition, our results indicate that removal of the hydroxyl group at the 5′ position of the B-ring (ECG) impairs the inhibiting function of the compound more significantly than elimination of the gallate moiety (EGC) (Figure 17D). Nonetheless, the AFM imaging of hCT incubated with either ECG or EGC does not indicate amyloid fibril formation; only spherical oligomeric aggregates were identified (Figures 17E and 17F). Taken together, these results demonstrate that ECG and EGC are also effective inhibitors of hCT amyloid formation.

To further evaluate the impact of the gallate moiety of EGCG in hCT amyloid inhibition, we tested the effect of gallic acid (GA) and a series of GA derivatives (Figure 18A below) on hCT aggregation. Neither 3-hydroxybenzoic acid (3-HBA) or 3,5-hydroxybenzoic acid (3,5-HBA) shows an appreciable influence on the aggregation of hCT (Figure 18B). The maximum ThT fluorescence intensity of hCT drops ~25% in the presence of 100 μM 3,4-hydroxybenzoic acid (3,4-HBA) (Figure 18B). The AFM imaging exhibits that amyloid fibrils still formed steadily after incubating hCT with 100 μM 3,4-

HBA or GA (Figures 18C and 18D). Taken together, these results show that these

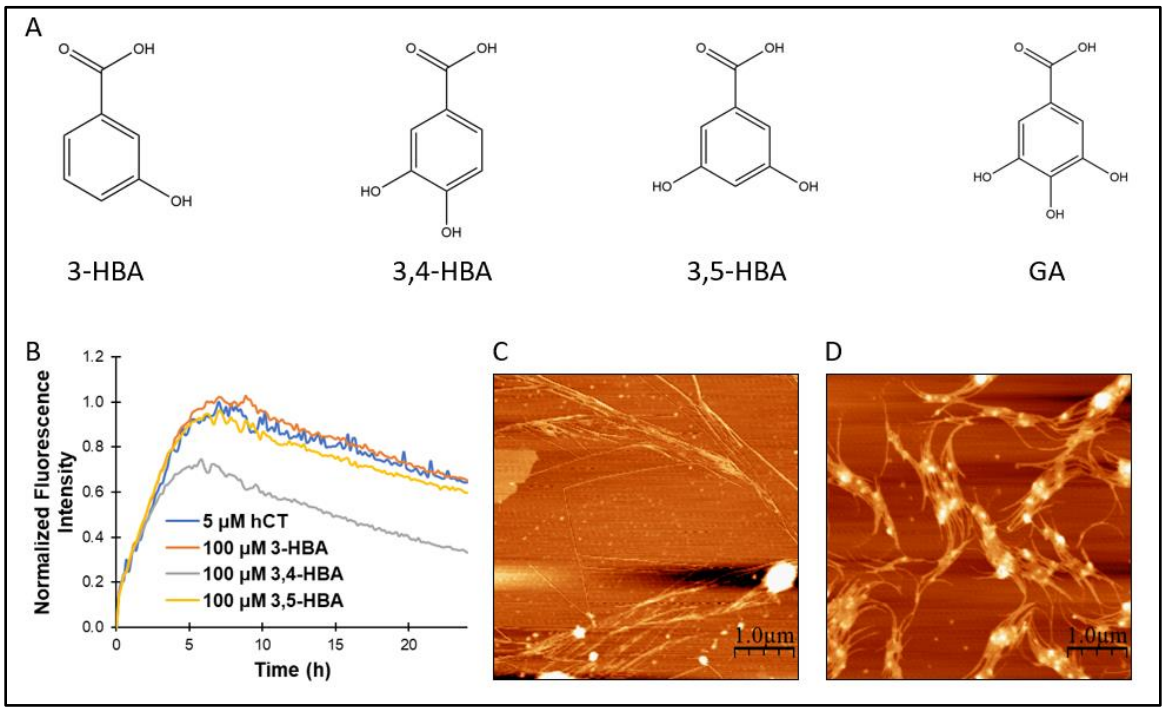

Figure 18. (A) Chemical structures of 3-HBA, 3,4-HBA, 3,5-HBA, and GA. (B) Aggregation kinetics of hCT (5 μM) in the absence or presence of 100 μM 3-HBA, 3,4-HBA, or 3,5-HBA measured by ThT fluorescence in sodium phosphate buffer (5 mM, pH 7.4) at 25 °C. (C-D) Tapping mode AFM images of hCT (5 μM)) in the presence of 100 μM 3,4-HBA (C) or 100 μM GA (D). The samples were incubated in sodium phosphate buffer (5 mM, pH 7.4) at 25 °C for 24 h before imaging.

compounds are not efficient inhibitors of hCT amyloid formation. This is consistent with the aforementioned result that removal of the gallate moiety in EGCG does not significantly weaken the amyloid inhibiting activity of the molecule. It is noteworthy that 3,4-HBA and GA both contain vicinal hydroxyl groups on the benzene ring with the potential to be oxidized and covalently linked to lysine or histidine residues in hCT to form adducts like Schiff base. Meanwhile, these compounds also contain a carboxylic acid group on the benzene ring. It is possible that the negatively charged carboxylic acid group under physiological conditions may form transient electrostatic interactions with Lys18 or His20 of hCT and thus hinder the covalent bond formation of the compound with the peptide.

Interestingly, methyl gallate, a molecule that has a similar structure to the gallate moiety of EGCG, is also a weak inhibitor of Aβ amyloid formation,[80] in accordance with our results.

3.3.2 Effect of the Vicinal Hydroxyl Groups in Flavonoids on hCT Amyloid Formation

To identify the roles of the aromatic skeletons and hydroxyl groups of flavonoids in hCT amyloid inhibition, we studied a group of flavone molecules that contain a similar base structure to EGCG without or with a hydroxyl group at different positions. Flavones

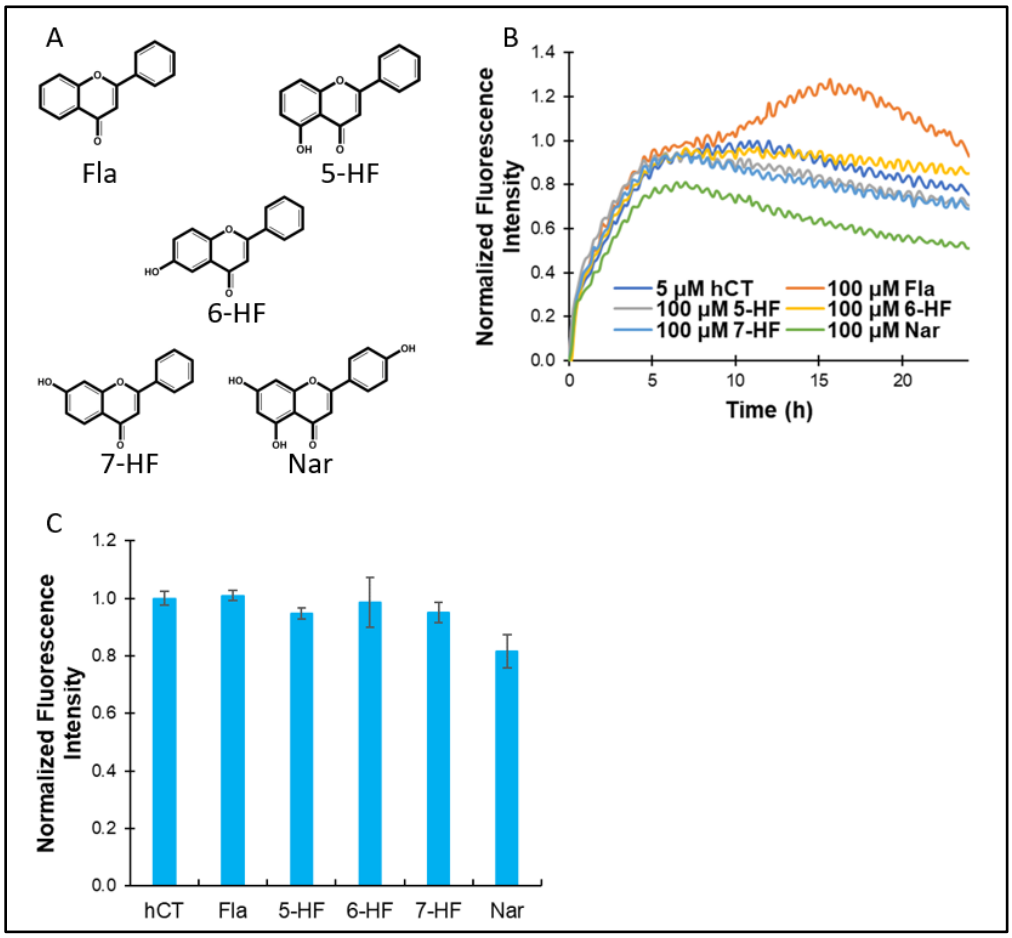

Figure 19. Chemical structures of Fla, 5-HF, 6-HF, 7-HF, and Nar. (B) Aggregation kinetics of hCT (5 μM) in the absence or presence of 100 μM Fla, 5-HF, 6-HF, 7-HF, or Nar measured by ThT fluorescence in sodium phosphate buffer (5 mM, pH 7.4) at 25 °C. (C) Comparison of the maximum ThT fluorescence intensity in the aggregation of hCT (5 μM) in the absence or the presence of 100 μM Fla, 5-HF, 6-HF, 7-HF, or Nar. Data are reported as means ± SD of triplicate results.

are a class of flavonoids most of which can be readily found in tea, citrus fruits, berries, red wine, apples, and legumes.[157] The base structure of the flavone (Fla) molecule contains two phenyl rings and a heterocyclic ring similar to that of EGCG (Figure 19A above). As shown in Figures 19B and 19C, Fla does not show a noticeable effect on the aggregation of hCT. Since there is no hydroxyl group in Fla, aromatic interactions would be speculated to play a major role in the interplay between Fla and the peptide. Nonetheless, the carbonyl group on the heterocyclic ring may be involved in hydrogen bonding and possibly Schiff base formation. However, it should be noted that most Schiff base reactions with aldehydes or ketones require acidic pH conditions.[158] Our results indicate that the interactions between the scaffold aromatic structure of flavone and hCT are not sufficient for inhibiting the peptide amyloid formation. These results are also consistent with the report of Malisauskas et al. that Fla does not influence the rate of human insulin fibril formation.[159] Addition of a hydroxyl group at the 5-, 6-, or 7-position of the A-ring of flavone (5-hydroxyflavone (5-HF), 6-hydroxyflavone (6-HF), and 7-hydroxyflavone (7-HF), Figure 19A) does not improve the inhibition activity of the molecule on hCT aggregation (Figures 19B and 19C). These compounds have been previously reported to be ineffective at inhibiting the aggregation of amylin or human insulin as well.[159-160]

On the other hand, a flavanone molecule naringenin (Nar) that contains two non-vicinal hydroxyl groups on the A-ring and one hydroxyl group on the B-ring (Figure 19A), shows a mild effect on hCT aggregation. A ~19% drop in ThT fluorescence intensity was observed with Nar compared to hCT alone (Figures 19B and 19C). Nar has been found to be able to inhibit Aβ amyloid-induced mitochondrial dysfunction.[80] However, Velander et al. reported that this compound is not effective at inhibiting amylin amyloid formation.[160]

As Nar contains three non-adjacent hydroxyl groups, the formation of hydrogen bonding interactions of Nar and the backbone and/or sidechains of hCT may putatively account for its mild inhibitory effect on hCT fibrillization.

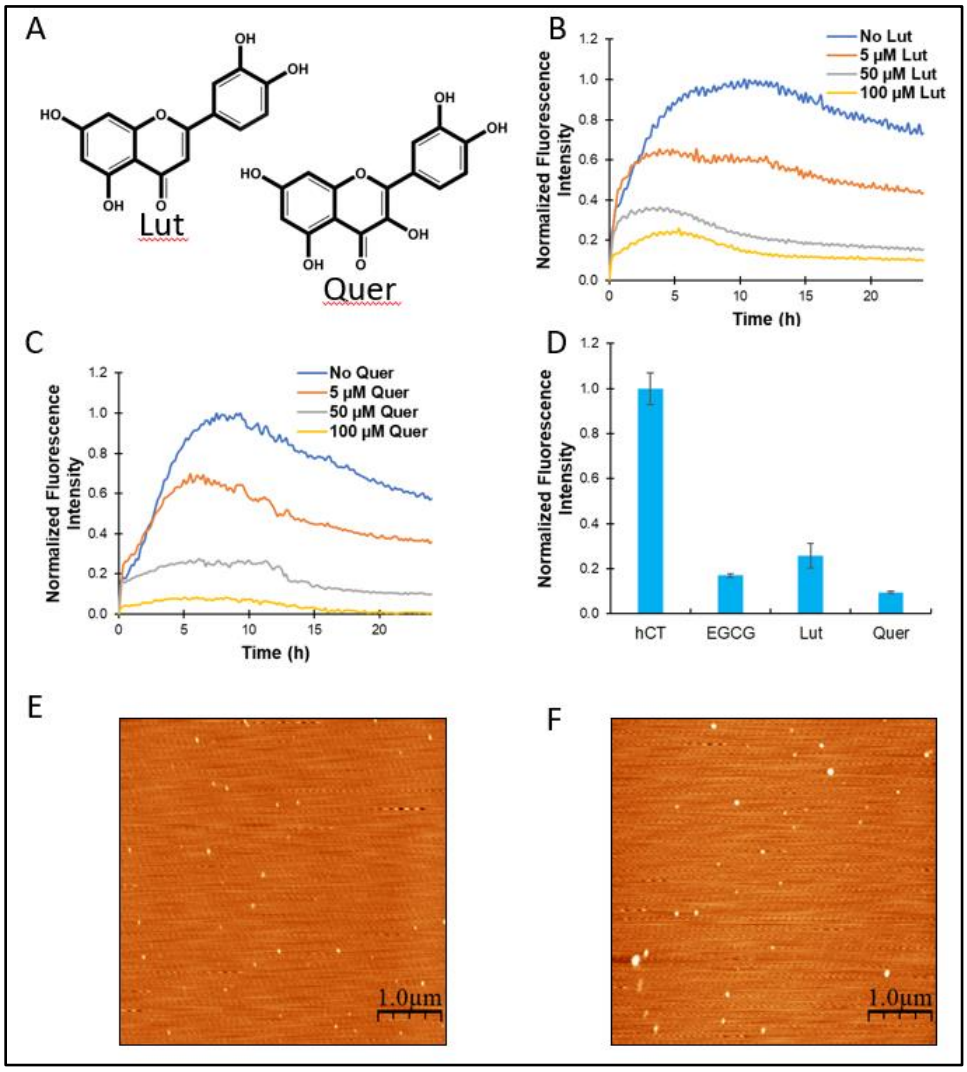

Figure 20. (A) Chemical structures of Lut and Quer. (B-C) Effect of Lut (B) or Quer (C) on the aggregation kinetics of hCT (5 μM) followed by ThT fluorescence in sodium phosphate buffer (5 mM, pH 7.4) at 25 °C. (D) Normalized maximum ThT fluorescence intensity in the aggregation of hCT in the absence or the presence of the flavonoid molecules (100 μM). Data are reported as means ± SD of triplicate results. (E-F) Tapping mode AFM images of hCT (5 μM) in the presence of 100 μM Lut (E) or 100 μM Quer (F). The samples were incubated in sodium phosphate buffer (5 mM, pH 7.4) at 25 °C for 24 h before imaging.

Next, we studied two flavonoid molecules, luteolin (Lut) and quercetin (Quer) that contain adjacent hydroxyl groups on the same benzene ring (Figure 20A above). Lut contains 4 hydroxyl groups, with two vicinal hydroxyls located on the 3' and 4' position of the B-ring. Lut is found in different dietary sources including chamomile tea, carrots, broccoli, celery, green pepper, and olive oil.[161-162] Lut has been recognized to be antiangiogenic and inhibit Aβ and insulin amyloidogenesis.[80, 159, 163] Compared to Lut, Quer contains one additional hydroxyl group at the C-3 position of the C-ring. Quer is found in red onions, apples, berries, grapes, tea, tomatoes, and other dietary sources.[164] Quer has been reported to possess strong anti-inflammatory effects and inhibit insulin fibril formation and destabilize the mature fibrils.[163-165] As shown in Figure 20B, Lut shows an efficient inhibitory activity on hCT amyloidogenesis in a dose-dependent manner. In the presence of 5 μM Lut, the maximum ThT fluorescence intensity decreases by ~40% compared to that of hCT only (Figure 20B). When 50 μM and 100 μM of Lut is added, the maximum ThT fluorescence intensity decreased by ~65% and ~75%, respectively. Quer also significantly interferes with the fibril formation of hCT and exhibits a slightly stronger inhibitory effect compared to Lut and EGCG at higher concentrations (Figures 20C and 20D). The ThT fluorescence trace of hCT aggregation is nearly flat in the presence of 100 μM Quer, implying an almost complete inhibition of the amyloid formation of hCT (Figure 20C). Only a few spherical oligomeric aggregates were observed in AFM imaging in the presence of Lut or Quer (Figures 20E and 20F), confirming the strong inhibition activity of these molecules on hCT fibril formation. Based on the structural features of these compounds, it appears that the catechol moiety on the B-ring likely makes both Lut and Quer stronger inhibitors of hCT fibril formation compared to Nar. Interestingly, Akaishi et

al. previously reported that the 3',4'-dihydroxyl group in fisetin is critical for its inhibitory effect on Aβ fibril formation.[166] Our results are in accord with their findings. The emerging crucial impact of the catechol moiety in these effective inhibitors indicates that the covalent linkage may likely be an important factor in the mechanism of inhibition of hCT aggregation as has been indicated by previous studies with other amyloidogenic proteins.[96, 151, 167] Quer contains an additional hydroxyl group on the heterocyclic ring, and this hydroxyl group could be involved in hydrogen bonding interactions with hCT, leading to a slightly stronger inhibition on hCT aggregation than Lut. In addition, Wang et al. suggested that factors such as hydrophobic interactions and aromatic stacking are important for Quer to inhibit bovine insulin fibril formation.[165] These interactions should also be taken into account as well in the inhibitory effects of these compounds on hCT amyloid formation.

Myricetin (Myr) is a flavonol that contains one additional hydroxyl at the C-5' position of the B-ring in comparison to Quer (Figure 21A below). It is found in fruits and vegetables such as onions, scallions, broccoli, apples, and berries.[157] Myr has been shown to be a strong amyloid inhibitor of Aβ and α-synuclein where it can reversibly bind to oligomers through noncovalent interactions such as hydrogen bonding and aromatic stacking.[168-169] Here, Myr shows a remarkably potent inhibitory activity on hCT fibril formation in a dose-dependent manner (Figure 21B). There is a ~60% drop in the maximum ThT fluorescence intensity of hCT aggregation when 5 μM Myr is added. In the presence of 100 μM Myr, the ThT fluorescence is negligible throughout the period of the measurement (Figure 21B), indicating a complete inhibition of hCT amyloid formation.

This inhibition activity is stronger than that of EGCG (Figure 21D). AFM imaging shows

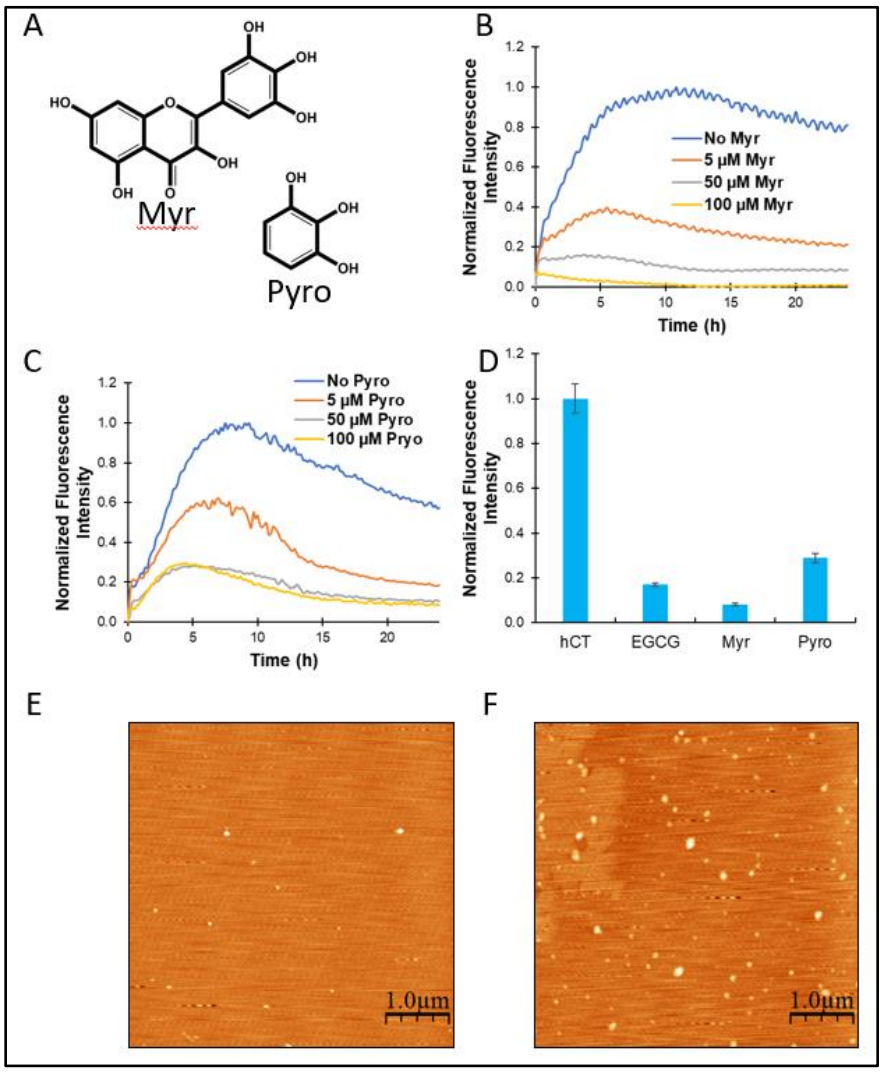

Figure 21. (A) Chemical structures of Myr and Pyro. (B-C) Effect of Myr (B) or Pyro (C) on the aggregation kinetics of hCT (5 μM) followed by ThT fluorescence in sodium phosphate buffer (5 mM, pH 7.4) at 25 °C. (D) Normalized maximum ThT fluorescence intensity in the aggregation of hCT in the absence or the presence of the small molecules (100 μM). Data are reported as means ± SD of triplicate results. (E-F) Tapping mode AFM images of hCT (5 μM) in the presence of 100 μM Myr (E) or 100 μM Pyro (F). The samples were incubated in sodium phosphate buffer (5 mM, pH 7.4) at 25 °C for 24 h before imaging.

that only few spherical oligomeric structures were observed when 5 μM hCT was incubated with 100 μM Myr (Figure 21E). These results show that Myr and Quer are the most potent inhibitors of hCT aggregation tested in this study. In light of the structural commonality of

these efficient inhibitors, our results suggest that the presence of vicinal hydroxyls, either a catechol moiety or a trihydroxyl group on the phenyl ring, is critical in the inhibiting function of these flavonoid molecules on hCT amyloid formation. In addition to the possible contribution of hydrogen bonding interactions with the backbone and side chains of the peptide, the adjacent hydroxyl groups on the benzyl ring may also favor the formation of a quinone structure to form a covalent linkage with the peptide.

To further investigate the impact of the multiple-hydroxyl phenyl structure on hCT fibrillization, we examined pyrogallol (Pyro) which is composed of a single vicinal trihydroxyl phenyl ring (Figure 21A). Remarkably, Pyro also inhibits hCT fibril formation (Figure 21C), although its inhibitory activity is weaker compared to that of EGCG (Figure 21D). No fibers were observed in the AFM imaging of 5 μM hCT incubated with 100 μM Pyro (Figure 21F), validating the inhibitory effect of this small molecule on hCT amyloid formation. Phan et al. reported that the pyrogallol moiety of gallocatechin gallate is one of the most potent groups that bind to Aβ through a combination of interactions such as aromatic and hydrogen bonding.[170] It is intriguing that the addition of a negatively charged carboxylic acid group on the trihydroxyl phenyl ring, such as in GA, dramatically hinders the inhibitory activity on hCT amyloid formation (Figure 18).

3.3.3 Effect of Baicalein and Polyphenols With Flexible Phenyl Rings on hCT Fibrillization

The effective flavonoid inhibitors on hCT amyloid formation tested so far all contain a catechol or pyrogallol moiety on the B-ring. Baicalein (Baic) is a flavone compound that has a vicinal trihydroxyl group on the A-ring (Figure 22A below). Baic is

used in traditional Chinese herbal medicine and exhibits antiallergic, anticarcinogenic, and

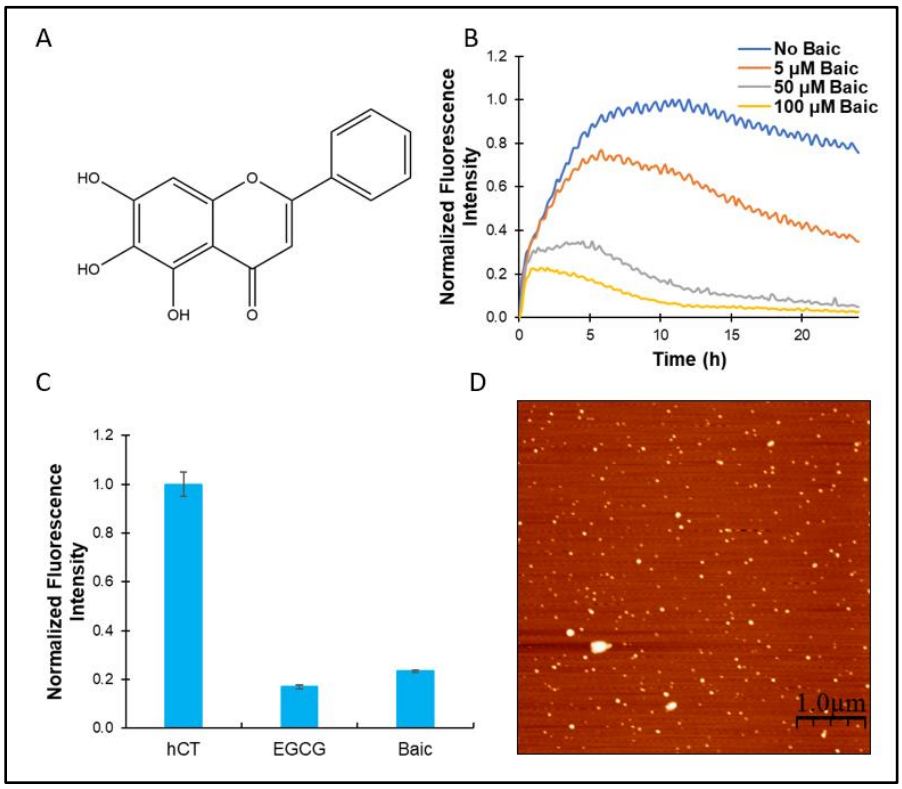

Figure 22. (A) Chemical structure of Baic. (B) Effect of Baic on the aggregation kinetics of hCT (5 μM) followed by ThT fluorescence in sodium phosphate buffer (5 mM, pH 7.4) at 25 °C. (C) Normalized maximum ThT fluorescence intensity in the aggregation of hCT in the absence or the presence of EGCG or Baic (100 μM). Data are reported as means ± SD of triplicate results. (D) Tapping mode AFM image of hCT (5 μM) in the presence of 100 μM Baic. The sample was incubated in sodium phosphate buffer (5 mM, pH 7.4) at 25 °C for 24 h before imaging.

anti-HIV effects.[171-175] Baic has also been shown to have inhibitory activities on the fibrillization of Aβ, α-synuclein, insulin, and amylin.[79-80, 87, 159-160, 169, 176-178] Our results here demonstrate that Baic is a potent inhibitor of hCT amyloidogenesis, validated by both the ThT kinetics results and AFM imaging (Figures 22B and 22D). Its inhibition efficiency is comparable to that of EGCG (Figure 22C). In comparison to the results of Fla (Figure 19), these results indicate that the vicinal hydroxyl groups located on the A-ring of

flavonoids also significantly enhance the inhibition efficiency of the molecule in hCT fibril formation.

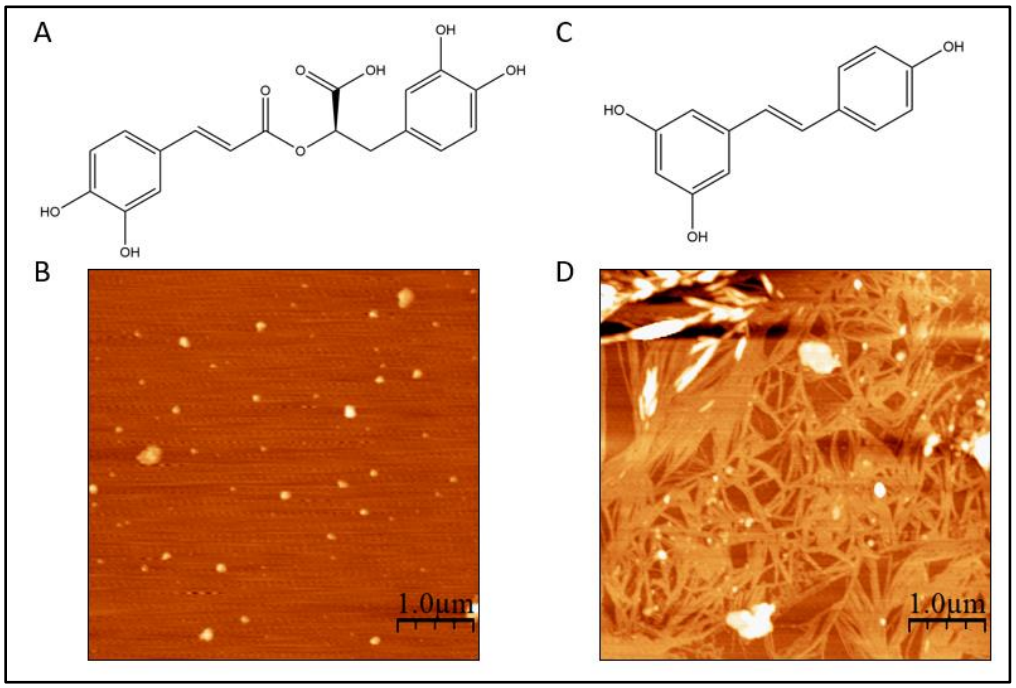

Figure 23. (A) Chemical structure of RA. (B) Tapping mode AFM image of hCT (5 μM) in the presence of 100 μM RA. The sample was incubated in sodium phosphate buffer (5 mM, pH 7.4) at 25 °C for 24 h before imaging. (C) Chemical structure of Resv. (D) Tapping mode AFM image of hCT (5 μM) in the presence of 100 μM Resv. The sample was incubated in sodium phosphate buffer (5 mM, pH 7.4) at 25 °C for 24 h before imaging.

Besides flavonoids, we also studied a polyphenol rosmarinic acid (RA) that is comprised of two flexible phenol rings (Figure 23A above). RA is found in herbs such as basil and rosemary[84] and has been reported to exhibit inhibitory activity in amyloidogenesis of Aβ and IAPP.[83] Each phenol group in RA contains a catechol moiety which could be involved in Schiff base formation as suggested in the vicinal hydroxyl containing flavonoids such as EGCG.[96] Our result shows that RA also blocks hCT amyloid formation, with only a few of spherical aggregates formed (Figure 23B). Resveratrol (Resv) is another polyphenol that has been found to inhibit Aβ and IAPP fibril formation and even disaggregate the preformed fibrils.[81] Resv is comprised of two polyphenolic residues with hydroxyl groups

that could be involved in aromatic interactions and hydrogen bonding, but does not contain vicinal hydroxyl structures (Figure 23C). Interestingly, Resv is not capable of inhibiting hCT fibril formation (Figure 23D). These results indicate that the presence of vicinal hydroxyl groups on the benzyl ring may also be crucial for non-flavonoid polyphenolic compounds to efficiently inhibit hCT amyloid formation. It worth noting that the amyloids formed when incubating hCT with Resv were thicker and more crystalline-like compared to that of hCT alone. This suggests that Resv can modulate the morphology of the hCT fibrils, although it cannot block the amyloid formation of hCT.

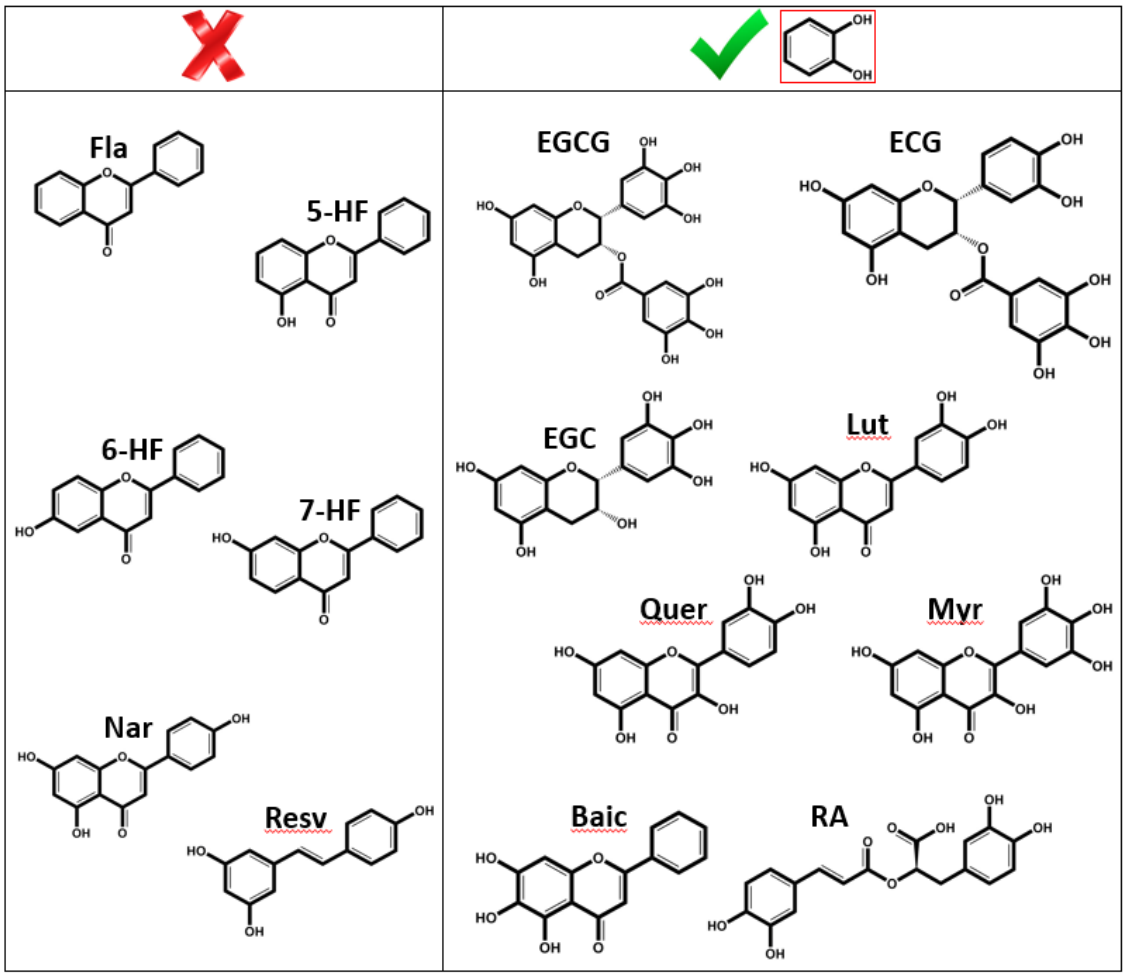

Figure 24. Summary of the effect of the polyphenols examined on hCT amyloidogenesis. The left group is nonefficient inhibitors of hCT amyloid formation, and the right group is efficient inhibitors.

As summarized in Figure 24 above, the examined polyphenols lacking the vicinal hydroxyl groups are not efficient inhibitors of hCT amyloid formation, whereas the presence of the vicinal hydroxyl groups on the phenyl rings can dramatically enhance the inhibitory activity. Our study suggests that the vicinal hydroxyl groups on the phenyl ring is a critical structural feature of the flavonoids and likely non-flavonoid polyphenolic molecules for their inhibitory activity of hCT fibril formation. It has been indicated that the inhibition ability of polyphenols on protein amyloid formation is influenced by various factors such as aromatic stacking, hydrogen bond formation, and Schiff base formation.[79, 87, 160] Our results imply that the aromatic and hydrogen bonding interactions between hCT and the flavonoids are not sufficient to prevent hCT amyloid formation. Therefore, the molecular mechanism of the vicinal hydroxyl groups of these polyphenol inhibitors may likely involve oxidation and subsequent covalent bond formation with hCT which consequently interferes with the crucial electrostatic and aromatic interactions of amino acid residues in hCT fibril formation.[46, 50, 52, 75] In addition, it is conceivable that the non-vicinal hydroxyl groups and the carbonyl group on the heterocyclic ring of flavonoids may also be involved in hydrogen bonding with the backbone and/or side chains of hCT. All these interactions need to be taken into account with regards to hCT amyloid inhibition. The inhibition activity of polyphenolic compounds on hCT fibril formation may likely be attributed to a combination of factors such as formation of covalent linkage, aromatic stacking, and hydrogen bonding interactions.

In this study, we investigated the effect of the polyphenolic compounds on the amyloid formation of hCT in aqueous sodium phosphate buffer solution. The aggregation of hCT *in vivo*, however, occurs under a rather complex physiological condition. For

instance, metal ions such as calcium, zinc, copper, and iron that steadily exist in the cellular environment have been implicated to play an important role in the formation of amyloid deposits in amyloid diseases.[179] A number of novel amyloid inhibitors have been reported to target metal chelation and metal-associated amyloid formation.[179-181] EGCG is also found to be an iron chelator and has been shown to reduce iron levels and Aβ amyloidogenesis.[182] Moreover, it has been well recognized that cellular membranes can significantly manipulate protein amyloid formation *in vivo*. Lorenzen et al. reported that EGCG moderately reduces the binding of α-synuclein oligomers to the surface of phospholipid membranes and thus blocks the toxicity of α-synuclein aggregates.[183] On the other hand, it has been found that EGCG becomes a much less efficient inhibitor of IAPP amyloid formation at a phospholipid interface than in bulk solution.[184] A systematic evaluation of the efficacy of the reported polyphenolic inhibitors in the presence of metal ions and/or in a membrane environment will provide mechanistic insight into the inhibiting function of these molecules on hCT amyloid formation in cellular environment. Assessment of the effects of these compounds against the hCT amyloid-induced cellular toxicity will provide more direct information on the potential application of these molecules in therapeutics. However, it should also be noted that these polar flavonoids may possibly exhibit poor pharmacokinetics in therapeutic applications.[185] The bioavailability of these compounds might be limited due to issues such as poor systematic absorption.[186-187] These factors should, therefore, be considered in designing novel flavonoid-based molecules for inhibiting hCT amyloidogenesis *in vivo*.

3.4 Conclusions

In conclusion, we report a group of polyphenolic compounds that inhibit hCT amyloid formation. Our results show that the gallate moiety in EGCG is not critical for the inhibition function on hCT amyloidogenesis. Remarkably, our results suggest that the presence of vicinal hydroxyl groups on the phenyl rings of flavonoids is essential for their capabilities of preventing hCT amyloid fibril formation. This structural feature may also be applied to non-flavonoid polyphenolic inhibitors. In addition to participating in hydrogen bonding interactions, this structural motif may favor the covalent bond formation with hCT to form adducts such as Schiff base. This could disrupt critical electrostatic and aromatic interactions in the process of amyloid formation of hCT. The inhibitory efficiency of polyphenolic molecules is likely dependent on the interplay of hCT and the compounds via synergistic interactions including covalent bond formation, hydrogen bonding, and aromatic interactions. Future studies with high resolution approaches such as NMR spectroscopy and molecular dynamics simulation will provide new insight into the interactions of the compounds and hCT at the molecular level. The knowledge obtained may facilitate the design of novel polyphenol molecules as effective inhibitors of hCT amyloidogenesis with appropriate bioavailability for treating hCT aggregation-related diseases. These advances would also allow for the return of hCT use in the clinic.

CHAPTER IV: CONCENTRATION, SIZE, AND CURVATURE EFFECTS OF LIPOSOMES ON HCT AMYLOID FORMATION

4.1 Introduction

Human calcitonin (hCT) interacts with osteoclast (breaks down bone) cell membranes and G protein-coupled receptors that are contained on the membranes to inhibit osteoclast activity and maintain calcium homeostasis.[11, 188] Unfortunately, hCT is a known amyloid peptide that can aggregate forming fibrils which have been shown to cause cellular toxicity when elevated concentrations are present.[11, 21] Salmon calcitonin (sCT), due to its amino acid sequence, is less likely to form amyloid fibrils[11] and contains increased monomeric alpha helical character than hCT.[189] These characteristics make for better receptor binding[190] and more potent biological activity[190] which is why it is a superior therapeutic agent in combating bone-related diseases such as osteoporosis and Paget's disease.[11, 32] Furthermore, the additional alpha helical character makes it easier for sCT to penetrate into the bilayer of membranes such, such as in osteoclasts, to facilitate ion channel formation and subsequent osteoclast inhibition.[11, 66]

A number of studies have suggested that the presence of phospholipid membranes, such as liposomes, can affect hCT self-association, amyloid formation and subsequent cellular toxicity.[21, 56-57, 64] Liposomes are spherical vesicles that are comprised of phospholipids that are organized in a bilayer where the hydrophilic head group is exposed to the aqueous solvent and the hydrophobic tail is sequestered on the inside of the bilayer

away from the aqueous solvent (Figure 25 below).[191-193] Since it is very difficult to replicate

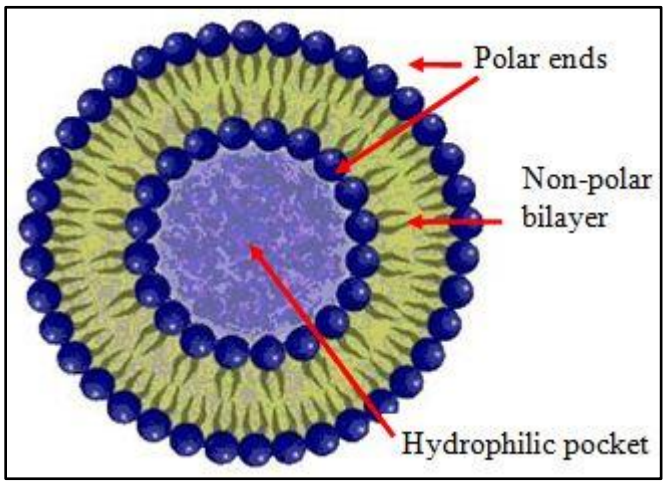

Figure 25. Scheme of a liposome. Adapted from ref. [193].

in vivo conditions, many studies use liposomes as models for artificial cell membranes.[191] It has been reported that liposomes containing cholesterol or gangliosides promoted β-sheet and amyloid content of bovine calcitonin (bCT) which consequently caused cell toxicity.[21, 56-57] In addition, Sheynis and Jelinek reported that liposomes containing cholesterol caused hCT to form fibrillar structures on the surface of membranes.[63] A similar result was reported where the presence of ganglioside GM1 caused sCT to form spherical aggregates on the surface of zwitterionic liposomes.[57] However, the use of negatively charged sodium dodecyl sulfate (SDS) can enhance alpha helical character in hCT which makes it easier for the alpha helical portion to bind and insert itself into the bilayer through a combination of hydrophobic and electrostatic interactions, thus enhancing the rate of channel formation.[190, 194] This has also been observed with negatively charged liposomes as well.[131] Calcitonin (CT) channel formation has been postulated to occur by the insertion of the central alpha helix portion of the peptide into the bilayer of the membrane.[11, 66] Under normal physiological concentrations, the solvent exposed portion of CT, that is not inserted

into the bilayer, can interact with other monomers to form an oligomer where pore formation can occur.[11, 66] This has been postulated to be biologically useful as a way of inhibiting osteoclast activity.[66] However, under abnormal concentrations of CT, this can cause excessive channel and fibril formation that can cause uncontrolled ion leakage and subsequent cell toxicity.[21, 64, 195]

It has been evidenced that size and curvature properties of liposomal vesicles are important factors in determining the binding of the vesicles to amyloidogenic proteins.[108, 139, 196-197] Terakawa et al. reported that small liposomes (≤ 50 nm) accelerated β-amyloid (Aβ) fibrillization while larger sized liposomes lessened the number of fibrils.[108] A similar result was seen with α-synuclein as well.[196-197] However, the role of membrane properties such as the structural characteristics of the lipids, size, and curvature on the fibrillization of hCT has not yet been studied in detail. In this study, we examined the effects of concentration, size, and curvature of liposomes on hCT amyloid formation. We used zwitterionic 1-palmitoyl-2-oleoyl-glycero-3-phosphocholine (POPC) and negatively charged 1-palmitoyl-2-oleoyl-phosphatidylglycerol (POPG) without cholesterol or GM1 to isolate and probe these effects between liposomes and hCT (Figures 26A and 26B below). hCT has been reported to interact with the surface of POPC, but not insertion into the bilayer.[66, 131] POPG has been reported to interact with hCT causing insertion into the bilayer through electrostatic interactions.[131] Investigating these interactions will aid in the mechanistic understanding of how hCT amyloid formation occurs in a physiological system and aid in the design of viable inhibitors for therapeutic use.

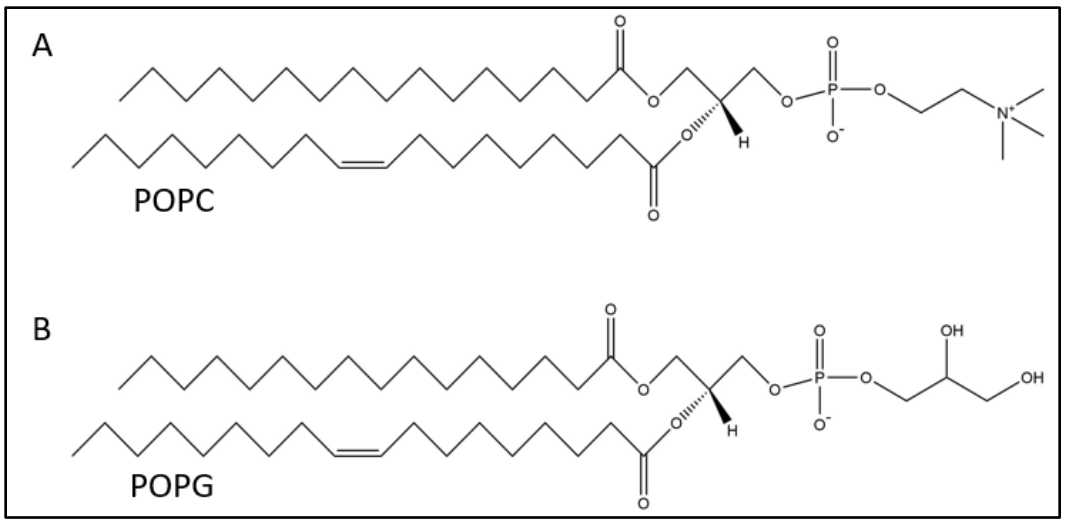

Figure 26. (A) Structure of POPC. (B) Structure of POPG.

4.2 Materials and Methods

4.2.1 Materials

All chemical reagents were purchased from commercial suppliers and used without further purification. POPC and POPG lipids were purchased from Avanti Polar Lipids, Inc.

4.2.2 Preparation of POPG and POPG Liposomes

POPC and POPG powder was dissolved in chloroform at a concentration of 5 mg/mL. Appropriate amounts of each were pipetted into a glass test tube and placed on a lyophilizer to evaporate off the solvent for 1-2 hours. The lipids were then hydrated using the thin film hydration method.[198] Briefly, the lipids were hydrated with 5 mM sodium phosphate buffer (pH 7.4) to make a stock solution of 3 mM lipid. The solution was vortexed vigorously and sonicated for 20 minutes. Once hydrated, the liposomes were prepared by the membrane extrusion method with the appropriate pore size (0.05 μm or 0.2 μm).[199] Extrusion was repeated 30 times to ensure sample homogeneity. The resulting liposomes where subsequently used in experiments within 24-48 hours of preparation.

4.2.3 Dynamic Light Scattering Liposome Size Measurements

5 μL of the resulting stock solutions of POPC and POPG liposomes from extrusion were diluted 1:20 v/v with 5 mM sodium phosphate buffer and dispensed 100 μL in 1 cm disposable micro cuvettes (Malvern, UK). Size measurements were performed on a Zetasizer Nano ZS (Malvern, UK) at 25 °C. The average diameter of the 50 nm and 200 nm vesicles were calculated as the mean of three measurements with 11-20 runs per measurement.

4.2.4 Aggregation Kinetics of hCT With Liposomes by ThT Fluorescence

5 μM of oxidized hCT was prepared in 5 mM sodium phosphate buffer (pH 7.4) containing 20 μM Thioflavin-T (ThT). A particular amount of POPC or POPG stock solutions was then added to the solutions containing 5 μM hCT, 20 μM ThT and 5 mM sodium phosphate buffer (pH 7.4). 100 μL of solution was pipetted to wells in a 96-well microplate (Costar black, clear bottom). The plate was then sealed with a microplate cover, para-filmed, and loaded into a Gemini SpectraMax EM fluorescence plate reader (Molecular Devices, Sunnyvale, California) where it was incubated at 25 °C for 24 hours. The ThT fluorescence was measured every 10 minutes after shaking for 5 seconds with an excitation wavelength of 440 nm and an emission of 480 nm. All fluorescence kinetics data are reported as a means of triplicate results.

4.2.5 Atomic Force Microscopy

To prepare the samples for atomic force microscopy (AFM) imaging, aliquots (15-20 μL) of hCT with or without liposomes were taken directly from the aggregation kinetics assay and were adsorbed onto the surface of freshly cleaved mica (5 × 5 mm). The samples

were covered and left to dry overnight. AFM images were acquired in tapping mode using the Asylum Research MFP 3D AFM system with MikroMasch NSC15/AI BS cantilevers.

4.3 Results and Discussion

The first set of liposomes we chose to work with were made up of zwitterionic POPC lipids as they are the most abundant phospholipid found in all mammalian cellular membranes.[197, 200] POPC liposomes were prepared by thin film hydration and extrusion methods with a membrane filter that contained 200 nm pore sizes and the size was determined by dynamic light scattering (DLS).[198-199] DLS uses a beam of light that scatters

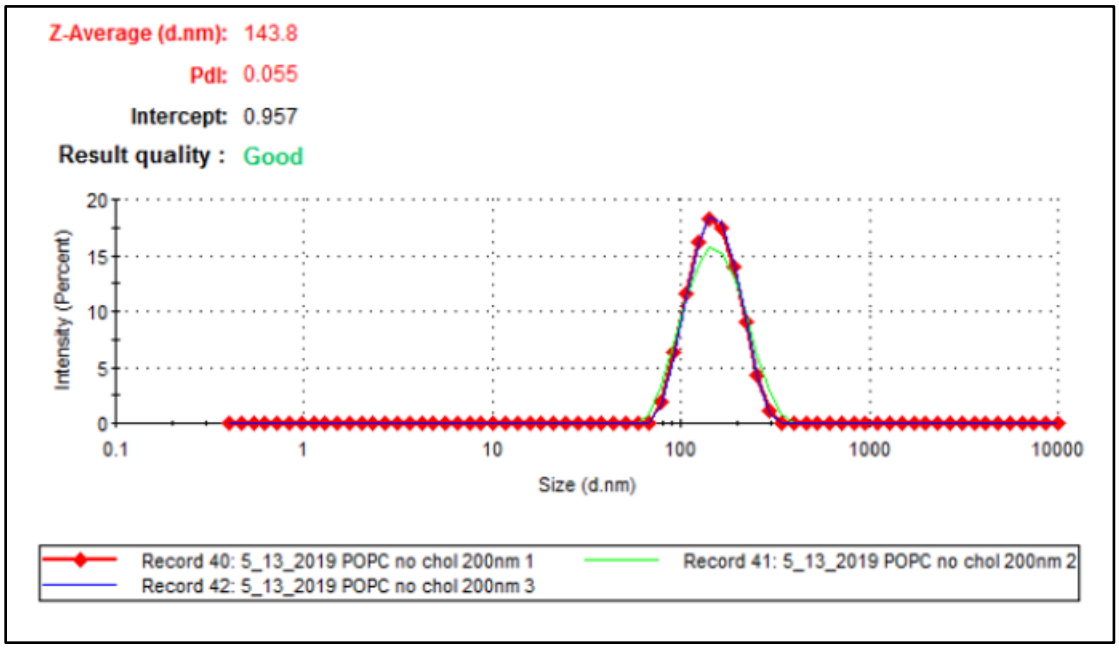

Figure 27. DLS size measurement of freshly prepared POPC liposomes using 200 nm pore filter in 5 mM sodium phosphate buffer (pH 7.4) at 25 °C.

off of a particle that displays Brownian motion.[106] The fluctuations in light intensity from this scattering is measured where a diffusion coefficient can be calculated and a radius of a particle can be determined using the Stokes-Einstein equation.[106] As shown in Figure 27 above, an average diameter of 143.8 nm was attained through the use of DLS which is smaller than the 200 nm filter pore size used. Ong et al. reported similar results when using

the same pore size and smaller pore sizes resulted in liposomes that were larger than the pore size selected when using the extrusion technique.[201] This is due to the elastic deformation of the liposomes where the liposome spheres become more ellipsoid in shape to make it easier to pass through the filter pores resulting in a differently sized liposome.[201-203] The polydispersity index (PdI) was 0.055 which indicates a homogenous size distribution of POPC liposomes.[201]

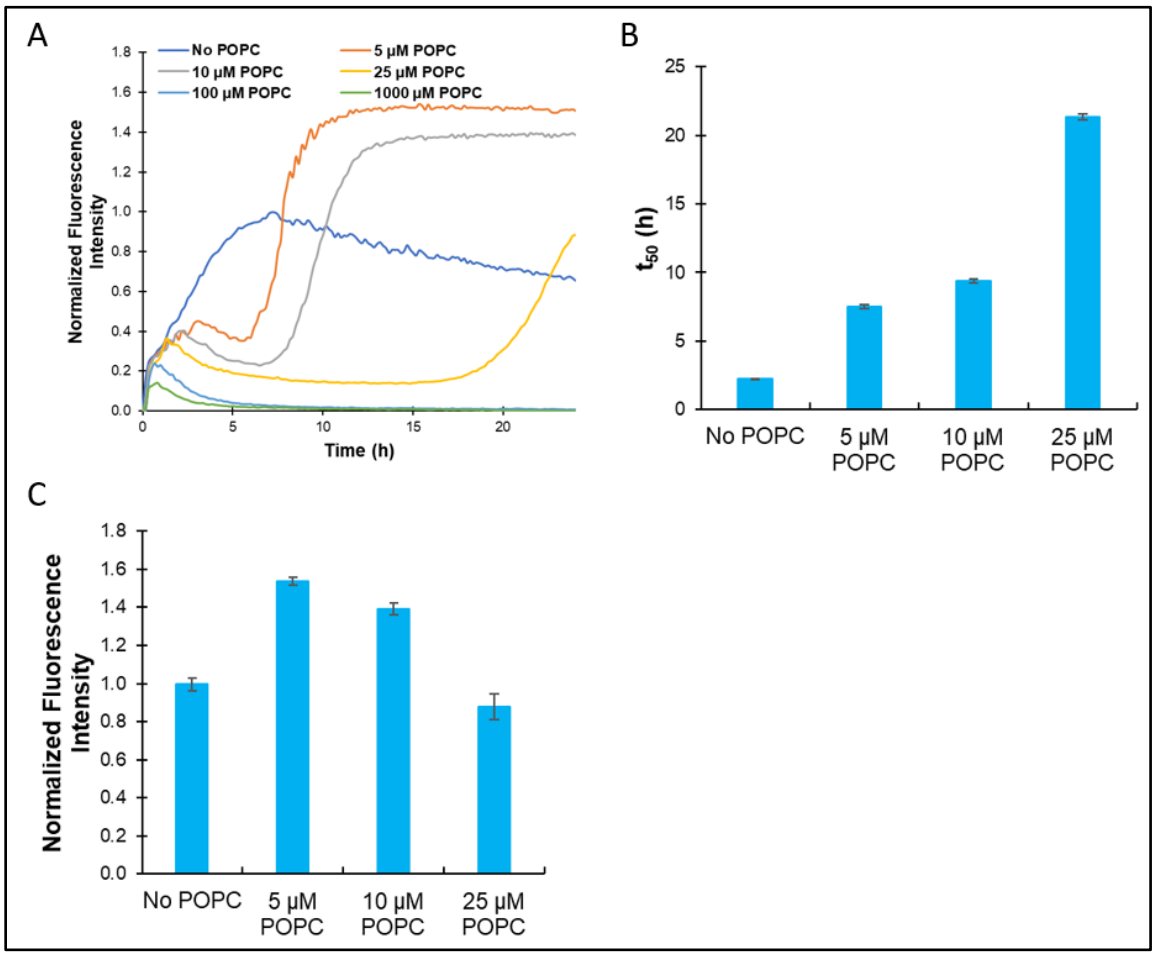

Figure 28. (A) Effect of POPC liposomes on the aggregation kinetics of hCT (5 μM) in sodium phosphate buffer (5 mM, pH 7.4) at 25 °C. (B) Aggregation half-time (t_{50}) of hCT in the presence or absence of POPC liposomes. (C) Normalized maximum fluorescence intensity of hCT in the presence or absence of POPC liposomes. Data are reported as means ± SD of triplicate results.

The aggregation kinetics of oxidized hCT (5 μM) in the presence or absence of POPC liposomes (5 mM sodium phosphate buffer, pH 7.4) was monitored by Thioflavin-T (ThT), a fluorescent dye that is widely used in the detection of amyloid fibril structure where the binding of the dye to the amyloid fibril leads to an increase in fluorescence intensity at around 480 nm (Figure 28A above).[95, 123-124] The aggregation of hCT in the absence of POPC liposomes shows a fast increase in fluorescence immediately after the start of the kinetics measurement until it reached a maximum fluorescence intensity at ~7 h (Figure 28A). This rapid rate of hCT fibril formation is consistent with previous reports and with the results in Chapters II & III.[31, 53, 58] In addition, after reaching the maximum, the fluorescence intensity slowly declines throughout the rest of the measurement. This phenomenon is likely attributed to hCT aggregates precipitating out of solution during incubation.[58, 99]

In the presence of 5 μM POPC liposomes, the aggregation curve looks more of a typical sigmoidal shape, but there is a delay in aggregation compared to when no POPC was added (Figure 28A). The aggregation half-time (t_{50}), which is the time it takes for the ThT fluorescence to reach half the maximum intensity, is ~7.5 h for when 5 μM of POPC liposomes were added compared to ~2.2 h when no POPC liposomes were added (Figure 28B). In addition, this increasing delay in aggregation continues in the presence of 10 μM and 25 μM large POPC liposomes (Figures 28A and 28B). The t_{50} value of when 25 μM POPC liposomes were added is ~21 h which is ~9.5 times longer than when no POPC was added (Figure 28B). Higher concentrations of POPC such as at 100 μM or 1000 μM exhibits little to no ThT fluorescence which indicates complete inhibition of fibril formation. Interestingly, the maximum fluorescence intensity in the presence of 5 μM

POPC liposomes is ~1.5 times higher than when no POPC was added, indicating a higher abundance of fibrils (Figure 28C). It has been reported that CT weakly interacts with the surface of zwitterionic liposomes, such as POPC. [120, 204-205] These weak surface interactions can cause CT to associate and form fibrils on the membrane surface to form a fibril network around the zwitterionic liposomes.[131-132, 204] Therefore, we propose that the increased formation of hCT fibrils in the presence of POPC is due to hCT monomers associating with the surface of POPC and acting as a seed for fibril formation. This could cause a nucleation point to occur where an oligomeric nucleus forms and leads to an enhancement of fibril formation. This increase in fluorescence is also seen in the presence of 10 μM POPC liposomes, but the maximum fluorescence intensity decreased to only ~1.4 times that of when no POPC was added. The maximum fluorescence intensity in the presence of 25 μM POPC liposomes is comparable to when no POPC was added, showing a decreasing trend in maximum ThT fluorescence with increasing POPC liposome concentration. This observed decrease in fluorescence intensity is possibly due to the presence of a greater number of POPC liposome vesicles as the concentration of POPC increases. This would lead to the binding of additional monomer to the liposome surface which would reduce the effective monomer concentration in solution, causing a reduction of peptide association and fibrillization. It should be noted that as the concentration of POPC liposomes increase, there is a fast increase in ThT intensity within 2-3 h of incubation and then quickly decreases afterward. This phenomenon has been seen in Chapter II and Chapter III with the incubation of hCT with DC-cholesterol or epigallocatechin gallate (EGCG).[58] This indicates that the early formed intermediate structures of hCT could interact with the POPC liposomes and be sequestered by the vesicles.[58]

The inhibitory activity of the POPC liposomes were also investigated by atomic force microscopy (AFM) imaging. The AFM imaging samples were aliquoted directly from the ThT aggregation assay that had been incubating for 24 h at 25 °C. In the absence of POPC, hCT formed long and stacked fibrillar structures (Figure 29A below). In the presence of 10 μM POPC liposomes, there is a greater abundance of long and stacked fibrils than in the absence of POPC. This is consistent with the increase in fluorescence intensity in the ThT kinetics results (Figure 29B). In the presence of 1000 μM POPC liposomes, there was no indication of any fibrillar structures and only oligomeric spherical intermediates and amorphous aggregates were seen (Figure 29C). These results are consistent with the ThT aggregation kinetics indicating that POPC liposomes have an inhibitory effect on hCT fibril formation.

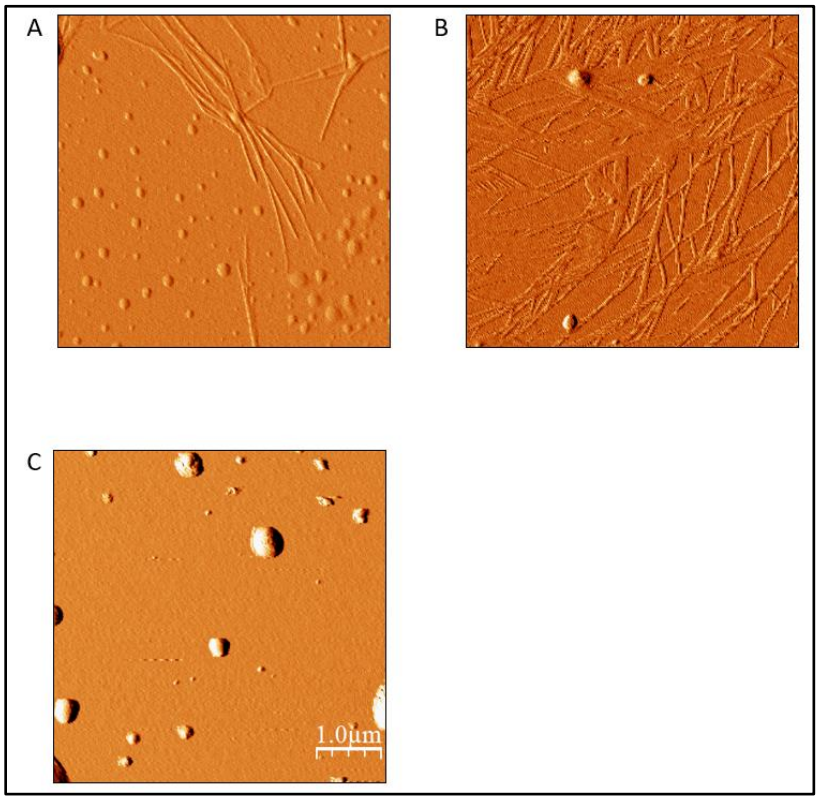

Figure 29. Tapping mode AFM images of hCT incubated in the presence or absence of POPC liposomes. (A) No POPC (B) 10 μM POPC. (C) 1000 μM POPC. The samples were incubated in 5 mM sodium phosphate buffer (pH 7.4) at 25 °C for 24 h before imaging.

From the kinetic and AFM results, there is an evident correlation between increasing concentration of POPC liposomes and hCT fibril inhibition, indicating interactions between them. From a charge perspective, POPC contains a negatively charged phosphate group and a positively charged quaternary ammonium cation on the head group of the phospholipid that would be exposed to the aqueous solvent at physiological pH. hCT contains one negatively charged aspartic acid (Asp15) and two positively charged lysine and histidine residues (Lys18 and His20). It has been reported that these residues are involved in intermolecular electrostatic interactions that help form and stabilize the antiparallel amyloid fibril structures formed by hCT (Chapter III, Figure 16).[46, 50] In addition, the disturbance of these interactions can cause instability and affects the elongation rate of hCT fibril formation.[46, 50] At physiological pH, Lys18 would be protonated, less than 10% of His20 would be protonated, and Asp15 would be deprotonated in hCT. It has been evidenced that the interactions between CT and zwitterionic liposomes are weak at physiological pH.[120, 204-205] However, these weak interactions could assist in the disruption of fibril formation and lead to retardation and inhibition as the concentration of POPC liposomes increase. It has been evidenced that electrostatic interactions of hCT with the vesicles formed by negatively charged cholesterol sulfate and positively charged DC-cholesterol in Chapter II can lead to delayed fibril formation and inhibition.[58] In addition, there are critical π-π stacking interactions that are in close proximity to the electrostatic residues which have been evidenced to be important in the formation and stability of hCT amyloid fibril formation as well.[52, 58] Therefore, these interactions could

also be disrupted if electrostatic interactions are occurring between hCT and POPC (Chapter III, Figure 16).

To further our understanding of the role electrostatic interactions have between hCT and liposomes in inhibiting amyloid fibril formation, we conducted hCT aggregation kinetics in the presence or absence of negatively charged POPG liposomes. The POPG liposomes were prepared with the same methods as the POPC liposomes. The DLS of the POPG liposomes shows that the average size of these vesicles was 129.4 nm with a PdI of

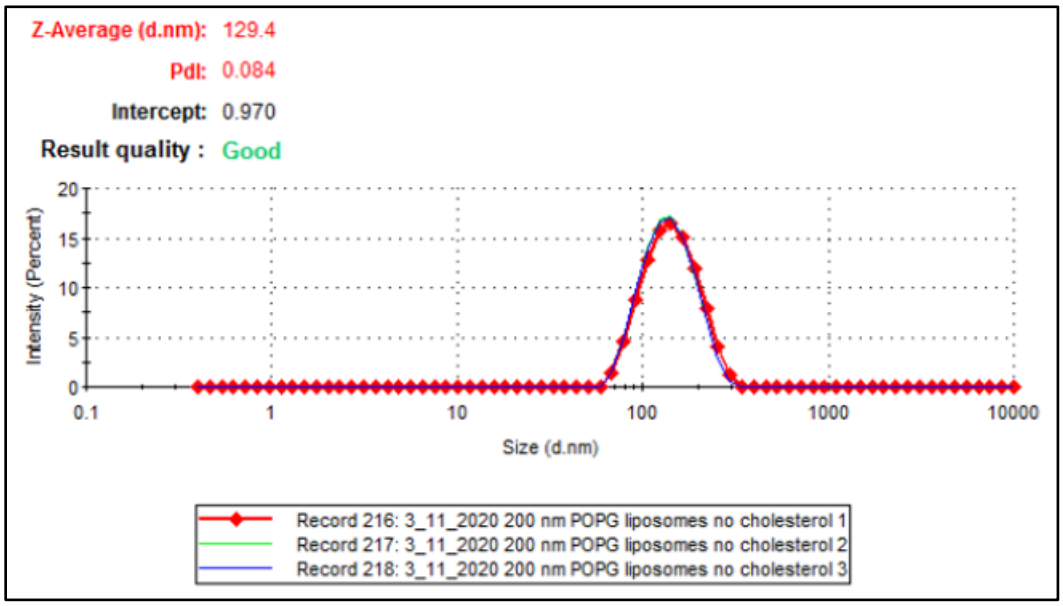

Figure 30. DLS size measurement of freshly prepared POPG liposomes using 200 nm pore filter in 5 mM sodium phosphate buffer (pH 7.4) at 25 °C.

0.084 (Figure 30 above). The size of the POPG liposomes are slightly less than the size of the POPC liposomes, but still are comparable to each other. Figure 31A below, shows the kinetics of incubating hCT with varying concentrations of POPG liposomes in 5 mM phosphate buffer (pH 7.4) at 25 °C. In the presence of 5 μM POPG liposomes, there is a delay in aggregation where the t_{50} is ~7.3 h (Figure 31B) which is about the same as the presence of 5 μM POPC liposomes (Figure 28B). However, the t_{50} in the presence of 10

μM or 25 μM POPG liposomes does not change significantly compared to the presence of 5 μM POPG liposomes. In addition, the presence of 100 μM POPG liposomes has a t_{50} of ~10.2 h (Figure 31B) whereas complete inhibition is seen with the same concentration of POPC liposomes (Figure 28B). Even in the presence of 1000 μM POPG liposomes, there is a small increase in ThT intensity signifying slight aggregation (Figure 31A). It should be noted that when in the presence of POPG liposomes, the maximum fluorescence intensity is below the maximum intensity in the absence of POPG liposomes indicating no enhanced fibril formation occurred from the presence of POPG liposomes (Figure 31C).

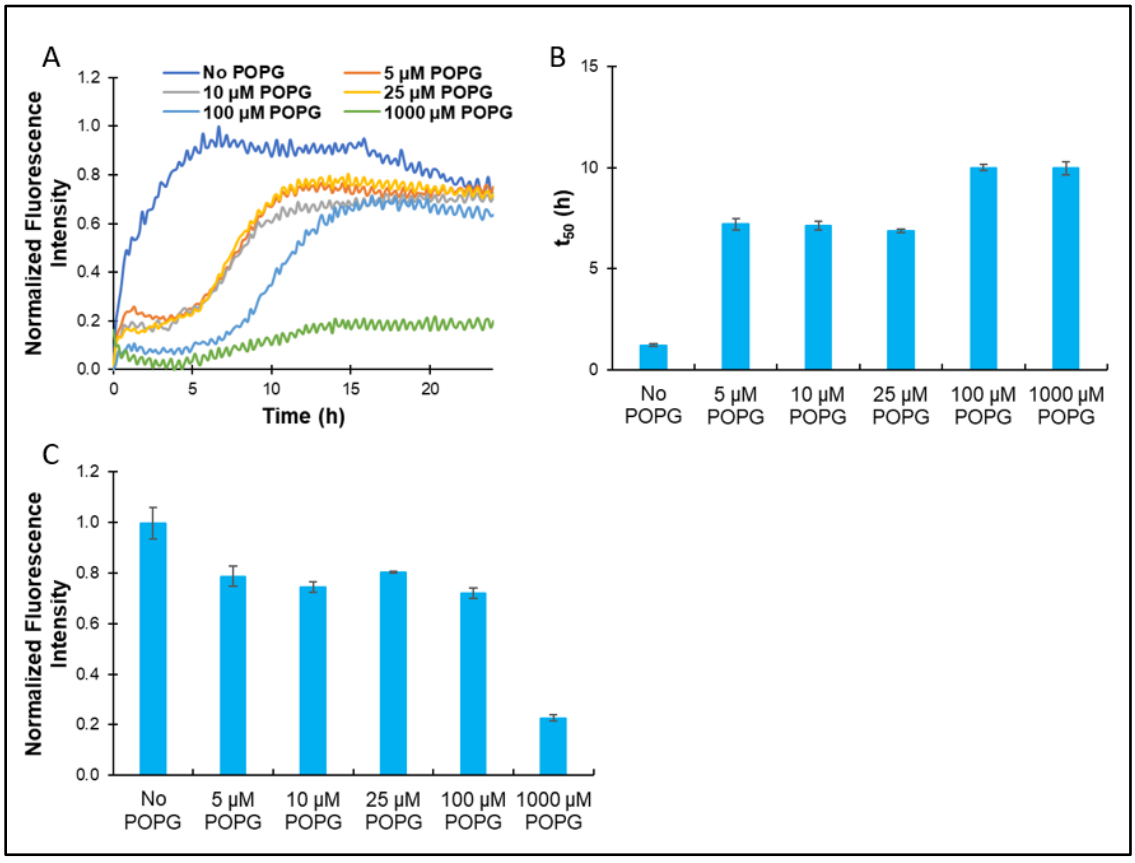

Figure 31. (A) Effect of POPG liposomes on the aggregation kinetics of hCT (5 μM) in sodium phosphate buffer (5 mM, pH 7.4) at 25 °C. (B) Aggregation half-time (t_{50}) of hCT in the presence or absence of POPG liposomes. (C) Normalized maximum fluorescence intensity of hCT in the presence or absence of POPG liposomes. Data are reported as means ± SD of triplicate results.

Several studies have indicated that hCT does interact with negatively charged liposomes and SDS by promotion of the peptide inserting itself into the bilayer.[131, 194, 206] Herbig et al. reported that electrostatic attraction to negatively charged phospholipids is a prerequisite for bilayer insertion by hCT.[131] Bradshaw reported that sCT was able to penetrate deep into the bilayer, further inserting its α-helix structure, by electrostatic interactions with a negatively charged phospholipid containing phosphatidylglycerol, which is the same head group found in POPG.[206] He suggested that the long side chain of lysine in salmon calcitonin would enable the amino acid to insert itself into the bilayer while maintaining its interaction with the negatively charged head group.[206] Another study reported similar results with a lipid that contained the same negatively charged head group and showed that hCT channel formation destabilizes the association between the amyloidogenic peptide molecules needed to form the seed for nucleation and fibril formation.[132] These results were further substantiated when it was reported that sCT prefibrillar oligomers were the culprits of channel formation, not monomers or fibrils.[64] From our fluorescence results, we hypothesize that hCT is interacting with the negatively charged POPG liposomes where the peptide may be inserting itself deep into the bilayer of the liposomes where fibril formation is avoided, but channel formation occurs.

It is known that proteins such as clathrin, BAR domain-containing proteins, and EHD-family proteins are able to deform cellular membranes into tubular shapes of high curvature in order to perform essential biological functions such as production of intracellular transport carriers.[207] It has been reported that the size and curvature of liposomes can affect amyloid fibril formation where increasing vesicle curvature causes the lipid head groups to be further apart and exposes water-accessible hydrophobic regions

for protein-membrane interactions to occur.[108, 139, 196-197] The proposed mechanism of how membrane deformation occurs is by shallow implanting of amphipathic helices and/or hydrophobic regions of the protein into the surface of the lipid monolayer which induces stress on the outer leaflet of the vesicle causing tubular formation.[207] Both POPC and POPG vesicles are known to form tubules induced by amyloidogenic proteins such as α-synuclein.[197, 208] Jiang et al. publicized that α-synuclein monomers are able to remodel spherical POPC vesicles into tubules with high curvature and these deformed vesicles inhibited fibril formation by reducing the number of available monomers to form fibrils.[197, 208] However, the binding of the intrinsically disordered α-synuclein monomer to the POPC vesicle surface lacked residue specificity and site dependence indicating that a helix is not necessarily needed for deforming the vesicle surface.[197] Therefore, the interactions of hCT with liposome vesicles may cause deformations and high curvature that leads to increased association due to the presence of water-accessible hydrophobic regions. However, α-synuclein induced tubular structures for POPC have been reported to have different dimensions than the tubules formed from POPG.[196, 208] Therefore, the difference in dimensions between these deformed lipid vesicles may be a contributing factor in the variance seen in inhibitory activity of hCT fibrillization. For example, the kinetics curves of hCT containing 5 μM, 10 μM, and 25 μM POPG liposomes are not significantly different from each other. Perhaps this may be due to hCT not being able to deform the POPG vesicles efficiently enough to assist in inhibition while the POPC vesicles deform to the appropriate tubular dimensions and curvature for enhanced hCT fibril inhibition. Also, the head group of POPC contains a quaternary ammonium cation while POPG contains a glycerol group. These structural differences should be taken into consideration as well.

Taken together, the effect of liposome vesicles on hCT aggregation may be determined by a rather complex mechanism. We hypothesize that hCT interacts with liposome vesicles through electrostatic and hydrophobic interactions. With POPG, electrostatic interactions between the negatively charged head group and the positively charged residues, Lys18 and His20, will facilitate hCT to anchor deep into the bilayer forming oligomeric ion-permeable channels and not fibrils. With POPC, hCT can interact with the vesicle surface through hydrophobic and weak electrostatic interactions. The interaction of hCT with both POPC and POPG may lead them to deform into tubular structures of higher curvature. This increase in curvature will allow for the interaction of water-accessible hydrophobic regions of the membrane and hCT to bind, leading to enhanced fibril inhibition. However, the dimensions of these induced tubular structures may be different between POPC and POPG which may affect their inhibitory activity towards hCT. The association between hCT and the liposome vesicles initially cause a delay in amyloid formation due to a greater number of hCT peptides interacting with the liposome vesicles instead of with each other. At low POPC vesicle concentrations, additional monomers can associate with hCT that is bound to the vesicle surface and create a nucleation point causing increased fibrillization. As the concentration of the POPC and POPG vesicles increase, there are more vesicles in solution that hCT can bind with which reduces the effective monomer concentration in solution. The combination of these effects can lead to retardation of hCT fibril formation and ultimately inhibition. In addition, both POPC and POPG contain phosphate groups which have been reported to hydrogen bond with the amino acid side chains of lysine, histidine, and glutamic acid.[209] These interactions should be taken into account as well with regards to hCT fibril inhibition.

To further investigate the role vesicle size and curvature has on hCT amyloid formation, we carried out hCT aggregation kinetics in the presence or absence of varying concentrations of smaller 50 nm POPC liposomes in 5 mM phosphate buffer (pH 7.4) at 25 °C. The 50 nm POPC liposomes were prepared the same way as described previously except that they were extruded through a 50 nm filter. DLS size measurements showed that the average diameter of these 50 nm liposomes was 88.2 nm in diameter with a PdI of 0.03 indicating a homogenous size distribution (Figure 32 below). Interestingly, the presence of 50 nm POPC liposomes show a stronger concentration-dependent inhibiting activity of

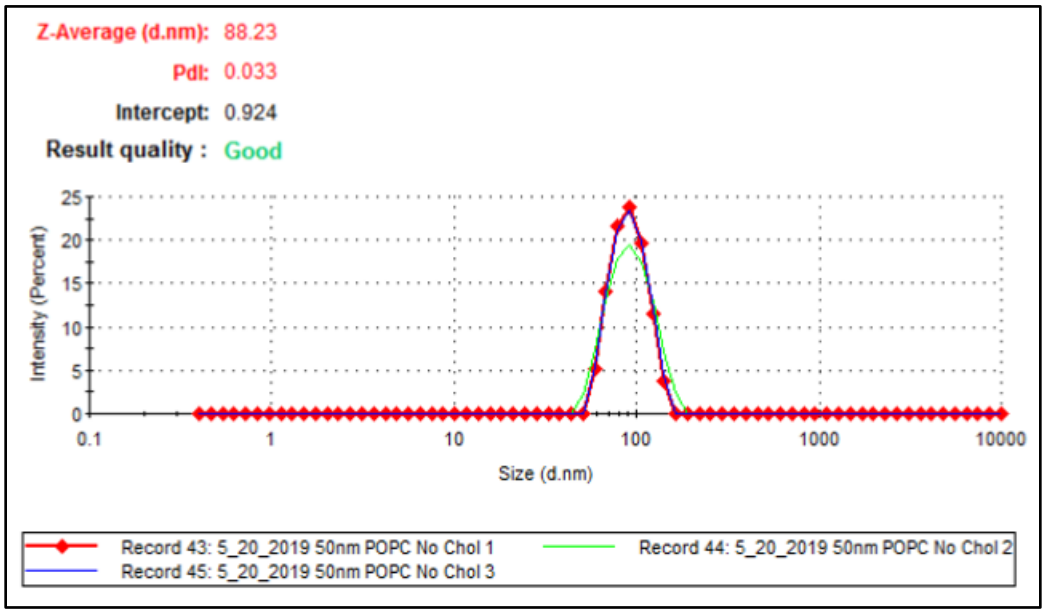

Figure 32. DLS size measurement of freshly prepared POPC liposomes using 50 nm pore filter in 5 mM sodium phosphate buffer (pH 7.4) at 25 °C.

hCT than the larger 200 nm POPC liposomes studied (Figure 33A below). For example, the addition of 5 μM 50 nm POPC liposomes delays fibril formation with a t_{50} of ~9.7 h (Figure 33B) which is about 30% longer than with the same concentration of 200 nm POPC liposomes (Figure 28B). The presence of 10 μM 50 nm POPC liposomes further delays fibril formation with a t_{50} of ~18 h (Figure 33B) which is nearly twice the t_{50} value of 200

nm POPC liposomes at the same concentration (Figure 28B). At concentrations of 25 μM or more, there is complete inhibition of hCT fibril formation (Figure 33A). In addition, the maximum fluorescence intensity in the presence of 5 μM 50 nm POPC liposomes is nearly 1.5 times more than in the absence of 50 nm POPC liposomes (Figure 33C) which is similar to what is seen with the same concentration of 200 nm POPC liposomes. This increase in fluorescence intensity is consistent with our hypothesis that hCT is interacting and loosely binding with the surface of POPC liposomes creating nucleation points and enhancing fibril formation. Also, the maximum fluorescence intensity decreases with increasing concentration which is consistent with the results seen with 200 nm POPC liposomes. This

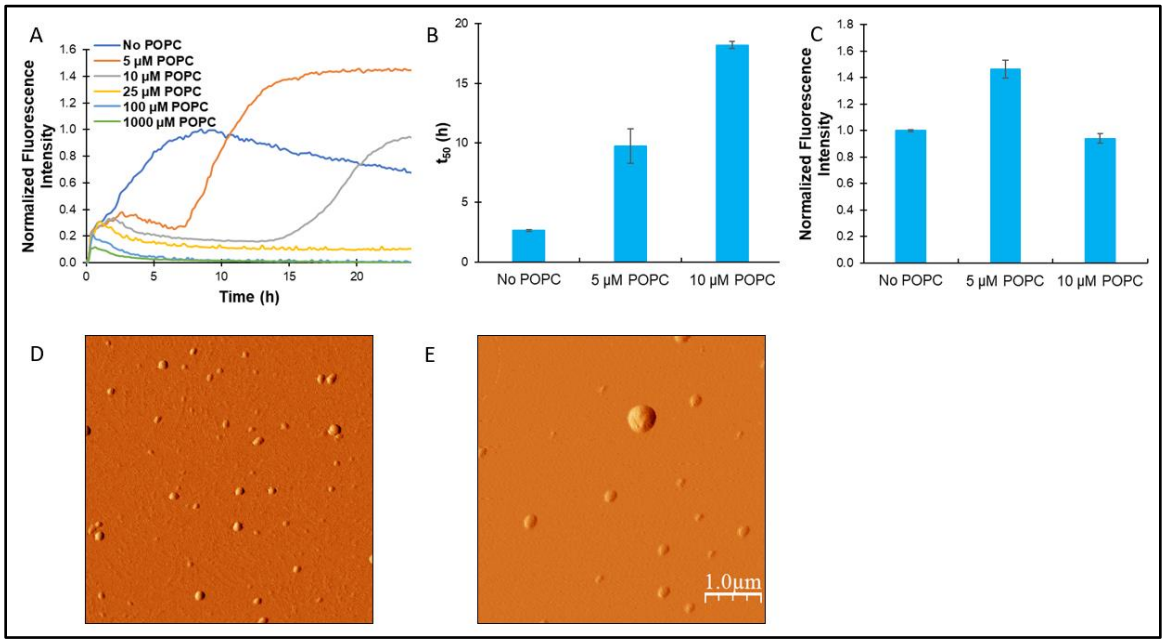

Figure 33. (A) Effect of 50 nm POPC liposomes on the aggregation kinetics of hCT (5 μM) in sodium phosphate buffer (5 mM, pH 7.4) at 25 °C. (B) Aggregation half-time (t_{50}) of hCT in the presence or absence of 50 nm POPC liposomes. (C) Normalized maximum fluorescence intensity of hCT in the presence or absence of 50 nm POPC liposomes. Data are reported as means ± SD of triplicate results. (D-E) Tapping mode AFM images of hCT incubated in the presence of 50 nm POPC liposomes. (D) 25 μM POPC. (E) 1000 μM POPC. The samples were incubated in 5 mM sodium phosphate buffer (pH 7.4) at 25 °C for 24 h before imaging.

further indicates that the presence of increased POPC vesicles reduces hCT nucleation by reduction of the effective monomer concentration in solution, leading to fibril inhibition. It should also be noted that as the concentration of liposomes increase, there is a fast increase in ThT intensity within 2-3 h of incubation and then swiftly decreases afterward. This likely indicates the inhibition of the elongation of hCT intermediates, which are further sequestered by the POPC liposome vesicles. AFM images of hCT in the presence of 25 μM and 1000 μM shows that there are only amorphous aggregates and spherical oligomeric intermediates, indicating hCT fibril inhibition (Figures 33D and 33E).

Since the 50 nm POPC liposome vesicles have a smaller diameter, they would exhibit higher curvature compared to their larger 200 nm POPC liposome counterparts. Also, the tubules of 50 nm POPC liposomes formed by hCT deformation may exhibit higher curvature compared to the 200 nm POPC tubules. This means that the head groups would be further apart from each other and have an increased number of water-accessible hydrophobic regions for the hCT peptide to bind to. This may cause a stronger and greater number of hCT peptides to bind to the vesicles compared to the 200 nm POPC vesicles. These interactions would further prevent the self-association and elongation needed to form the critical nuclei that is needed to form fibrils. Elbassal et al. reported that $A\beta_{40}$ binds more strongly to DC-cholesterol vesicles of higher curvature which led to enhanced amyloid inhibition in a concentration-dependent manner.[115] Similar results were seen with DC-cholesterol in Chapter II with hCT.[58] However, it should be noted that the head group of DC-cholesterol contains a positively charged tertiary amine whereas the head group of POPC contains a quaternary ammonium cation which may be a contributing factor in their common ability to cause hCT inhibition. Additionally, there would be a greater number of

50 nm POPC liposomes than 200 nm POPC liposomes at the same concentration. The combination of additional 50 nm POPC vesicles with higher curvature may make it more difficult for hCT to aggregate and form fibrils due to their stronger binding to the surface of the vesicles. Also, the binding to a greater number of 50 nm POPC vesicles would reduce the effective hCT monomer concentration, leading to the delay and inhibition of hCT amyloid formation. Van der Waals interactions between hCT and the liposome vesicles may also be a contributing factor to the liposome inhibiting activity as well.

4.4 Conclusions

In conclusion, we report the effects of concentration, size and curvature of POPC and POPG liposomes on their inhibitory activity towards hCT fibril formation. The presence of either POPC or POPG liposome vesicles show inhibition of hCT fibril formation in a concentration-dependent manner. However, zwitterionic POPC liposomes exhibit a stronger inhibitory effect than the negatively charged POPG liposomes. The potential electrostatic interactions between the sulfate group of POPG and the lysine residue of hCT may allow hCT to bury deep into the lipid bilayer where fibrillization is avoided. In contrast, hCT monomers are able to associate with the surface of POPC liposomes through hydrophobic and weak electrostatic interactions that can act as a seed for the creation of nucleation points that can enhance hCT fibrillization. The binding of hCT may cause POPC and POPG liposomal vesicles to deform into tubular shapes of high curvature which exposes water-accessible hydrophobic regions that hCT can bind to, thus enhancing inhibition. However, the dimensions of these tubules vary between POPC and POPG which may be a contributing factor in their difference in inhibition of hCT. The smaller 50 nm POPC vesicles exhibit higher curvature than their larger counterparts which

may make them superior for hCT amyloid inhibition due to the exposure of an increased number of water-exposed hydrophobic regions. In addition, the binding of hCT to liposomal vesicles will ultimately reduce the effective monomer in solution. This would lead to a reduction in hCT self-association and inhibit fibril formation as the concentration of the liposomal vesicles increase. Furthermore, van der Waals interactions and hydrogen bonding between the phosphate group of the vesicles and select amino acids in hCT may aid in their inhibitory activity as well. These findings provide new insights into the mechanism of how hCT interacts with cellular membranes. Future studies will include the incorporation of cholesterol and cholesterol sulfate in these liposomes to be more physiologically relevant. This will aid in the development of novel inhibitors to prevent the formation of hCT amyloid fibril and excessive channel formation.

APPENDIX A:

Vibrational Approach to the Dynamics and Structure of Protein Amyloids

This appendix was adapted from the following publication

> Li H., Lantz R., and Du, D. (2019) Vibrational Approach to the Dynamics and Structure of Protein Amyloids. *Molecules* 24, 186

Abstract

Amyloid diseases, including neurodegenerative diseases such as Alzheimer's and Parkinson's, are linked to a poorly understood progression of protein misfolding and aggregation events that culminate in tissue-selective deposition and human pathology. Elucidation of the mechanistic details of protein aggregation and the structural features of the aggregates is critical for a comprehensive understanding of the mechanisms of protein oligomerization and fibrillization. Vibrational spectroscopies, such as Fourier transform infrared (FTIR) and Raman, are powerful tools that are sensitive to the secondary structure of proteins and have been widely used to investigate protein misfolding and aggregation. We address the application of the vibrational approaches in recent studies of conformational dynamics and structural characteristics of protein oligomers and amyloid fibrils. In particular, introduction of isotope labelled carbonyl into a peptide backbone, and incorporation of the extrinsic unnatural amino acids with vibrational moieties on the side chain, have greatly expanded the ability of vibrational spectroscopy to obtain site-specific structural and dynamic information. The applications of these methods in recent studies of protein aggregation are also reviewed.

1. Introduction

Protein aggregation and amyloid formation has become an important topic in protein biophysics as well as in molecular medicine, in part because amyloidogenesis of a number of aggregation-prone proteins has been recognized as a common pathogenic event in a variety of human diseases including Alzheimer's, Parkinson's, Huntington's, type II diabetes, and others [1,2]. In 1854, Rudolph Virchow coined the term amyloid [3]. Amyloids are protein aggregates composed of insoluble fibers with monomeric strands packed in a cross-β pattern that are stabilized by interstrand interactions such as hydrogen bonding, electrostatic interactions, aromatic interactions (π–π stacking), and hydrophobic interactions [4,5]. The amyloid fibrils themselves, however, are not necessarily the major toxic species. Growing lines of evidence has indicated that the oligomeric intermediates formed during protein fibrillization appear to be more toxic and responsible for neurological damage in some neurodegenerative diseases [6,7]. There is therefore great interest in elucidating the mechanistic details of protein aggregation and the molecular structures formed along the aggregation pathway, for a more comprehensive understanding of the mechanisms of protein oligomerization and fibrillization and development of pharmacological means to ameliorate amyloid toxicity.

Protein amyloid formation is usually proposed as a nucleated polymerization mechanism in vitro (Figure 1) [8–10]. The rate limiting step of this process is the formation of the oligomeric nucleus, the highest energy species on the amyloidogenesis pathway. After the nucleus is formed, additional monomeric peptides or oligomers can be added in a step that is thermodynamically favorable, leading to a fast growth phase to the fibrillar forms (Figure 1). In the past two decades, a combination of widespread techniques has

been employed in studying the dynamics of protein amyloidogenesis and the structures of the aggregated species. The cross-β-sheet fibrils can be selectively detected by fluorescent dyes Congo red and thioflavin T (ThT) [11,12]. Techniques such as electron microscopy [13], atomic force microscopy (AFM) [14,15], small-angle X-ray scattering [16], solid/solution state NMR [17–20], have been used extensively to explore the morphology and structural characteristics of the mature fibrils and oligomeric intermediates. X-ray crystallography, a powerful tool for determining the three-dimensional structure of proteins, has also been employed recently to study amyloid structures formed by relatively short peptides at atomic resolution [21]. However, crystallization of amyloids of larger peptides/proteins is still difficult.

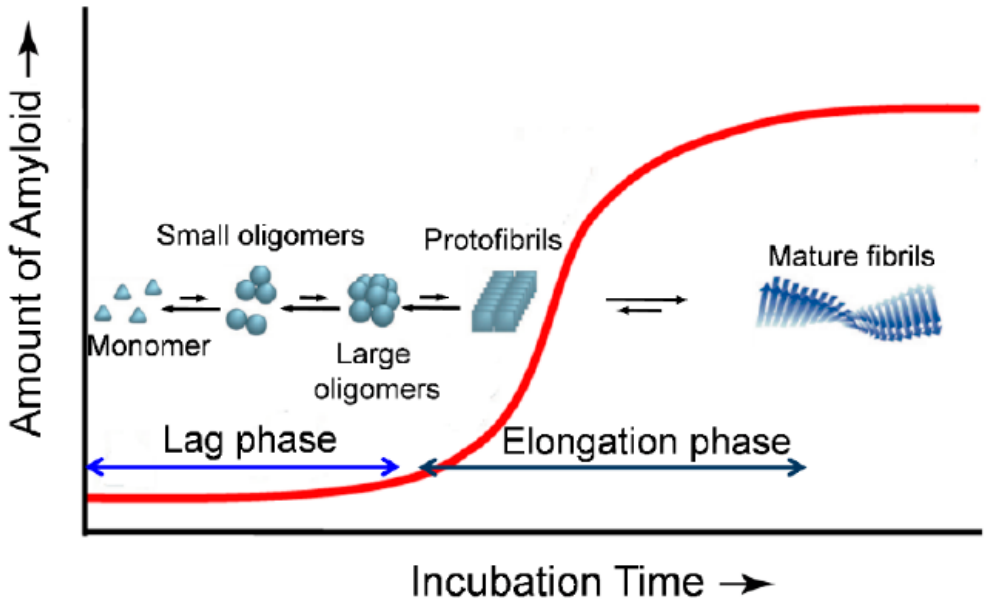

Figure 1. Schematic representation of a typical nucleated polymerization process of protein aggregation. Oligomeric nuclei are formed in the early lag phase stage, being a critical rate limiting step. In an elongation phase, addition of monomers and/or oligomers onto the nucleus allows formation of fibrils which is energetically favorable.

Vibrational spectroscopies, such as infrared (IR) and Raman, are classical methods for investigation of protein structure, dynamics, folding/unfolding, and misfolding [22–

24]. The molecular vibrations of proteins can be monitored with IR and Raman spectroscopy on the picosecond timescale when used in conjunction with a femtosecond laser [25]. In IR spectroscopy, infrared radiation is used to excite the vibrational modes of the molecule of interest due to a net dipole change [26]. Most molecules, except for homonuclear diatomic molecules, show IR absorption. Technically, Fourier transform infrared (FTIR) spectroscopy is widely used because of its high signal-to-noise ratio, fast data acquisition, and reliable digital subtraction [26,27]. Unlike IR spectroscopy, Raman spectroscopy uses the polarizability of the molecule instead of the net dipole change to observe molecular vibrations. In Raman spectroscopy, the incident radiation excites the sample and causes inelastic scattering where the scattered light is either higher or lower than the incident radiation [28]. Raman spectroscopy shows strong potential for providing noninvasive structural information of proteins. Different techniques, e.g., ultraviolet resonance Raman (UVRR) spectroscopy with higher sensitivity than conventional Raman spectroscopy, have also been successfully applied for studies including protein structures and protein–protein interaction.

Protein misfolding and amyloidogenesis is always associated with changes of secondary structures. The high sensitivity of the vibrational spectroscopies to the secondary structure of proteins makes them particularly valuable for studying the conformational dynamics in protein self-assembly and amyloid formation. The vibrational spectroscopies are well suited for determining the structural features of proteins both in solution and as insoluble aggregates. In addition to the determination of the global structural changes from analysis of the backbone vibration, recent applications of site-specific approaches, such as isotopic labeling of specific amino acid(s) [23], and use of unnatural amino acids with

unique mutated side chains (e.g., nitrile, thiocyanate, azide) as vibrational probes [24], has greatly expanded the application of vibrational spectroscopies to explore local dynamics and conformational changes with residue specific resolution. In this paper, we attempt to review some recent research achievements of protein aggregation and amyloidogenesis studies using vibrational approaches including the backbone amide band, isotopic decoupling, and side chain vibrational probes.

2. Backbone Vibrational Probe

In the mid-IR region, a polypeptide or protein vibration spectrum that covers the 400 to 4000 cm^{-1} range can be characteristically described as nine frequency regions according to different modes of vibrations [29,30]. Of these, the two most prominent vibrational band regions of proteins are amide I (1610–1700 cm^{-1}), arising primarily from the C=O stretching vibration, and amide II (1480–1600 cm^{-1}), mainly deriving from the combination of the NH in-plane bend and CN stretching vibration [31]. In particular, the amide I vibration is little affected by the nature of the side chain, and mainly depends on the secondary structure of the backbone. Therefore, the amide I band is the most sensitive spectral region to protein secondary structures of α-helix, β-sheet, turn, and disordered conformations [32–35]. From the amide I band, one can differentiate between different secondary structures. The absorbance range in the amide I band for a particular secondary structure is summarized in Table 1. For instance, random coil structures show a broad amide I band located at 1640–1650 cm^{-1} [36], while the α-helices and β-sheets have amide I frequencies at approximately 1655 and 1630 cm^{-1}, respectively [36,37].

Table 1. Assignment of amide I band positions to secondary structure [30].

Secondary Structure	Band Position in H_2O/cm^{-1}		Band Position in D_2O/cm^{-1}	
	Average	Extremes	Average	Extremes
α-helix	1654	1648–1657	1652	1642–1660
β-sheet	1633	1623–1641	1630	1615–1638
β-sheet	1684	1674–1695	1679	1672–1694
Turns	1672	1662–1686	1671	1653–1691
Disordered	1654	1642–1657	1645	1639–1654

Based on the experimental data and assignments of various authors collected and evaluated by Goormaghtigh et al [38].

Amyloidogenic peptides, when aggregated, normally exhibit a characteristic cross-β-sheet structure [2,39]. This structure can be probed sensitively by analyzing the amide I band in vibrational spectroscopy. The native β-sheet features an amide I band at 1630–1640 cm^{-1}, whereas the amide I band of the aggregated amyloid β-sheets is generally in the range of 1610–1630 cm^{-1}, possibly due to being in a more hydrophobic environment and formation of stronger hydrogen bonding [40,41]. More ordered fibers absorb at around 1620 cm^{-1} while more disordered fibers absorb at approximately 1635 cm^{-1} due to stronger coupling [42]. In addition, amyloid fibrils may be composed of parallel or antiparallel _-sheets. In comparison to parallel β-sheets, antiparallel β-sheets exhibit an additional weaker high frequency amide I transition at approximately 1670–1690 cm^{-1} [32,41].

When probing proteins in solution with FTIR, D_2O is normally used instead of H_2O due to the strong water bending mode that overlaps the amide I vibrational mode [43]. The spectrum analysis methods like Fourier self-deconvolution, second derivative, and curve-fitting, are commonly used to acquire the secondary structural information. For sampling methods, besides the conventional transmission measurement, attenuated total reflectance (ATR) where the sample is placed on a crystal that has an index of refraction larger than the sample itself, is also commonly used [26]. This technique is advantageous in certain

aspects because of the very short pathlength into the sample. It is more amenable to study aqueous samples and the sample preparation is generally much simpler. Moreover, in the past two decades, two-dimensional infrared spectroscopy (2D-IR) has been established as a powerful tool to determine the dynamics of proteins structures in complex systems with high temporal resolution [44,45]. 2D-IR spectroscopy is sensitive to protein secondary structure, vibrational coupling, and solvent exposure based on frequencies and cross-peaks. In comparison to FTIR, 2D-IR allows the resolution of cross-peaks, which reveal coupling between different vibrational modes. Unlike FTIR spectroscopy, 2D-IR signals scale with the fourth power of the transition dipole moment, resulting in enhanced resolution of peaks in the spectra [46]. In Raman spectroscopy, the H_2O bending vibration mode that obscures the amide I band in IR spectroscopy has a low intensity, obviating the need to use D_2O in Raman spectroscopy measurement, and reduces the errors inherent in large solvent background subtractions.

With these vibrational techniques, one can study structure characteristics of protein aggregates, and probe the conformational dynamics in real-time along the aggregation process. Discussed below, are examples of some recent studies in the structural properties and kinetics of aggregation of a number of amyloidogenic peptides/proteins using the backbone vibrational probe.

2.1 Amyloid-β

Alzheimer's disease (AD) is the most common neurodegenerative disorder. One of the hallmarks of AD is the formation of extracellular deposits of amyloid-β (Aβ) in the brain. Aβ peptides are cleaved from the amyloid-β precursor protein (APP) and aggregate to form oligomers and then ultimately to insoluble fibrils that are made up of β-sheets [47].

The majority of the secreted Aβ peptides are $A\beta_{1-40}$ and $A\beta_{1-42}$, which start at Asp1 and end at either Val40 or Ala42, respectively. Compelling genetic, biochemical and pathological evidence indicates that the etiology of AD is mechanistically linked to the production and aggregation of Aβ [48,49]. A growing body of recent studies has suggested that the oligomeric, diffusible assemblies of Aβ peptides formed in the early stages of aggregation, rather than the mature amyloid fibrils, may be the primary neurotoxic species in AD. The mechanisms of the conformational changes in the formation of oligomers and fibrils of Aβ therefore have been the subject of numerous in vitro studies. FTIR spectroscopy has been extensively used to study the conformational dynamics and the alignment of β-strands in the formation of Aβ oligomers and amyloid fibrils in vitro. In an ATR-FTIR study, Sarroukh et al. reported that conversion of $A\beta_{1-40}$ oligomers into fibrils results from a transition from antiparallel to parallel β-sheet, by observing a progressive vanishing of a peak at 1695 cm^{-1} which is typical of an antiparallel arrangement of the β-strands [50]. The presence of an amide I band at ~1630 cm^{-1} in the intermediates suggests the formation of β-sheet structure in oligomers. The signature of this low frequency β-sheet band in $A\beta_{1-40}$ oligomers was also reported in another recent study of Klementieva et al. [51]. A broad band centered around 1640cm^{-1} (black, M) corresponds to unstructured $A\beta_{1-40}$ monomers (Figure 2). A band centered at around 1623cm^{-1} (blue, F) suggests the existence of fibrillar β-structures of amyloids. Importantly, as shown in Figure 2, the $A\beta_{1-40}$ oligomers prepared in the presence of ions of Cu(II) show a peak at about 1630cm^{-1} (red, Õ), which indicates the presence of β-sheets, although the electron microscopy, small angle X-ray scattering and ThT spectroscopy data support the non-fibrillar nature of these $A\beta_{40}$ oligomers. The secondary structural features of the oligomers can therefore be

discriminated from that of the amyloid fibrils. The spectroscopic signatures of the stable amyloid fibrils have been also distinguished from oligomeric intermediates using more sensitive 2D-IR spectroscopy. A unique transition at 1610 cm^{-1} is observed in the 2D-IR spectra of the mature fibrils of both $A\beta_{1–40}$ and $A\beta_{1–42}$ [52]. This band does not appear in other Aβ aggregates including β-sheet-structure-like oligomers, and is not seen in linear IR spectroscopy because it is occluded by the broad band at ~1625 cm^{-1}. Interestingly, the 1610 cm^{-1} band still exists even when the Aβ aggregates are solubilized in sodium dodecyl sulfate (SDS), indicating that the 1610 cm^{-1} transition corresponds to highly stable amyloid species that are not disaggregated by SDS.

IR spectroscopy has also been applied to illuminate the secondary structure characteristics of Aβ in complex biological conditions. In a study of Klementieva et al., the FTIR spectra maps were recorded in brain sections of both AD transgenic Tg19959 mice and wild-type mice to identify the increase of β-sheet contents in AD mice over time [51]. Similarly, FTIR spectroscopy was used to compare the structural characteristics of the Aβ aggregates formed in vivo to that formed by chemically induced aggregation ex vivo [53]. Recently, Wiltfang and co-workers developed an immune-infrared sensor to measure the Aβ peptide secondary structure distribution in cerebrospinal fluid (CSF) and blood plasma [54]. The amide I band frequency downshifts to a β-sheet secondary structure in Dementia Alzheimer type patients, and the discrimination between the Dementia Alzheimer type patients and the disease control patients reaches an accuracy of 90% for CSF. This kind of method holds a promise for simple, robust, and label-free diagnosis of this devastating disease.

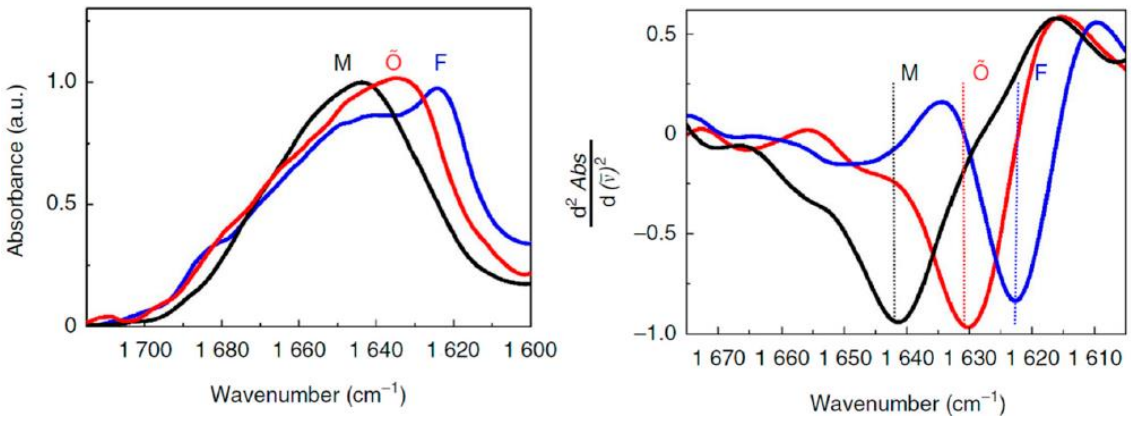

Figure 2. Left panel: normalized FTIR spectra of $A\beta_{1-40}$ monomers (M) in 10 mM HEPES/D_2O pD11, fibrils (F) after 24 h incubation in 10 mM HEPES pD7.4, and Cu(II)-induced oligomers ($A\beta_{1-40}$-Cu(II)Õ) after 24 h incubation at 37 °C, pD7.4 [51]. **Right panel**: second derivatives of the FTIR spectra. Reprinted with permission.

2.2 Islet Amyloid Polypeptide

Human islet amyloid polypeptide (IAPP) is a 37-residue peptide hormone secreted by pancreatic β-cells that acts with insulin as a regulator of glucose homeostasis. IAPP is a natively disordered and highly amyloidogenic peptide that easily self-assembles into amyloid fibrils via a multistep process. The aggregation and amyloid formation of IAPP is strongly associated with β-cell degeneration in type II diabetes [55,56]. Similar to Aβ, it has been proposed that the oligomers of IAPP might be the major toxic species that lead to β-cell death [57]. The structural characteristics of the IAPP oligomers have also been investigated by vibrational spectroscopy. Rawat and co-workers used both FTIR and Raman spectroscopy to investigate the conformation of the peptide chain in the different aggregation states of IAPP [58]. Both FTIR and Raman spectra of the IAPP oligomers suggest a predominantly α-helical conformation (together with significant β-sheet content) of the peptide chain in the oligomeric state, while in fibrils the peptide is predominantly in a β-sheet conformation. This is consistent with circular dichroism (CD) studies of IAPP revealing the formation of α-helical states in IAPP aggregation [59]. 2D-IR spectroscopy

is also applied to discriminate different secondary structural elements during amyloid formation without the need of deconvolution of the spectra [60]. Abedini et al. performed a 2D-IR study on IAPP oligomers to define the structural properties of the toxic IAPP intermediates [61]. Their results indicated that the more toxic oligomers contain flexible and low order structure with modest overall β-sheet and α-helical content.

The structural features of the mature fibrils of IAPP and their different isoforms have also been studied by vibrational spectroscopy of the backbone. Zanni and co-workers used 2D-IR to investigate the structural diversity of the amyloid fibrils of human IAPP [62]. The presence of an inhomogeneously broadened β-sheet peak and strong coupling to random coil conformations reveals a large structural distribution of the fibrils. In a later publication, they analyzed the secondary structural properties of human IAPP and rat IAPP in solution, membrane, or micelle bound forms by measuring the transition dipole strengths of the samples using both 1D and 2D-IR spectroscopy [63]. The amide I band has also been used to evaluate the function of inhibitors in blocking IAPP aggregation [64–67]. The inhibition activity of small compounds, such as rhodamine derivatives and red wine compound resveratrol, on IAPP aggregation was confirmed by monitoring the amide I band change using ATR-FTIR [64,65]. Using similar methods, Sellin et al. reported that a non-amyloidogenic human IAPP analog and a hexapeptide have strong inhibitory effects on IAPP fibrillization at the membrane interface, suggesting that these peptides may be able to suppress pathogenic self-association of IAPP also in vivo [66].

2.3 α-Synuclein

Parkinson's disease (PD) is the second most common neurodegenerative disorder characterized by formation of cytosolic inclusions known as Lewy bodies in the neurons

of the brain [68]. α-Synuclein, a 140-residue presynaptic protein, has been shown to be a major fibrillar component of Lewy bodies, and the mutations to the α-synuclein gene cause early onset of PD [69–71], implicating the aggregation of α-synuclein as a key step in the etiology of PD. Along with Aβ and IAPP, it has been suggested that the oligomeric species of α-synuclein are more toxic than mature fibrils to cause neuronal death [72]. While being natively disordered under neutral pH, α-synuclein is transformed into a partially folded conformation with a significant amount of β-structure at acidic pH, evidenced by appearance of a new band in the vicinity of 1626 cm^{-1} [73]. The amide I absorption of α-synuclein in the oligomer-forming conditions exhibits a band at 1625 cm^{-1} along with a prominent shoulder at 1695 cm^{-1}, indicating the components of antiparallel β-sheet structure in oligomers; whereas the amyloid fibrils displayed the typical parallel β-sheet features characterized by a maximum band at 1628 cm^{-1} [74]. However, a deconvolution analysis of the FTIR spectra of α-synuclein and three variants reveals the antiparallel β-sheet structure in α-synuclein fibrils [75]. These contradictory results may imply the sensitivity of the structure of α-synuclein aggregates to environments. Indeed, a recent study of Roeters et al. using a combination of FTIR, 2D-IR and AFM suggested that α-synuclein fibrils formed in low-salt buffers are composed of loosely packed parallel β-sheet structure with extended conformation, while the fibrils formed in high-salt buffers mainly adopt a more tightly-packed, antiparallel intramolecular conformation [76].

In addition to IR, Raman spectroscopy has also been applied to characterize the conformation of the natively unfolded α-synuclein in various solvents before fibrillization using Raman amide I and III (which is also sensitive to secondary structure) bands [77–79]. The amide III band is a combination of CN and NH stretching in the region of 1200–

1340 cm^{-1} [80]. This band is also known to be structurally sensitive owing to its dependence on the psi and phi dihedral angles [80–82]. The Raman studies on monomeric α-synuclein, conducted by Anderson group, showed that the secondary structure is largely α-helical in hexafluoro-2-propanol (HFIP) and SDS, and predominantly β-sheet in 25% methanol in H_2O [77]. The characterization of the secondary structure of α-synuclein oligomers by analyzing the Raman amide I band profiles showed that the spherical oligomers have a significant amount of α-helical structure [78], which decreases in protofilaments and filaments accompanied by the increase of the β-sheet structure. Upon filament formation, the Raman amide I band narrows dramatically accompanied by a red shift of the peak maximum, consistent with a progressive increase in β-sheet structure and the formation of more ordered aggregates.

2.4 Examples of Other Disease-Associated Proteins and Model Peptides

In addition to the aforementioned amyloidogenic proteins, the backbone amide I spectra have been widely used in aggregation studies of other disease-associated amyloidogenic proteins, e.g., crystallin [83], prion [84,85], polyglutamine (polyQ) [86], and model peptides [87,88]. For instance, deposits of aggregated crystallin on the lens of the eye cause blurred vision or blindness in cataracts. The antiparallel β-sheet structure was identified by FTIR when γD-crystallin was incubated at acidic pH mimicking the lysosome compartments of the eye [83]. In a recent study, although not observable in TEM imaging because of the small size, Zhang et al. was able to identify the formation of the ordered β-sheet amyloid structure of γD-crystallin in UV-induced cataracts of porcine lenses, owing to the enhanced sensitivity of 2D-IR to amyloid β-sheet secondary structure by non-linear scaling of 2D-IR intensities and cross peaks [89]. Such pioneering work expands the ability

of application of 2D-IR spectroscopy in more complex tissues studies. Taken together, the vibrational spectrum arising from protein backbone have been continuously employed as a versatile and convenient method for identifying the secondary structural features and monitoring the conformational dynamics of both the metastable oligomers and the mature fibrils of amyloidogenic proteins with distinct primary sequences. Differentiating the structural characteristics of oligomers from fibrils may be crucial for understanding the strong cytotoxicity of the oligomeric species.

3. Isotopic Labeling Probe

The amide I band of peptides and proteins is generally applied as a global probe of the assembled secondary structures, but it is hard to be assigned to specific residues or local regions of the protein. To overcome this limit, development of site-specific isotopic labelling method combined with vibrational spectroscopy, has greatly advanced the ability of vibrational approaches to provide information of protein structure and dynamics with higher resolution [90–92]. Isotopic editing allows one to replace residue(s) of interest with analogues bearing an isotope-labeled $^{13}C=^{16}O$ or $^{13}C=^{18}O$ carboxylic group in a noninvasive manner [93–95]. Labelling with $^{13}C=^{16}O$ induces ~40 cm^{-1} red shift of the amide I frequency, and labeling with $^{13}C=^{18}O$ induces a more significant red shift of ~65 cm^{-1} [23,24,96], allowing the frequency of the labeled residues resolved from the bulk unlabeled amide I frequencies. Because of this great advantage, there is already a wealth of studies to identify the local conformational dynamics in protein folding using isotope-edited vibrational spectroscopy [97–101]. Here, we address some of the recent accomplishments of this technique in exploring local structural characteristics along the formation of oligomers and amyloid fibrils of amyloidogenic proteins, e.g., Aβ and IAPP.

3.1 Amyloid-β

Although the parallel β-sheet structure has been well resolved in amyloid structures of $A\beta_{1-40}$ and $A\beta_{1-42}$, a shorter Aβ fragment, $A\beta_{16-22}$, forms aggregates with antiparallel in register β-sheet with the central residue (Phe19) in alignment across all the strands, validated by the FTIR study of a series of $A\beta_{16-22}$ mutants with a single $^{13}C=^{16}O$ label or two residues labeled simultaneously [102]. This result is consistent with a following study of Shanmugam et al. through isotope-assisted vibrational circular dichroism [103]. In a recent study, Hochstrasser and co-workers incorporated $^{13}C=^{18}O$ isotopic substitution to five residues of $A\beta_{1-40}$, respectively, and investigated the 2D-IR spectra of the isotopically diluted amyloid fibrils of $A\beta_{1-40}$ [104]. Their results identified 1D excitation formed by the isotope dilution of parallel in-register β-sheets. The variability of the spectral shifts of the amide I modes for different residues further reveals a structural and/or environmental heterogeneity of the fibrils. To elucidate the structure features of monomeric Aβ, Zhuang et al. investigated the spectral characteristics of $A\beta_{1-42}$ conformers by simulating the 2D-IR spectra of Aβ with $^{13}C=^{18}O$ labels at 31–34 and the 38–41 regions [105], which are basically random coil in the monomeric state. In addition, the residue-specific binding of the copper ion with the N-terminal region of Aβ at various pH conditions was also identified by ATR-FTIR spectroscopy in combination with isotopic labeling of the amino acids involved in the coordination sphere [106].

Isotopic labelling was also applied to investigate Aβ aggregation under different environments. There is accumulating evidence suggesting that membranes play a crucial role in amyloidogenesis of Aβ under physiological conditions. Ganglioside GM1 is abundant in the brain and has multiple roles in the function of the brain. It has been

demonstrated that GM1 can act as a seed for Aβ growth and the fibrils formed are more toxic than fibrils grown in aqueous solution [107]. Okada and co-workers conducted ^{13}C labelled FTIR to distinguish the structural characteristics of $A\beta_{1-40}$ fibrils formed in aqueous solution or on GM1 clusters, and their results suggested a novel mixed parallel and antiparallel β-sheet structure formed on GM1 clusters with almost the entire sequence of Aβ included in the β-sheet [108]. Their findings also showed that GM1 bound fibrils formed faster, had a flat tape like structure, and exhibited stronger hydrogen bonding than fibrils grown in aqueous solution [108,109]. Isotopic labeling was also applied to reveal the vibrational frequency dynamics of 18 individual residues between Val12 and Val39 of $A\beta_{1-40}$ fibrils, to identify the presence of water at specific locations in the fibril [110]. There was water trapped within the fibrils even after years of incubation [111]. This observation was later supported by molecular simulations on $A\beta_{1-40}$ in two different protonation states (one ionized and one neutral) [112]. The authors compared the simulation results to the isotope-edited 2D-IR experiment and concluded that water molecules trapped inside the fibrils play a major role in the frequency fluctuation.

3.2 Islet Amyloid Polypeptide

Isotopic labeling has also been used to probe the aggregated structure of human IAPP. In one example, $^{13}C=^{18}O$ isotopic labels were put in seven positions along the human IAPP sequence. The results, in combination with the experiments and simulations, showed that the amide I frequency corresponding to a β-sheet is sensitive to the length of β-sheet and the position of isotopic labels [46]. A high frequency at ~1665 cm^{-1}, assigned to coupling in the turn region, was also observed and sensitive to the label position within the turn. In a follow-up study, Zanni and co-workers monitored the kinetics of IAPP

aggregation at six isotopically labeled sites [113]. For example, as depicted in Figure 3, for the IAPP mutant with $^{13}C=^{18}O$ label at Ala25, the 2D-IR spectrum shows that the isotope-labeled features appear near 1580 cm^{-1}. The difference spectra highlight that concurrent with the growth of the β-strand, 2 isotope-labeled features appear at 1574 and 1585 cm^{-1}. The growth of the large cross-peaks between the isotope labels and the unlabeled β-strand peak at 1617 cm^{-1} indicates that Ala25 is strongly coupled to the β-sheets. Interestingly, the kinetic traces of the intensity of the peaks for the unlabeled β-strand, Ala25, and the cross-peak as a function of time are virtually identical, indicating a direct assembly of the Ala25 residue into a β-strand structure when it becomes part of the ordered fibril structure. A detailed multistep aggregation pathway of IAPP starting with formation of nucleus at the loop region was proposed accordingly from this thorough residue-specific amyloidogenesis study [113]. Since parallel β-sheet formation seems to be significant in the formation of IAPP amyloids, the vibrational coupling was further systematically investigated by six combinations of doubly $^{13}C=^{18}O$ isotopic labeling in a synthetic cyclic peptide containing parallel β-sheet structure to establish calculated and experimentally verified coupling models that link spectra to structure [114]. Furthermore, the disruptive effect of a post-translational modification, deamidation of asparagine and glutamine, on N- and C-terminal β-sheet in IAPP amyloid structure was also elucidated by Zanni group using isotope-edited 2D-IR [115].

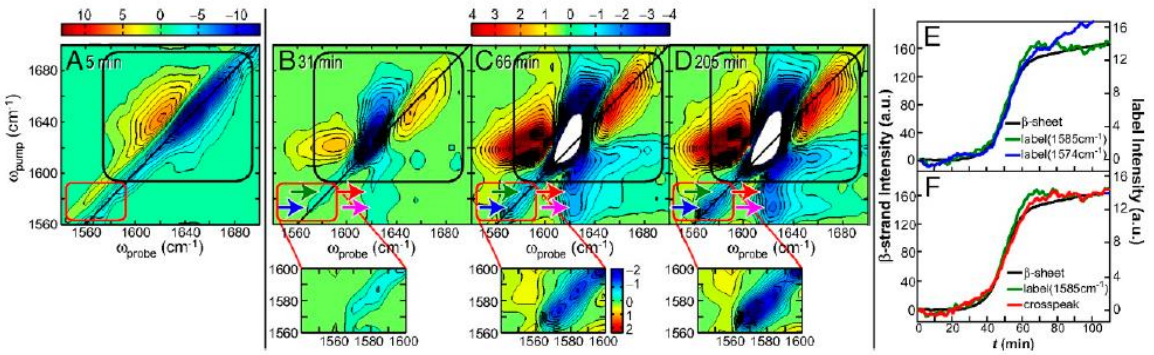

Figure 3. 2D-IR spectra and kinetics curves of human IAPP with $^{13}C{=}^{18}O$ labeled at the Ala25 residue [113]. (**A**) The first 2D-IR spectrum at t = 5 min. (**B**–**D**) Difference 2D-IR spectra at t = 31, 66, and 205 min, calculated by subtracting the t = 5 min spectrum. Black boxes surround the spectral features of the unlabeled portion of the peptide, whereas red boxes enclose the diagonal peaks of the isotope labeled Ala25. Blue and green arrows highlight the 2 labeled features, whereas magenta and red arrows point to the cross-peak between the $^{13}C{=}^{18}O$ Ala25 and the unlabeled β-sheet. (**E**) Kinetics of the diagonal peaks of the unlabeled β-sheet at 1617 cm^{-1} and the 2 label features (blue and green arrows). (**F**) Comparison of the kinetics of the cross-peak and the diagonal peaks. Reprinted with permission.

The structural properties of the transiently populated oligomers of IAPP have also been probed using isotopic labels. By using 2D-IR coupled with isotopic $^{13}C{=}^{18}O$ labelling, Buchanan et al. discovered that an oligomeric intermediate containing a parallel β-sheet structure extending over a hydrophobic fragment 23–27 (FGAIL) forms in the lag phase of IAPP amyloid formation [116]. This local hydrophobic region initially starts out as a random coil structure and evolves into β-sheet oligomers, then is disrupted and forms partially disordered loop during fibril formation [117]. A further study by isotopically labeling two neighboring amino acids in IAPP showed that up to 38% of monomeric IAPP peptides in aqueous solution adopt an α-helical structure at the L12A13 region, but not at the L16V17 residual region [118]. The N-terminal helices of IAPP monomers may help seed IAPP oligomer formation by stabilizing small β-sheet oligomers.

In addition, isotopic labelling has been applied to identify the structural information of amyloid-inhibitor complexes [116,119]. Rat IAPP has been found to be a modest inhibitor of human IAPP aggregation [120]. The residue-specific structural information of human IAPP-rat IAPP complex was studied using isotope-edited 2D-IR spectroscopy [119]. The results showed that rat IAPP inhibited the N-terminal β-sheet instead of the hypothesized C-terminal β-sheet of the human IAPP. Interestingly, it was found that the rat IAPP formed its own β-sheet which was not previously recognized. This kind of study provides residue-specific details of the inhibition mechanism, and may illuminate the development of novel means for blocking IAPP aggregation via targeting the key local residues/regions involved in the oligomer and amyloid formation.

3.3 Examples of Other Disease-Associated Proteins and Model Peptides

The local mechanistic details of aggregation of γD-crystallin were thoroughly investigated by the Zanni group using isotopic labelling 2D-IR [121–124]. The ^{13}C labeled N-terminal or C-terminal domains of γD-crystallin were expressed to prepare the full-length protein via protein ligation, and the 2D-IR studies demonstrated that the C-terminal domain is the fibril nucleation site and forms amyloid β-sheets, whereas the N-terminal domain is largely disordered while lying in close proximity to the β-sheets [121]. Misfolding and conformational conversion of prion protein (PrP) into β-sheet rich aggregates is associated with a group of fatal neurodegenerative disorders also known as prion diseases. The structure and mechanism of the aggregation of the prion peptide H1 (residues 109–122 of the prion protein) was addressed using isotope-edited FTIR [125,126]. The residue-level alignment of a kinetically trapped intermediate with antiparallel β-sheet and the subsequent rearrangement of the structure into a more stable

conformation with nonexponential local kinetics were reported [127]. In addition, the β-sheet packing pattern of the oligomers and fibrils of the model polyglutamic acids was studied by Keiderling and co-workers using the ^{13}C labelled ATR-FTIR and vibrational CD (VCD) spectra [128]. They deduced that the oligomers are made up of antiparallel β-sheets that are stacked and twisted. The amyloid fibril structure and aggregation kinetics of a model polyQ peptide was also investigated by Buchanan et al. via studying fibril formation of a mixture of ^{12}C and ^{13}C protein mixtures [129]. Investigation of the structural ordering in aggregation of a synthetic hexapeptide $AcWL_5$ with a single isotopic label in the presence of lipid bilayer via 2D-IR provides novel insight into the residue-level structural ordering of the aggregated peptide in membrane environments [130,131]. Elucidation of the mechanistic roles of the key residues and local regions in protein aggregation significantly facilitates a comprehensive understanding of the mechanisms of protein amyloidogenesis, and will illuminate future simulation approaches to address protein aggregation process at an atomic-level.

4. Side Chain Vibrational Probe

Albeit the power of the isotopic labelling in studying high resolution dynamics of proteins, the method has its own limitations. The natural abundance of ^{13}C of ~1% can cause a significant fraction of $^{13}C=^{16}O$ amide I modes at random positions. In addition, isotope labeled amide I vibrations are normally located at the 1550–1600 cm^{-1} region, where it is often congested with side-chain vibrations from some of the amino acids [132]. In the past decade, alternative strategies of development and application of extrinsic vibrational probes, many of which are unnatural amino acids with vibrational moieties at the side-chain, have also received great interest for improving the structural resolution of

vibrational spectroscopy at a site-specific level. Many of the suitable labels show a vibrational spectrum window at a much less congested region, e.g., between 1900 and 2900 cm^{-1} [133]. These probes can sensitively detect side chain environmental changes and the interactions that don't necessarily involve the backbone. In order to be useful for monitoring the local dynamics, the probe should be sensitive to the local environment with a relatively intense absorption in a frequency region that is not overcrowded with other vibrations, and importantly, it should cause minimal structural perturbation of the target molecules [134]. Up to now, a large group of useful vibrational probes have been developed and successfully employed in studying monomeric protein structure and dynamics, which are summarized in a number of reviews [24,135,136]. Here, we will more specifically focus on the application of some vibrational probes including azide, nitrile, and ester carbonyl, in studying local dynamics and environmental information in protein amyloidogenesis. There is no doubt that the application of side chain vibrational probes in protein aggregation studies is not restricted to the ones discussed below. It is expected that other extrinsic vibrational moieties, e.g., thiocyanate [137,138], carbon-deuterium (C-D) [139–141], may also be employed as valuable local probes in future protein misfolding and aggregation studies.

4.1 Azide Probe

Azide-functionalized amino acids, such as β-azidoalanine, azidohomoalanine, and *para*-azidophenylalaline normally show an asymmetric stretch vibration in the region of ~2100 cm^{-1} [133,142]. This region is uncongested because few functional groups present in proteins absorb in this region of the IR spectrum. The size of the azide moiety is relatively small, so the presence of this group on amino acid side chain is unlikely to perturb

aggregation significantly. These azide labelled amino acids also have moderately strong extinction coefficients of around 300–500 M^{-1} cm^{-1} which makes them useful for measurement at lower concentrations [133,142]. Although the presence of a Fermi resonance between a combinational band and the N3 asymmetric stretching band may complicate the band profile of the vibration [143], these vibrational probes have been proven to be useful to examine local dynamics and folding of proteins [144–148]. The application of the azide probe to study protein aggregation is still in its early stages. Cho and co-workers incorporated an unnatural β-azidoalanine in $A\beta_{16–22}$ (a peptide with residues 16–22 of the full-length Aβ) to replace Ala, for studying site-specific information of the local electrostatic environments in the aggregates [149]. They found that the azido peak frequency in the aggregates is the same to that in DMSO, suggesting that the vibrational probe is surrounded by a hydrophobic environment in the aggregated state of the peptide, instead of exposed to water. The study suggests that the azide probe can provide sufficient sensitivity with strong intensity for monitoring the local environmental change along the aggregation pathway. Future studies of using these tools will be expected for elucidating high resolution dynamic information in protein aggregation.

4.2 Nitrile Probe

Nitrile groups are also excellent vibrational probes of protein structure and dynamics. Like the azide probe, the vibrational frequency of the nitrile groups is also in a relatively clear region of 2100–2400 cm^{-1} [150], and highly sensitive to the local environment. The extinction coefficient varies from 120 M^{-1} cm^{-1} to 800 M^{-1} cm^{-1} and is large enough to make it a viable vibrational probe [134,137,151,152]. There are several nitrile labelled amino acids, e.g., 5-cyanotryptophan, β-cyanoalanine, and *p*-

cyanophenylalanine that have been developed in recent years [134,151,153]. Among these, *p*-cyanophenylalanine (Phe_{CN}) has received a great deal of attention as a useful spectroscopic reporter of protein structure and dynamics [154–159]. Phe_{CN} is a good fluorophore, and the fluorescence quantum yield decreases upon dehydration [154–157]. Furthermore, the CN stretching frequency of Phe_{CN} at 2220–2250 cm^{-1} is sensitive to the electric field in its environment [160,161] and solvent polarity [134,135,162], making it a suitable vibrational probe to the local environment. For example, in H_2O, the CN stretching vibrational band of Phe_{CN} is centered at ~2237 cm^{-1}, whereas this band shifts to ~2229 cm^{-1} in a less polar tetrahydrofuran (THF) solvent [134,163]. Moreover, substitution of Phe/Tyr with Phe_{CN} introduces little structural perturbation because of their structural similarity. The Phe_{CN} residue can be incorporated into the sequence by either chemical peptide synthesis, or site-specific genetic incorporation methods via evolved aminoacyl-tRNA synthetase/tRNA pair that can specifically target on the unnatural amino acid [134,164,165]. Phe_{CN} has been used widely as a site-specific spectroscopic reporter of protein conformational changes, folding, and hydration states of proteins [156,165–169].

Recently, Phe_{CN} has been used to monitor local structural characteristics of amyloid fibrils [170-172]. Inouye et al. substituted Phe19 and Phe20 with Phe_{CN} to probe the local hydration states in Aβ16–22 [171]. In addition, Raleigh and co-workers replaced the aromatic residues in IAPP with Phe_{CN} to distinguish their local environments upon aggregation [170]. They concluded that the Phe_{CN} residues at 23 and 37 are in a more hydrophobic environment (CN vibration at ~2229 cm^{-1}) while residue 15 is in a more water exposed environment (CN vibration at ~2233 cm^{-1}) [163]. In a study of the aggregation of an $A\beta_{1–23}$ peptide, Liu and co-workers substituted the aromatic amino acids in the sequence

to Phe_{CN} and studied the Raman spectra of CN upon aggregation to reveal distinct local environmental changes of specific residues during the aggregation [172]. For instance, after amyloid formation, the peak of the CN stretching band of the $Phe_{CN}19$ residue shows a significant red shift from 2237 cm^{-1} to 2229 cm^{-1} ($A\beta_{1–23}M2$, Figure 4), indicating a more hydrophobic and less solvent accessible environment for the CN probe in fibrillar structure [163]; whereas the CN band of the $Phe_{CN}20$ residue only shows a red shift of only 2 cm^{-1} of the peak upon aggregation ($A\beta_{1–23}M3$, Figure 4), suggesting a much more polar local environment of this residue in fibrils. In a similar study of the $A\beta_{1–40}$, the CN stretching vibration band in the Raman spectra of all the mutants is centered at approximately 2229 cm^{-1} after aggregation, suggesting a dehydrated and hydrophobic local environment at the mutating positions in the amyloids [173].

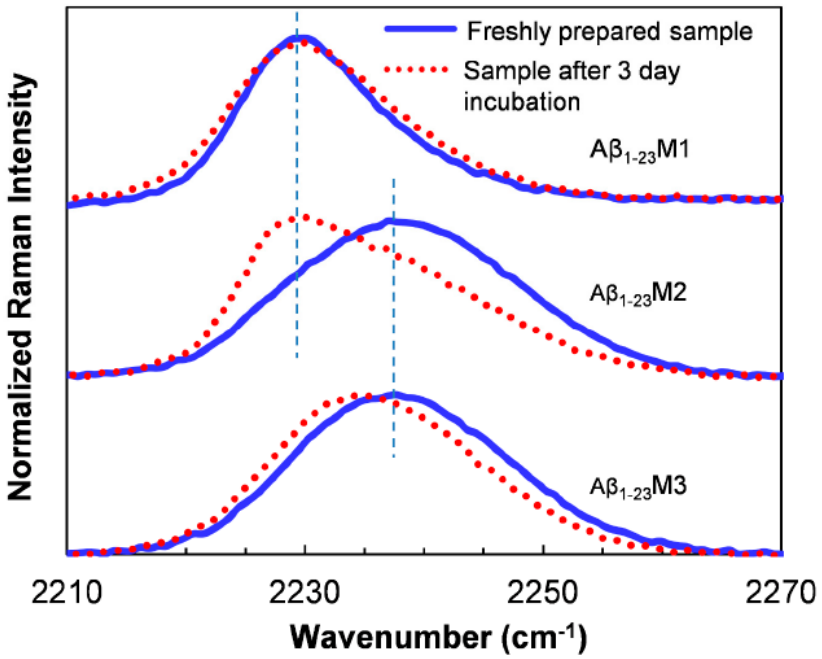

Figure 4. Raman spectra of three $A\beta_{1–23}$ mutants before and after being incubated for 3 day for aggregation [172]. In the mutants, the PheCN residue was used to replace Tyr10 ($A\beta_{1–23}M1$), Phe19 ($A\beta_{1–23}M2$), and Phe20 ($A\beta_{1–23}M3$), respectively. The vertical dashed lines indicate Raman wavenumbers at 2229 and 2237 cm^{-1}, respectively. Reprinted with permission.

4.3 Ester Carbonyl Probe

The stretching vibration of the ester carbonyl side chain of a number of unnatural amino acids has also been employed to examine the local electrostatic environment during protein folding and aggregation. A computational study by Choi and Cho predicted that the stretching mode of such a carbonyl group is not only localized, but its frequency also varies linearly with the electrostatic field for both hydrogen bonding and non-hydrogen-bonding environments [174]. The ester carbonyl group absorbs in a spectral region (1700–1800 cm^{-1}). Recently, the ester carbonyl stretching vibration of unnatural amino acids, e.g., L-aspartic acid 4-methyl ester, and L-glutamic acid 5-methyl ester, has been reported to be a sensitive probe for local electrostatic and/or hydration environment in a site-specific manner [175]. Gai and co-workers made this probe more applicable to amyloid aggregation by demonstrating that L-aspartic acid 4-methyl ester is sensitive to the hydration and hydrogen bonding of the residue and the local electrostatic field in aggregation of a model peptide of $A\beta_{16–22}$ derivative [175]. The same probe was also introduced to another $A\beta_{16–22}$ peptide derivative to discriminate the hydration status of local residues for dry fibrils and fibrils in aqueous solution by measuring the ester carbonyl stretching vibration [176]. Similarly, a methyl ester group was also introduced to the side chain of the cysteine residue of amyloidogenic peptides via cysteine alkylation, to successfully probe the local hydration state and the structural integrity of the amyloid fibrils [177]. These studies highlight the potential utility of the ester carbonyl stretching vibration as a convenient means for structural determination of amyloids fibrils and local environmental information along the aggregation pathway. Future efforts to further identify and develop novel side chain groups that fulfill the requirements of useful vibrational probes will continue to expand the

application of the vibrational spectroscopy in studying protein aggregation with enhanced structural and spatial resolution. It is worth noting that the potential perturbation of the introduced probes on the aggregation properties of the target proteins should always be taken into consideration in such studies.

5. Conclusions and Outlook

In summary, being one of the most widely used techniques in the analysis of protein secondary structure, vibrational spectroscopy is still employed as a convenient and powerful means in dissecting structural dynamics and conformational changes of peptides and proteins. The versatility of the vibrational approach and the wide range of time scales makes it particularly valuable in the analysis and understanding of the complex aggregation problem of proteins, complementing other traditional techniques. Furthermore, application of backbone isotopic labelling or side chain vibrational probes, combined with the traditional vibrational technique, allows dissecting the structural and dynamic information of protein oligomer and fibril formation at a site-specific level. We anticipate that the application of these techniques will improve the elucidation of the protein aggregation process in more complex environments, leading to a better understanding of protein aggregation mechanism in vivo. Moreover, in the future, it is expected that the ongoing advances in vibrational spectroscopy, in combination with other experimental and computational methods, will hold promise for facilitating the development of novel strategies for diagnosis and therapeutic treatment of amyloid diseases.

References

1. Selkoe, D.J. Folding proteins in fatal ways. *Nature* **2003,** *426*, 900-904.
2. Chiti, F.; Dobson, C.M. Protein misfolding, functional amyloid, and human disease. *Annu. Rev. Biochem.* **2006,** *75*, 333-366.

3. Sipe, J.D.; Cohen, A.S. Review: history of the amyloid fibril. *J. Struct. Biol.* **2000,** *130*, 88-98.
4. Jahn, T.R.; Makin, O.S.; Morris, K.L.; Marshall, K.E.; Tian, P.; Sikorski, P.; Serpell, L.C. The common architecture of cross-β amyloid. *J. Mol. Biol.* **2010,** *395*, 717-727.
5. Eisenberg, D.; Jucker, M. The amyloid state of proteins in human diseases. *Cell* **2012,** *148*, 1188-1203.
6. Kayed, R.; Head, E.; Thompson, J.L.; McIntire, T.M.; Milton, S.C.; Cotman, C.W.; Glabe, C.G. Common structure of soluble amyloid oligomers implies common mechanism of pathogenesis. *Science* **2003,** *300*, 486-489.
7. Shankar, G.M.; Li, S.; Mehta, T.H.; Garcia-Munoz, A.; Shepardson, N.E.; Smith, I.; Brett, F.M.; Farrell, M.A.; Rowan, M.J.; Lemere, C.A. Amyloid-β protein dimers isolated directly from Alzheimer's brains impair synaptic plasticity and memory. *Nat. Med.* **2008,** *14*, 837-842
8. Harper, J.D.; Lansbury, P.T. Models of amyloid seeding in Alzheimier's disease and scrapie: Mechanistic truths and physiological consequences of the time-dependent solubility of amyloid proteins. *Annu. Rev. Biochem.* **1997,** *66*, 385-407.
9. Naiki, H.; Hasegawa, K.; Yamaguchi, I.; Nakamura, H.; Gejyo, F.; Nakakuki, K. Apolipoprotein E and antioxidants have different mechanisms of inhibiting Alzheimer's β-amyloid fibril formation in vitro. *Biochemistry* **1998,** *37*, 17882-17889.
10. Powers, E.T.; Powers, D.L. Mechanisms of protein fibril formation: nucleated polymerization with competing off-pathway aggregation. *Biophys. J.* **2008,** *94*, 379-391.
11. Howie, A.J.; Brewer, D.B. Optical properties of amyloid stained by Congo red: history and mechanisms. *Micron* **2009,** *40*, 285-301.
12. Biancalana, M.; Koide, S. Molecular mechanism of Thioflavin-T binding to amyloid fibrils. *Biochim. Biophys. Acta.* **2010,** *1804*, 1405-1412.
13. Mechaly, A.E.; Bellomio, A.; Gil-Carton, D.; Morante, K.; Valle, M.; Gonzalez-Manas, J.M.; Guerin, D.M. Structural insights into the oligomerization and architecture of eukaryotic membrane pore-forming toxins. *Structure* **2011,** *19*, 181-191.

14. Mustata, M.; Capone, R.; Jang, H.; Arce, F.T.; Ramachandran, S.; Lal, R.; Nussinov, R. K3 fragment of amyloidogenic β2-microglobulin forms ion channels: implication for dialysis related amyloidosis. *J. Am. Chem. Soc.* **2009,** *131*, 14938-14945.
15. Pires, R.H.; Saraiva, M.J.; Damas, A.M.; Kellermayer, M.S. Structure and assembly-disassembly properties of wild-type transthyretin amyloid protofibrils observed with atomic force microscopy. *J. Mol. Recognit.* **2011,** *24*, 467-476.
16. Vestergaard, B.; Groenning, M.; Roessle, M.; Kastrup, J.S.; van de Weert, M.; Flink, J.M.; Frokjaer, S.; Gajhede, M.; Svergun, D.I. A helical structural nucleus is the primary elongating unit of insulin amyloid fibrils. *PLoS Biol.* **2007,** *5*, e134.
17. Chimon, S.; Shaibat, M.A.; Jones, C.R.; Calero, D.C.; Aizezi, B.; Ishii, Y. Evidence of fibril-like β-sheet structures in a neurotoxic amyloid intermediate of Alzheimer's β-amyloid. *Nat. Struct. Mol. Biol.* **2007**, 14, 1157-1164.
18. Walsh, P.; Yau, J.; Simonetti, K.; Sharpe, S. Morphology and secondary structure of stable β-oligomers formed by amyloid peptide PrP(106-126). *Biochemistry* **2009,** *48*, 5779-5781.
19. Patel, H.R.; Pithadia, A.S.; Brender, J.R.; Fierke, C.A.; Ramamoorthy, A. In Search of Aggregation Pathways of IAPP and Other Amyloidogenic Proteins: Finding Answers through NMR Spectroscopy. *J. Phys. Chem. Lett.* **2014,** *5*, 1864-1870.
20. Wälti, M.A.; Ravotti, F.; Arai, H.; Glabe, C.G.; Wall, J.S.; Böckmann, A.; Güntert, P.; Meier, B.H.; Riek, R. Atomic-resolution structure of a disease-relevant Aβ (1–42) amyloid fibril. *Proc. Natl. Acad. Sci. USA.* **2016,** *113*, E4976-E4984.
21. Sawaya, M.R.; Sambashivan, S.; Nelson, R.; Ivanova, M.I.; Sievers, S.A.; Apostol, M.I.; Thompson, M.J.; Balbirnie, M.; Wiltzius, J.J.; McFarlane, H.T.; Madsen, A.O.; Riekel, C.; Eisenberg, D. Atomic structures of amyloid cross-β spines reveal varied steric zippers. *Nature* **2007,** *447*, 453-457.
22. Kim, H.; Cho, M. Infrared probes for studying the structure and dynamics of biomolecules. *Chem. Rev.* **2013,** *113*, 5817-5847.
23. Moran, S.D.; Zanni, M.T. How to Get Insight into Amyloid Structure and Formation from Infrared Spectroscopy. *J. Phys. Chem. Lett.* **2014,** *5*, 1984-1993.
24. Ma, J.; Pazos, I.M.; Zhang, W.; Culik, R.M.; Gai, F. Site-specific infrared probes of proteins. *Annu. Rev. Phy.s Chem.* **2015,** *66*, 357-377.

25. Schweitzer-Stenner, R. Visible and UV-resonance Raman spectroscopy of model peptides. *J. Raman Spectrosc.* **2001,** *32*, 711-732.
26. Barth, A. Infrared spectroscopy of proteins. *Biochim. Biophys. Acta.* **2007,** *1767*, 1073-1101.
27. McDonald, R.S. Infrared spectrometry. *Anal. Chem.* **1986,** *58*, 1906-1925.
28. Rostron, P.; Gaber, S.; Gaber, D. Raman Spectroscopy, Review. *IJETR* **2016,** *6*, 50-64.
29. Krimm, S.; Bandekar, J. Vibrational spectroscopy and conformation of peptides, polypeptides, and proteins. *Adv. Prot. Chem.* **1986,** *38*, 181-364.
30. Barth, A.; Zscherp, C. What vibrations tell us about proteins. *Q. Rev. Biophys.* **2002,** *35*, 369-430.
31. Haris, P.I.; Severcan, F. FTIR spectroscopic characterization of protein structure in aqueous and non-aqueous media. *J. Mol. Catal. B Enzym.* **1999,** *7*, 207-221.
32. Moore, W.H.; Krimm, S. Transition dipole coupling in Amide I modes of βpolypeptides. *Proc. Natl. Acad. Sci. USA.* **1975,** *72*, 4933-4935.
33. Woutersen, S.; Ham, S. Structure Determination of Trialanine in Water Using Polarization Sensitive Two-Dimensional Vibrational Spectroscopy. *J. Phys. Chem. B* **2000,** *104*, 11316-11320.
34. Lee, C.; Cho, M. Local Amide I Mode Frequencies and Coupling Constants in Multiple-Stranded Antiparallel β-Sheet Polypeptides. *J. Phys. Chem. B* **2004,** *108*, 20397-20407.
35. Myshakina, N.S.; Asher, S.A. Peptide bond vibrational coupling. *J. Phys. Chem. B* **2007,** *111*, 4271-4279.
36. Ganim, Z.; Chung, H.S.; Smith, A.W.; Deflores, L.P.; Jones, K.C.; Tokmakoff, A. Amide I two-dimensional infrared spectroscopy of proteins. *Acc. Chem. Res.* **2008,** *41*, 432-441.
37. Rygula, A.; Majzner, K.; Marzec, K.M.; Kaczor, A.; Pilarczyk, M.; Baranska, M. Raman spectroscopy of proteins: a review. *J. Raman Specrosc.* **2013,** *44*, 1061-1076.
38. Goormaghtigh, E.; Cabiaux, V.; Ruysschaert, J.-M., Determination of soluble and membrane protein structure by Fourier transform infrared spectroscopy. In *Physicochemical methods in the study of biomembranes*, Springer: 1994; pp 405-450.

39. Dobson, C.M. Protein folding and misfolding. *Nature* **2003,** *426,* 884-890.
40. Zandomeneghi, G.; Krebs, M.R.; McCammon, M.G.; Fandrich, M. FTIR reveals structural differences between native β-sheet proteins and amyloid fibrils. *Protein Sci.* **2004,** *13,* 3314-3321.
41. Lomont, J.P.; Ostrander, J.S.; Ho, J.J.; Petti, M.K.; Zanni, M.T. Not All β-Sheets Are the Same: Amyloid Infrared Spectra, Transition Dipole Strengths, and Couplings Investigated by 2D IR Spectroscopy. *J. Phys. Chem. B* **2017,** *121,* 8935-8945.
42. Sarroukh, R.; Goormaghtigh, E.; Ruysschaert, J.M.; Raussens, V. ATR-FTIR: a "rejuvenated" tool to investigate amyloid proteins. *Biochim. Biophys. Acta.* **2013,** *1828,* 2328-2338.
43. Venyaminov, S.; Prendergast, F.G. Water (H2O and D2O) molar absorptivity in the 1000-4000 cm-1 range and quantitative infrared spectroscopy of aqueous solutions. *Anal. Biochem.* **1997,** *248,* 234-245.
44. Fayer, M.D. Dynamics of liquids, molecules, and proteins measured with ultrafast 2D IR vibrational echo chemical exchange spectroscopy. *Annu. Rev. Phys. Chem.* **2009,** *60,* 21-38.
45. Kim, Y.S.; Hochstrasser, R.M. Applications of 2D IR spectroscopy to peptides, proteins, and hydrogen-bond dynamics. *J. Phys. Chem. B* **2009,** *113,* 8231-8251.
46. Strasfeld, D.B.; Ling, Y.L.; Gupta, R.; Raleigh, D.P.; Zanni, M.T. Strategies for extracting structural information from 2D IR spectroscopy of amyloid: application to islet amyloid polypeptide. *J. Phys. Chem. B* **2009,** *113,* 15679-15691.
47. Mattson, M.P. Pathways towards and away from Alzheimer's disease. *Nature* **2004,** *430,* 631-639.
48. Hardy, J.; Selkoe, D.J. Medicine - The amyloid hypothesis of Alzheimer's disease: Progress and problems on the road to therapeutics. *Science* **2002,** *297,* 353-356.
49. Tanzi, R.E.; Bertram, L. Twenty years of the Alzheimer's disease amyloid hypothesis: A genetic perspective. *Cell* **2005,** *120,* 545-555.
50. Sarroukh, R.; Cerf, E.; Derclaye, S.; Dufrene, Y.F.; Goormaghtigh, E.; Ruysschaert, J.M.; Raussens, V. Transformation of amyloid β(1-40) oligomers into fibrils is characterized by a major change in secondary structure. *Cell. Mol. Life Sci.* **2011,** *68,* 1429-1438.

51. Klementieva, O.; Willén, K.; Martinsson, I.; Israelsson, B.; Engdahl, A.; Cladera, J.; Uvdal, P.; Gouras, G. Pre-plaque conformational changes in Alzheimer's disease-linked Aβ and APP. *Nat. Commun.* **2017,** *8*, 14726.
52. Lomont, J.P.; Rich, K.L.; Maj, M.; Ho, J.J.; Ostrander, J.S.; Zanni, M.T. Spectroscopic Signature for Stable β-Amyloid Fibrils versus β-Sheet-Rich Oligomers. *J. Phys. Chem. B* **2018,** *122*, 144-153.
53. Tidy, R.J.; Lam, V.; Fimognari, N.; Mamo, J.C.; Hackett, M.J. FTIR studies of the similarities between pathology induced protein aggregation in vivo and chemically induced protein aggregation ex vivo. *Vib. Spec.* **2017,** *91*, 68-76.
54. Nabers, A.; Ollesch, J.; Schartner, J.; Kotting, C.; Genius, J.; Hafermann, H.; Klafki, H.; Gerwert, K.; Wiltfang, J. Amyloid-β-Secondary Structure Distribution in Cerebrospinal Fluid and Blood Measured by an Immuno-Infrared-Sensor: A Biomarker Candidate for Alzheimer's Disease. *Anal. Chem.* **2016,** *88*, 2755-2762.
55. Hull, R.L.; Westermark, G.T.; Westermark, P.; Kahn, S.E. Islet amyloid: a critical entity in the pathogenesis of type 2 diabetes. *J. Clin. Endocrinol. Metab.* **2004,** *89*, 3629-3643.
56. Westermark, P.; Andersson, A.; Westermark, G.T. Islet amyloid polypeptide, islet amyloid, and diabetes mellitus. *Physiol. Rev.* **2011,** *91*, 795-826.
57. Janson, J.; Ashley, R.H.; Harrison, D.; McIntyre, S.; Butler, P.C. The mechanism of islet amyloid polypeptide toxicity is membrane disruption by intermediate-sized toxic amyloid particles. *Diabetes* **1999,** *48*, 491-498.
58. Rawat, A.; Maity, B.K.; Chandra, B.; Maiti, S. Aggregation-induced conformation changes dictate islet amyloid polypeptide (IAPP) membrane affinity. *Biochim. Biophys. Acta. Biomembr*. **2018**, 1860, 1734-1740.
59. Goldsbury, C.; Goldie, K.; Pellaud, J.; Seelig, J.; Frey, P.; Müller, S.; Kistler, J.; Cooper, G.; Aebi, U. Amyloid fibril formation from full-length and fragments of amylin. *J. Struct. Biol.* **2000,** *130*, 352-362.
60. Strasfeld, D.B.; Ling, Y.L.; Shim, S.H.; Zanni, M.T. Tracking fiber formation in human islet amyloid polypeptide with automated 2D-IR spectroscopy. *J. Am. Chem. Soc.* **2008,** *130*, 6698-6699.

61. Abedini, A.; Plesner, A.; Cao, P.; Ridgway, Z.; Zhang, J.; Tu, L.H.; Middleton, C.T.; Chao, B.; Sartori, D.J.; Meng, F.; Wang, H.; Wong, A.G.; Zanni, M.T.; Verchere, C.B.; Raleigh, D.P.; Schmidt, A.M. Time-resolved studies define the nature of toxic IAPP intermediates, providing insight for anti-amyloidosis therapeutics. *Elife* **2016,** *5*.

62. Shim, S.H.; Strasfeld, D.B.; Ling, Y.L.; Zanni, M.T. Automated 2D IR spectroscopy using a mid-IR pulse shaper and application of this technology to the human islet amyloid polypeptide. *Proc. Natl. Acad. Sci. USA.* **2007,** *104*, 14197-14202.

63. Dunkelberger, E.B.; Grechko, M.; Zanni, M.T. Transition Dipoles from 1D and 2D Infrared Spectroscopy Help Reveal the Secondary Structures of Proteins: Application to Amyloids. *J. Phys. Chem. B* **2015,** *119*, 14065-14075.

64. Mishra, R.; Bulic, B.; Sellin, D.; Jha, S.; Waldmann, H.; Winter, R. Small-molecule inhibitors of islet amyloid polypeptide fibril formation. *Angew. Chem. In.t Ed. Engl.* **2008,** *47*, 4679-4682.

65. Mishra, R.; Sellin, D.; Radovan, D.; Gohlke, A.; Winter, R. Inhibiting islet amyloid polypeptide fibril formation by the red wine compound resveratrol. *ChemBioChem* **2009,** *10*, 445-449.

66. Sellin, D.; Yan, L.M.; Kapurniotu, A.; Winter, R. Suppression of IAPP fibrillation at anionic lipid membranes via IAPP-derived amyloid inhibitors and insulin. *Biophys. Chem.* **2010,** *150*, 73-79.

67. Gao, M.; Estel, K.; Seeliger, J.; Friedrich, R.P.; Dogan, S.; Wanker, E.E.; Winter, R.; Ebbinghaus, S. Modulation of human IAPP fibrillation: cosolutes, crowders and chaperones. *Phys. Chem. Chem. Phys.* **2015,** *17*, 8338-8348.

68. Forno, L.S. Neuropathology of Parkinson's disease. *J. Neuropathol. Exp. Neuro.l* **1996,** *55*, 259-272.

69. Polymeropoulos, M.H.; Lavedan, C.; Leroy, E.; Ide, S.E.; Dehejia, A.; Dutra, A.; Pike, B.; Root, H.; Rubenstein, J.; Boyer, R.; Stenroos, E.S.; Chandrasekharappa, S.; Athanassiadou, A.; Papapetropoulos, T.; Johnson, W.G.; Lazzarini, A.M.; Duvoisin, R.C.; Di Iorio, G.; Golbe, L.I.; Nussbaum, R.L. Mutation in the α-synuclein gene identified in families with Parkinson's disease. *Science* **1997,** *276*, 2045-2047.

70. Kruger, R.; Kuhn, W.; Muller, T.; Woitalla, D.; Graeber, M.; Kosel, S.; Przuntek, H.; Epplen, J.T.; Schols, L.; Riess, O. Ala30Pro mutation in the gene encoding α-synuclein in Parkinson's disease. *Nat. Genet.* **1998,** *18,* 106-108.
71. Spillantini, M.G.; Crowther, R.A.; Jakes, R.; Hasegawa, M.; Goedert, M. α-Synuclein in filamentous inclusions of Lewy bodies from Parkinson's disease and dementia with lewy bodies. *Proc. Natl. Acad. Sci. USA.* **1998,** *95,* 6469-6473.
72. Deas, E.; Cremades, N.; Angelova, P.R.; Ludtmann, M.H.; Yao, Z.; Chen, S.; Horrocks, M.H.; Banushi, B.; Little, D.; Devine, M.J.; Gissen, P.; Klenerman, D.; Dobson, C.M.; Wood, N.W.; Gandhi, S.; Abramov, A.Y. α-Synuclein Oligomers Interact with Metal Ions to Induce Oxidative Stress and Neuronal Death in Parkinson's Disease. *Antioxid. Redox. Signal.* **2016,** *24,* 376-391.
73. Uversky, V.N.; Li, J.; Fink, A.L. Evidence for a partially folded intermediate in α-synuclein fibril formation. *J. Biol. Chem.* **2001,** *276,* 10737-10744.
74. Celej, M.S.; Sarroukh, R.; Goormaghtigh, E.; Fidelio, G.D.; Ruysschaert, J.-M.; Raussens, V. Toxic prefibrillar α-synuclein amyloid oligomers adopt a distinctive antiparallel β-sheet structure. *Biochem. J.* **2012,** *443,* 719-726.
75. Conway, K.A.; Harper, J.D.; Lansbury, P.T. Fibrils formed in vitro from α-synuclein and two mutant forms linked to Parkinson's disease are typical amyloid. *Biochemistry* **2000,** *39,* 2552-2563.
76. Roeters, S.J.; Iyer, A.; Pletikapić, G.; Kogan, V.; Subramaniam, V.; Woutersen, S. Evidence for intramolecular antiparallel β-sheet structure in alpha-synuclein fibrils from a combination of two-dimensional infrared spectroscopy and atomic force microscopy. *Sci. Rep.* **2017,** *7,* 41051.
77. Maiti, N.C.; Apetri, M.M.; Zagorski, M.G.; Carey, P.R.; Anderson, V.E. Raman spectroscopic characterization of secondary structure in natively unfolded proteins: α-synuclein. *J. Am. Chem. Soc.* **2004,** *126,* 2399-2408.
78. Apetri, M.M.; Maiti, N.C.; Zagorski, M.G.; Carey, P.R.; Anderson, V.E. Secondary structure of α-synuclein oligomers: characterization by raman and atomic force microscopy. *J. Mol. Biol.* **2006,** *355,* 63-71.

79. Flynn, J.D.; McGlinchey, R.P.; Walker, R.L.; Lee, J.C. Structural features of α-synuclein amyloid fibrils revealed by Raman spectroscopy. *J. Biol. Chem.* **2018,** *293*, 767-776.
80. Schweitzer-Stenner, R. Advances in vibrational spectroscopy as a sensitive probe of peptide and protein structure - A critical review. *Vib. Spec.* **2006,** *42*, 98-117.
81. Asher, S.A.; Ianoul, A.; Mix, G.; Boyden, M.N.; Karnoup, A.; Diem, M.; Schweitzer-Stenner, R. Dihedral psi angle dependence of the amide III vibration: a uniquely sensitive UV resonance Raman secondary structural probe. *J. Am. Chem. Soc.* **2001,** *123*, 11775-11781.
82. Ianoul, A.; Boyden, M.N.; Asher, S.A. Dependence of the peptide amide III vibration on the phi dihedral angle. *J. Am. Chem. Soc.* **2001,** *123*, 7433-7434.
83. Papanikolopoulou, K.; Mills-Henry, I.; Thol, S.L.; Wang, Y.; Gross, A.A.; Kirschner, D.A.; Decatur, S.M.; King, J. Formation of amyloid fibrils in vitro by human γD-crystallin and its isolated domains. *Mol. Vis.* **2008,** *14*, 81-89.
84. Gustiananda, M.; Haris, P.I.; Milburn, P.J.; Gready, J.E. Copper-induced conformational change in a marsupial prion protein repeat peptide probed using FTIR spectroscopy. *FEBS letters* **2002,** *512*, 38-42.
85. Sokolowski, F.; Naumann, D. FTIR study on thermal denaturation and aggregation of recombinant hamster prion protein SHaPrP90–232. *Vib. Spec.* **2005,** *38*, 39-44.
86. Heck, B.S.; Doll, F.; Hauser, K. Length-dependent conformational transitions of polyglutamine repeats as molecular origin of fibril initiation. *Biophys. Chem.* **2014,** *185*, 47-57.
87. Dzwolak, W.; Muraki, T.; Kato, M.; Taniguchi, Y. Chain-length dependence of α-helix to β-sheet transition in polylysine: Model of protein aggregation studied by temperature-tuned FTIR spectroscopy. *Biopolymers* **2004,** *73*, 463-469.
88. Markiewicz, B.N.; Oyola, R.; Du, D.; Gai, F. Aggregation Gatekeeper and Controlled Assembly of Trpzip beta-Hairpins. *Biochemistry* **2014,** *53*, 1146-1154.
89. Zhang, T.O.; Alperstein, A.M.; Zanni, M.T. Amyloid β-Sheet Secondary Structure Identified in UV-Induced Cataracts of Porcine Lenses using 2D IR Spectroscopy. *J. Mol. Biol.* **2017,** *429*, 1705-1721.

90. Fang, C.; Hochstrasser, R.M. Two-Dimensional Infrared Spectra of the 13C 18O Isotopomers of Alanine Residues in an α-Helix. *J. Phys. Chem. B* **2005,** *109*, 18652-18663.
91. Arkin, I.T. Isotope-edited IR spectroscopy for the study of membrane proteins. *Curr. Opin. Chem. Biol.* **2006,** *10*, 394-401.
92. Middleton, C.T.; Woys, A.M.; Mukherjee, S.S.; Zanni, M.T. Residue-specific structural kinetics of proteins through the union of isotope labeling, mid-IR pulse shaping, and coherent 2D IR spectroscopy. *Methods* **2010,** *52*, 12-22.
93. Tadesse, L.; Nazarbaghi, R.; Walters, L. Isotopically Enhanced Infrared Spectroscopy: A Novel Method for Examining Secondary Structure at Specific Sites in Conformationally Heterogeneous Peptides. *J. Am. Chem. Soc.* **1991,** *113*, 7036-7037.
94. Decatur, S.M.; Antonic, J. Isotope-Edited Infrared Spectroscopy of Helical Peptides. *J. Am. Chem. Soc.* **1999,** *121*, 11914-11915.
95. Decatur, S.M. Elucidation of residue-level structure and dynamics of polypeptides via isotope-edited infrared spectroscopy. *Acc. Chem. Res.* **2006,** *39*, 169-175.
96. Wang, L.; Middleton, C.T.; Singh, S.; Reddy, A.S.; Woys, A.M.; Strasfeld, D.B.; Marek, P.; Raleigh, D.P.; de Pablo, J.J.; Zanni, M.T.; Skinner, J.L. 2DIR spectroscopy of human amylin fibrils reflects stable β-sheet structure. *J. Am. Chem. Soc.* **2011,** *133*, 16062-16071.
97. Huang, C.Y.; Getahun, Z.; Wang, T.; DeGrado, W.F.; Gai, F. Time-resolved infrared study of the helix-coil transition using (13)C-labeled helical peptides. *J. Am. Chem. Soc.* **2001,** *123*, 12111-12112.
98. Backus, E.H.; Bloem, R.; Pfister, R.; Moretto, A.; Crisma, M.; Toniolo, C.; Hamm, P. Dynamical transition in a small helical peptide and its implication for vibrational energy transport. *J. Phys. Chem. B* **2009,** *113*, 13405-13409.
99. Backus, E.H.; Bloem, R.; Donaldson, P.M.; Ihalainen, J.A.; Pfister, R.; Paoli, B.; Caflisch, A.; Hamm, P. 2D-IR study of a photoswitchable isotope-labeled α-helix. *J. Phys. Chem. B* **2010,** *114*, 3735-3740.

100. Remorino, A.; Korendovych, I.V.; Wu, Y.; DeGrado, W.F.; Hochstrasser, R.M. Residue-specific vibrational echoes yield 3D structures of a transmembrane helix dimer. *Science* **2011,** *332*, 1206-1209.
101. Ghosh, A.; Qiu, J.; DeGrado, W.F.; Hochstrasser, R.M. Tidal surge in the M2 proton channel, sensed by 2D IR spectroscopy. *Proc. Natl. Acad. Sci. USA.* **2011,** *108,* 6115-6120.
102. Petty, S.A.; Decatur, S.M. Experimental evidence for the reorganization of β-strands within aggregates of the Aβ(16-22) peptide. *J. Am. Chem. Soc.* **2005,** *127*, 13488-13489.
103. Shanmugam, G.; Polavarapu, P.L. Isotope-assisted vibrational circular dichroism investigations of amyloid β peptide fragment, Aβ(16-22). *J. Struct. Biol.* **2011,** *176*, 212-219.
104. Kim, Y.S.; Liu, L.; Axelsen, P.H.; Hochstrasser, R.M. Two-dimensional infrared spectra of isotopically diluted amyloid fibrils from Aβ40. *Proc. Natl. Acad. Sci. USA.* **2008,** *105*, 7720-7725.
105. Zhuang, W.; Sgourakis, N.G.; Li, Z.; Garcia, A.E.; Mukamel, S. Discriminating early stage Aβ42 monomer structures using chirality-induced 2DIR spectroscopy in a simulation study. *Proc. Natl. Acad. Sci. USA.* **2010,** *107*, 15687-15692.
106. El Khoury, Y.; Dorlet, P.; Faller, P.; Hellwig, P. New insights into the coordination of Cu (II) by the amyloid-β 16 peptide from Fourier transform IR spectroscopy and isotopic labeling. *J. Phys. Chem. B* **2011,** *115,* 14812-14821.
107. Yanagisawa, K.; Odaka, A.; Suzuki, N.; Ihara, Y. GM1 ganglioside-bound amyloid β-protein (Aβ): a possible form of preamyloid in Alzheimer's disease. *Nat. Med.* **1995,** *1*, 1062-1066.
108. Okada, Y.; Okubo, K.; Ikeda, K.; Yano, Y.; Hoshino, M.; Hayashi, Y.; Kiso, Y.; Itoh-Watanabe, H.; Naito, A.; Matsuzaki, K. Toxic Amyloid Tape: A Novel Mixed Antiparallel/Parallel β-Sheet Structure Formed by Amyloid β-Protein on GM1 Clusters. *ACS Chem. Neurosci.* **2018,** *Article ASAP*.
109. Fukunaga, S.; Ueno, H.; Yamaguchi, T.; Yano, Y.; Hoshino, M.; Matsuzaki, K. GM1 cluster mediates formation of toxic Aβ fibrils by providing hydrophobic environments. *Biochemistry* **2012,** *51*, 8125-8131.

110. Kim, Y.S.; Liu, L.; Axelsen, P.H.; Hochstrasser, R.M. 2D IR provides evidence for mobile water molecules in β-amyloid fibrils. *Proc. Natl. Acad. Sci. USA.* **2009,** *106*, 17751-17756.
111. Ma, J.; Komatsu, H.; Kim, Y.S.; Liu, L.; Hochstrasser, R.M.; Axelsen, P.H. Intrinsic structural heterogeneity and long-term maturation of amyloid β peptide fibrils. *ACS Chem. Neurosci.* **2013,** *4*, 1236-1243.
112. Falvo, C.; Zhuang, W.; Kim, Y.S.; Axelsen, P.H.; Hochstrasser, R.M.; Mukamel, S. Frequency distribution of the amide-I vibration sorted by residues in amyloid fibrils revealed by 2D-IR measurements and simulations. *J. Phys. Chem. B* **2012,** *116*, 3322-3330.
113. Shim, S.H.; Gupta, R.; Ling, Y.L.; Strasfeld, D.B.; Raleigh, D.P.; Zanni, M.T. Two-dimensional IR spectroscopy and isotope labeling defines the pathway of amyloid formation with residue-specific resolution. *Proc. Natl. Acad. Sci. USA.* **2009,** *106*, 6614-6619.
114. Woys, A.M.; Almeida, A.M.; Wang, L.; Chiu, C.C.; McGovern, M.; de Pablo, J.J.; Skinner, J.L.; Gellman, S.H.; Zanni, M.T. Parallel β-sheet vibrational couplings revealed by 2D IR spectroscopy of an isotopically labeled macrocycle: quantitative benchmark for the interpretation of amyloid and protein infrared spectra. *J. Am. Chem. Soc.* **2012,** *134*, 19118-19128.
115. Dunkelberger, E.B.; Buchanan, L.E.; Marek, P.; Cao, P.; Raleigh, D.P.; Zanni, M.T. Deamidation accelerates amyloid formation and alters amylin fiber structure. *J. Am. Chem. Soc.* **2012,** *134*, 12658-12667.
116. Buchanan, L.E.; Dunkelberger, E.B.; Tran, H.Q.; Cheng, P.N.; Chiu, C.C.; Cao, P.; Raleigh, D.P.; de Pablo, J.J.; Nowick, J.S.; Zanni, M.T. Mechanism of IAPP amyloid fibril formation involves an intermediate with a transient β-sheet. *Proc. Natl. Acad. Sci. USA.3* **2013,** *110*, 19285-19290.
117. Serrano, A.L.; Lomont, J.P.; Tu, L.H.; Raleigh, D.P.; Zanni, M.T. A Free Energy Barrier Caused by the Refolding of an Oligomeric Intermediate Controls the Lag Time of Amyloid Formation by hIAPP. *J. Am. Chem. Soc.* **2017,** *139*, 16748-16758.

118. Maj, M.; Lomont, J.P.; Rich, K.L.; Alperstein, A.M.; Zanni, M.T. Site-specific detection of protein secondary structure using 2D IR dihedral indexing: a proposed assembly mechanism of oligomeric hIAPP. *Chem. Sci.* **2018,** *9*, 463-474.
119. Middleton, C.T.; Marek, P.; Cao, P.; Chiu, C.C.; Singh, S.; Woys, A.M.; de Pablo, J.J.; Raleigh, D.P.; Zanni, M.T. Two-dimensional infrared spectroscopy reveals the complex behaviour of an amyloid fibril inhibitor. *Nat. Chem.* **2012,** *4*, 355-360.
120. Cao, P.; Meng, F.; Abedini, A.; Raleigh, D.P. The ability of rodent islet amyloid polypeptide to inhibit amyloid formation by human islet amyloid polypeptide has important implications for the mechanism of amyloid formation and the design of inhibitors. *Biochemistry* **2010,** *49*, 872-881.
121. Moran, S.D.; Woys, A.M.; Buchanan, L.E.; Bixby, E.; Decatur, S.M.; Zanni, M.T. Two-dimensional IR spectroscopy and segmental 13C labeling reveals the domain structure of human γD-crystallin amyloid fibrils. *Proc. Natl. Acad. Sci. USA.* **2012,** *109*, 3329-3334.
122. Moran, S.D.; Decatur, S.M.; Zanni, M.T. Structural and sequence analysis of the human γD-crystallin amyloid fibril core using 2D IR spectroscopy, segmental 13C labeling, and mass spectrometry. *J. Am. Chem. Soc.* **2012,** *134*, 18410-18416.
123. Lam, A.R.; Moran, S.D.; Preketes, N.K.; Zhang, T.O.; Zanni, M.T.; Mukamel, S. Study of the γD-crystallin protein using two-dimensional infrared (2DIR) spectroscopy: experiment and simulation. *J. Phys. Chem. B* **2013,** *117*, 15436-15443.
124. Moran, S.D.; Zhang, T.O.; Zanni, M.T. An alternative structural isoform in amyloid-like aggregates formed from thermally denatured human γD-crystallin. *Protein Sci.* **2014,** *23*, 321-331.
125. Silva, R.A.; Barber-Armstrong, W.; Decatur, S.M. The organization and assembly of a β-sheet formed by a prion peptide in solution: an isotope-edited FTIR study. *J. Am. Chem. Soc.* **2003,** *125*, 13674-13675.
126. Petty, S.A.; Adalsteinsson, T.; Decatur, S.M. Correlations among morphology, β-sheet stability, and molecular structure in prion peptide aggregates. *Biochemistry* **2005,** *44*, 4720-4726.

127. Petty, S.A.; Decatur, S.M. Intersheet rearrangement of polypeptides during nucleation of β-sheet aggregates. *Proc. Natl. Acad. Sci. USA.* **2005,** *102*, 14272-14277.
128. Chi, H.; Welch, W.R.; Kubelka, J.; Keiderling, T.A. Insight into the packing pattern of β2 fibrils: a model study of glutamic acid rich oligomers with 13C isotopic edited vibrational spectroscopy. *Biomacromolecules* **2013,** *14*, 3880-3891.
129. Buchanan, L.E.; Carr, J.K.; Fluitt, A.M.; Hoganson, A.J.; Moran, S.D.; de Pablo, J.J.; Skinner, J.L.; Zanni, M.T. Structural motif of polyglutamine amyloid fibrils discerned with mixed-isotope infrared spectroscopy. *Proc. Natl. Acad. Sci. USA.* **2014,** *111*, 5796-5801.
130. Paul, C.; Wang, J.; Wimley, W.C.; Hochstrasser, R.M.; Axelsen, P.H. Vibrational coupling, isotopic editing, and β-sheet structure in a membrane-bound polypeptide. *J. Am. Chem. Soc.* **2004,** *126*, 5843-5850.
131. Londergan, C.H.; Wang, J.; Axelsen, P.H.; Hochstrasser, R.M. Two-dimensional infrared spectroscopy displays signatures of structural ordering in peptide aggregates. *Biophys. J.* **2006,** *90*, 4672-4685.
132. Barth, A. The infrared absorption of amino acid side chains. *Prog. Biophys. Mol. Biol.* **2000,** *74*, 141-173.
133. Bloem, R.; Koziol, K.; Waldauer, S.A.; Buchli, B.; Walser, R.; Samatanga, B.; Jelesarov, I.; Hamm, P. Ligand binding studied by 2D IR spectroscopy using the azidohomoalanine label. *J. Phys. Chem. B* **2012,** *116*, 13705-13712.
134. Getahun, Z.; Huang, C.Y.; Wang, T.; De Leon, B.; DeGrado, W.F.; Gai, F. Using nitrile-derivatized amino acids as infrared probes of local environment. *J. Am. Chem. Soc.* **2003,** *125*, 405-411.
135. Waegele, M.M.; Culik, R.M.; Gai, F. Site-Specific Spectroscopic Reporters of the Local Electric Field, Hydration, Structure, and Dynamics of Biomolecules. *J. Phys. Chem. Lett.* **2011,** *2*, 2598-2609.
136. Lindquist, B.A.; Furse, K.E.; Corcelli, S.A. Nitrile groups as vibrational probes of biomolecular structure and dynamics: an overview. *Phys. Chem. Chem. Phys.* **2009,** *11*, 8119-8132.

137. Fafarman, A.T.; Webb, L.J.; Chuang, J.I.; Boxer, S.G. Site-specific conversion of cysteine thiols into thiocyanate creates an IR probe for electric fields in proteins. *J. Am. Chem. Soc.* **2006,** *128*, 13356-13357.
138. van Wilderen, L.J.; Kern-Michler, D.; Müller-Werkmeister, H.M.; Bredenbeck, J. Vibrational dynamics and solvatochromism of the label SCN in various solvents and hemoglobin by time dependent IR and 2D-IR spectroscopy. *Phys. Chem. Chem. Phys.* **2014,** *16*, 19643-19653.
139. Miller, C.S.; Ploetz, E.A.; Cremeens, M.E.; Corcelli, S.A. Carbon-deuterium vibrational probes of peptide conformation: alanine dipeptide and glycine dipeptide. *J. Chem. Phys.* **2009,** *130*, 125103.
140. Yu, W.; Dawson, P.E.; Zimmermann, J.; Romesberg, F.E. Carbon-deuterium bonds as probes of protein thermal unfolding. *J. Phys. Chem. B* **2012,** *116*, 6397-6403.
141. Hoffman, K.W.; Romei, M.G.; Londergan, C.H. A new Raman spectroscopic probe of both the protonation state and noncovalent interactions of histidine residues. *J. Phys. Chem. A* **2013,** *117*, 5987-5996.
142. Bazewicz, C.G.; Liskov, M.T.; Hines, K.J.; Brewer, S.H. Sensitive, site-specific, and stable vibrational probe of local protein environments: 4-azidomethyl-L-phenylalanine. *J. Phys. Chem. B* **2013,** *117*, 8987-8993.
143. Lipkin, J.S.; Song, R.; Fenlon, E.E.; Brewer, S.H. Modulating Accidental Fermi Resonance: What a Difference a Neutron Makes. *J. Phys. Chem. Lett.* **2011,** *2011*, 1672-1676.
144. Garcia-Viloca, M.; Nam, K.; Alhambra, C.; Gao, J. Solvent and protein effects on the vibrational frequency shift and energy relaxation of the azide ligand in carbonic anhydrase. *J. Phys. Chem. B* **2004,** *108*, 13501-13512.
145. Ye, S.; Huber, T.; Vogel, R.; Sakmar, T.P. FTIR analysis of GPCR activation using azido probes. *Nat. Chem. Biol.* **2009,** *5*, 397-399.
146. Tucker, M.J.; Gai, X.S.; Fenlon, E.E.; Brewer, S.H.; Hochstrasser, R.M. 2D IR photon echo of azido-probes for biomolecular dynamics. *Phys. Chem. Chem. Phys.* **2011,** *13*, 2237-2241.
147. Thielges, M.C.; Axup, J.Y.; Wong, D.; Lee, H.S.; Chung, J.K.; Schultz, P.G.; Fayer, M.D. Two-dimensional IR spectroscopy of protein dynamics using two vibrational

labels: a site-specific genetically encoded unnatural amino acid and an active site ligand. *J. Phys. Chem. B* **2011,** *115*, 11294-11304.

148. Wolfshorndl, M.P.; Baskin, R.; Dhawan, I.; Londergan, C.H. Covalently bound azido groups are very specific water sensors, even in hydrogen-bonding environments. *J. Phys. Chem. B* **2012,** *116*, 1172-1179.
149. Oh, K.I.; Lee, J.H.; Joo, C.; Han, H.; Cho, M. β-azidoalanine as an IR probe: application to amyloid Aβ(16-22) aggregation. *J. Phys. Chem. B* **2008,** *112*, 10352-10357.
150. Velarde, L.; Wang, H.F. Capturing inhomogeneous broadening of the -CN stretch vibration in a Langmuir monolayer with high-resolution spectra and ultrafast vibrational dynamics in sum-frequency generation vibrational spectroscopy (SFG-VS). *J. Chem. Phys.* **2013,** *139*, 084204.
151. Waegele, M.M.; Tucker, M.J.; Gai, F. 5-Cyanotryptophan as an Infrared Probe of Local Hydration Status of Proteins. *Chem. Phys. Lett.* **2009,** *478*, 249-253.
152. Tucker, M.J.; Kim, Y.S.; Hochstrasser, R.M. 2D IR photon echo study of the anharmonic coupling in the OCN region of phenyl cyanate. *Chem. Phys. Lett.* **2009,** *470*, 80-84.
153. Weeks, C.L.; Jo, H.; Kier, B.; DeGrado, W.F.; Spiro, T.G. Cysteine-linked aromatic nitriles as UV resonance Raman probes of protein structure. *J. Raman Specrosc.* **2012,** *43*, 1244-1249.
154. Tucker, M.J.; Oyola, R.; Gai, F. Conformational distribution of a 14-residue peptide in solution: a fluorescence resonance energy transfer study. *J. Phys. Chem. B* **2005,** *109*, 4788-4795.
155. Tucker, M.J.; Oyola, R.; Gai, F. A novel fluorescent probe for protein binding and folding studies: p-cyano-phenylalanine. *Biopolymers* **2006,** *83*, 571-576.
156. Aprilakis, K.N.; Taskent, H.; Raleigh, D.P. Use of the novel fluorescent amino acid p-cyanophenylalanine offers a direct probe of hydrophobic core formation during the folding of the N-terminal domain of the ribosomal protein L9 and provides evidence for two-state folding. *Biochemistry* **2007,** *46*, 12308-12313.

157. Tang, J.; Yin, H.; Qiu, J.; Tucker, M.J.; DeGrado, W.F.; Gai, F. Using two fluorescent probes to dissect the binding, insertion, and dimerization kinetics of a model membrane peptide. *J. Am. Chem. Soc.* **2009,** *131,* 3816-3817.
158. Zimmermann, J.; Thielges, M.C.; Seo, Y.J.; Dawson, P.E.; Romesberg, F.E. Cyano groups as probes of protein microenvironments and dynamics. *Angew. Chem. Int. Ed. Engl.* **2011,** *50,* 8333-8337.
159. Chung, J.K.; Thielges, M.C.; Fayer, M.D. Conformational dynamics and stability of HP35 studied with 2D IR vibrational echoes. *J. Am. Chem. Soc.* **2012,** *134,* 12118-12124.
160. Suydam, I.T.; Snow, C.D.; Pande, V.S.; Boxer, S.G. Electric fields at the active site of an enzyme: direct comparison of experiment with theory. *Science* **2006,** *313,* 200-204.
161. Fafarman, A.T.; Boxer, S.G. Nitrile bonds as infrared probes of electrostatics in ribonuclease S. *J. Phys. Chem. B* **2010,** *114,* 13536-13544.
162. Lindquist, B.A.; Corcelli, S.A. Nitrile Groups as Vibrational Probes: Calculations of the CN Infrared Absorption Line Shape of Acetonitrile in Water and Tetrahydrofuran. *J. Phys. Chem. B* **2008,** *112,* 6301-6303.
163. Weeks, C.L.; Polishchuk, A.; Getahun, Z.; Degrado, W.F.; Spiro, T.G. Investigation of an unnatural amino acid for use as a resonance Raman probe: Detection limits, solvent and temperature dependence of the vCN band of 4-cyanophenylalanine. *J. Raman Spectrosc.* **2008,** *39,* 1606-1613.
164. Schultz, K.C.; Supekova, L.; Ryu, Y.; Xie, J.; Perera, R.; Schultz, P.G. A genetically encoded infrared probe. *J. Am. Chem. Soc.* **2006,** *128,* 13984-13985.
165. Miyake-Stoner, S.J.; Miller, A.M.; Hammill, J.T.; Peeler, J.C.; Hess, K.R.; Mehl, R.A.; Brewer, S.H. Probing protein folding using site-specifically encoded unnatural amino acids as FRET donors with tryptophan. *Biochemistry* **2009,** *48,* 5953-5962.
166. Tucker, M.J.; Tang, J.; Gai, F. Probing the kinetics of membrane-mediated helix folding. *J. Phys. Chem. B* **2006,** *110,* 8105-8109.
167. Glasscock, J.M.; Zhu, Y.; Chowdhury, P.; Tang, J.; Gai, F. Using an amino acid fluorescence resonance energy transfer pair to probe protein unfolding: application

to the villin headpiece subdomain and the LysM domain. *Biochemistry* **2008,** *47*, 11070-11076.

168. Taskent-Sezgin, H.; Chung, J.; Patsalo, V.; Miyake-Stoner, S.J.; Miller, A.M.; Brewer, S.H.; Mehl, R.A.; Green, D.F.; Raleigh, D.P.; Carrico, I. Interpretation of p-cyanophenylalanine fluorescence in proteins in terms of solvent exposure and contribution of side-chain quenchers: a combined fluorescence, IR and molecular dynamics study. *Biochemistry* **2009,** *48*, 9040-9046.
169. Taskent-Sezgin, H.; Marek, P.; Thomas, R.; Goldberg, D.; Chung, J.; Carrico, I.; Raleigh, D.P. Modulation of p-cyanophenylalanine fluorescence by amino acid side chains and rational design of fluorescence probes of α-helix formation. *Biochemistry* **2010,** *49*, 6290-6295.
170. Marek, P.; Mukherjee, S.; Zanni, M.T.; Raleigh, D.P. Residue-specific, real-time characterization of lag-phase species and fibril growth during amyloid formation: a combined fluorescence and IR study of p-cyanophenylalanine analogs of islet amyloid polypeptide. *J. Mol. Biol.* **2010,** *400*, 878-888.
171. Inouye, H.; Gleason, K.A.; Zhang, D.; Decatur, S.M.; Kirschner, D.A. Differential effects of Phe19 and Phe20 on fibril formation by amyloidogenic peptide Aβ 16-22 (Ac-KLVFFAE-NH2). *Proteins* **2010,** *78*, 2306-2321.
172. Liu, H.; Lantz, R.; Cosme, P.; Rivera, N.; Andino, C.; Gonzalez, W.G.; Terentis, A.C.; Wojcikiewicz, E.P.; Oyola, R.; Miksovska, J.; Du, D. Site-specific dynamics of amyloid formation and fibrillar configuration of Aβ(1-23) using an unnatural amino acid. *Chem. Commun.* **2015,** *51*, 7000-7003.
173. Liu, H.; Morris, C.; Lantz, R.; Kent, T.W.; Elbassal, E.A.; Wojcikiewicz, E.P.; Du, D. Residue-Specific Dynamics and Local Environmental Changes in Aβ40 Oligomer and Fibril Formation. *Angew. Chem. Int. Ed. Engl.* **2018,** *57*, 8017-8021.
174. Choi, J.H.; Cho, M. Vibrational solvatochromism and electrochromism of infrared probe molecules containing C≡O, C≡N, C=O, or C-F vibrational chromophore. *J. Chem. Phys.* **2011,** *134*, 154513.
175. Pazos, I.M.; Ghosh, A.; Tucker, M.J.; Gai, F. Ester carbonyl vibration as a sensitive probe of protein local electric field. *Angew. Chem. Int. Ed. Engl.* **2014,** *53*, 6080-6084.

176. Pazos, I.M.; Ma, J.; Mukherjee, D.; Gai, F. Ultrafast Hydrogen-Bonding Dynamics in Amyloid Fibrils. *J. Phys. Chem. B* **2018,** 122, 11023-11029.
177. Ahmed, I.A.; Gai, F. Simple method to introduce an ester infrared probe into proteins. *Prot. Sci.* **2017,** *26*, 375-381.

APPENDIX B

Permission of Copyright

Letter of Permission Granting Use of Copyrighted Materials

To whom it may concern,

I am Deguo Du, PhD, Department of Chemistry and Biochemistry and I am the dissertation advisor of Richard Lantz (Z#15111930). I am the corresponding author of the publications listed below. This letter is to confirm the full permission to reproduce the materials of the publications, and the corresponding supporting information, for one of the original authors, Richard Lantz, in his dissertation titled "Human Calcitonin: An Investigation of Amyloid Formation and Inhibition" for Doctoral of Philosophy in Chemistry.

Publications:

1. Effects of Disulfide Bond and Cholesterol Derivatives on Human Calcitonin Amyloid Formation. R. Lantz, B. Busbee, E. P. Wojcikiewicz, and D. Du, *Biopolymers* **2020**, 111, e23343.

2. Flavonoids with Vicinal Hydroxyl Groups Inhibit Human Calcitonin Amyloid Formation. R. Lantz, B. Busbee, E. P. Wojcikiewicz, and D. Du, *Chemistry – A European Journal* **2020**, 10.1002/chem.202002027.

3. Vibrational Approach to the Dynamics and Structure of Protein Amyloids. H. Li, R. Lantz, and D. Du, *Molecules* **2019**, 24, 186.

Regards,

Signature: Deguo Du (Jun 25, 2020 15:37 EDT)

Date: June 25, 2020

REFERENCES

1. Kubelka, J.; Hofrichter, J.; Eaton, W. A., The protein folding 'speed limit'. *Curr. Opin. Struct. Biol.* **2004,** *14* (1), 76-88.
2. Levinthal, C., How to fold graciously. In *Mossbauer Spectroscopy in Biological Systems*, University of Illinois Press: Proceedings of a Meeting held at Allerton House (Monticello, I.L., ed.), 1969; pp 22-44.
3. Levinthal, C., Are there pathways for protein folding? *Extrait du Journal de Chimie Physique* **1968,** *65*, 44-45.
4. Leopold, P. E.; Montal, M.; Onuchic, J. N., Protein folding funnels: a kinetic approach to the sequence-structure relationship. *Proc. Natl. Acad. Sci. U. S. A.* **1992,** *89* (18), 8721-8725.
5. Onuchic, J. N.; Wolynes, P. G., Theory of protein folding. *Curr. Opin. Struct. Biol.* **2004,** *14* (1), 70-75.
6. Finkelstein, A. V.; Badretdin, A. J.; Galzitskaya, O. V.; Ivankov, D. N.; Bogatyreva, N. S.; Garbuzynskiy, S. O., There and back again: Two views on the protein folding puzzle. *Phys. Life Rev.* **2017,** *21*, 56-71.
7. Salahuddin, P., Protein folding, misfolding, aggregation and amyloid formation: Mechanisms of AB oligomer mediated toxicities. *Journal of Biochemistry and Molecular Biology Research* **2015,** *1* (2), 36-45.

8. Sipe, J. D.; Benson, M. D.; Buxbaum, J. N.; Ikeda, S.; Merlini, G.; Saraiva, M. J.; Westermark, P., Nomenclature 2014: Amyloid fibril proteins and clinical classification of the amyloidosis. *Amyloid* **2014,** *21* (4), 221-224.

9. Copp, D. H.; Cameron, E. C.; Cheney, B. A.; Davidson, A. G.; Henze, K. G., Evidence for calcitonin--a new hormone from the parathyroid that lowers blood calcium. *Endocrinology* **1962,** *70*, 638-649.

10. Wallach, S.; Rousseau, G.; Martin, L.; Azria, M., Effects of calcitonin on animal and in vitro models of skeletal metabolism. *Bone* **1999,** *25* (5), 509-516.

11. Kamgar-Parsi, K., Tolchard, J., Habenstein, B., Loquet, A., Naito, A., and Ramamoorthy, A., Structural biology of calcitonin: From aqueous therapeutic properties to amyloid aggregation. *Isr. J. Chem.* **2016,** *57*, 634-650.

12. Zaidi, M.; Inzerillo, A. M.; Moonga, B. S.; Bevis, P. J.; Huang, C. L., Forty years of calcitonin--where are we now? A tribute to the work of Iain Macintyre, FRS. *Bone* **2002,** *30* (5), 655-663.

13. Jaeger, P.; Jones, W.; Clemens, T. L.; Hayslett, J. P., Evidence that calcitonin stimulates 1,25-dihydroxyvitamin D production and intestinal absorption of calcium in vivo. *J. Clin. Invest.* **1986,** *78* (2), 456-461.

14. Riniker, B.; Brugger, M.; Kamber, B.; Rittel, W.; Sieber, P.; Neher, R., Structure and synthesis of human calcitonin M. *Biochem. J.* **1969,** *111* (3), 14P.

15. Niall, H. D.; Keutmann, H. T.; Copp, D. H.; Potts, J. T., Jr., Amino acid sequence of salmon ultimobranchial calcitonin. *Proc. Natl. Acad. Sci. U. S. A.* **1969,** *64* (2), 771-778.

16. Brewer, H. B., Jr.; Ronan, R., Amino acid sequence of bovine thyrocalcitonin. *Proc. Natl. Acad. Sci. U. S. A.* **1969,** *63* (3), 940-947.

17. Potts, J. T., Jr.; Niall, H. D.; Keutmann, H. T.; Brewer, H. B., Jr.; Deftos, L. J., The amino acid sequence of porcine thyrocalcitonin. *Proc. Natl. Acad. Sci. U. S. A.* **1968,** *59* (4), 1321-1328.

18. Raulais, D.; Hagaman, J.; Ontjes, D. A.; Lundblad, R. L.; Kingdon, H. S., The complete amino-acid sequence of rat thyrocalcitonin. *Eur. J. Biochem.* **1976,** *64* (2), 607-611.

19. Arvinte, T.; Cudd, A.; Drake, A. F., The structure and mechanism of formation of human calcitonin fibrils. *J. Biol. Chem.* **1993,** *268* (9), 6415-6422.

20. Gilchrist, P. J.; Bradshaw, J. P., Amyloid formation by salmon calcitonin. *Biochim. Biophys. Acta* **1993,** *1182* (1), 111-114.

21. Wang, S. S.; Good, T. A.; Rymer, D. L., The influence of phospholipid membranes on bovine calcitonin peptide's secondary structure and induced neurotoxic effects. *Int. J. Biochem. Cell Biol.* **2005,** *37* (8), 1656-1669.

22. Siligardi, G.; Samori, B.; Melandri, S.; Visconti, M.; Drake, A. F., Correlations between biological activities and conformational properties for human, salmon, eel, porcine calcitonins and Elcatonin elucidated by CD spectroscopy. *Eur. J. Biochem.* **1994,** *221* (3), 1117-1125.

23. Murphy, M. P.; LeVine, H., 3rd, Alzheimer's disease and the amyloid-beta peptide. *J. Alzheimers Dis.* **2010,** *19* (1), 311-323.

24. Westermark, P.; Andersson, A.; Westermark, G. T., Islet amyloid polypeptide, islet amyloid, and diabetes mellitus. *Physiol. Rev.* **2011,** *91* (3), 795-826.

25. Spillantini, M. G.; Schmidt, M. L.; Lee, V. M.; Trojanowski, J. Q.; Jakes, R.; Goedert, M., Alpha-synuclein in Lewy bodies. *Nature* **1997,** *388* (6645), 839-840.

26. Adachi, I.; Abe, K.; Tanaka, M.; Yamaguchi, K.; Miyakawa, S., Plasma human calcitonin (hCT) levels in normal and pathologic conditions, and their responses to short calcium or tetragastrin infusion. *Endocrinol. Jpn.* **1976,** *23* (6), 517-526.

27. Silver, M. M.; Hearn, S. A.; Lines, L. D.; Troster, M., Calcitonin and chromogranin A localization in medullary carcinoma of the thyroid by immunoelectron microscopy. *J. Histochem. Cytochem.* **1988,** *36* (8), 1031-1036.

28. Diociaiuti, M.; Gaudiano, M. C.; Malchiodi-Albedi, F., The slowly aggregating salmon Calcitonin: a useful tool for the study of the amyloid oligomers structure and activity. *Int. J. Mol. Sci.* **2011,** *12* (12), 9277-9295.

29. Fowler, S. B.; Poon, S.; Muff, R.; Chiti, F.; Dobson, C. M.; Zurdo, J., Rational design of aggregation-resistant bioactive peptides: reengineering human calcitonin. *Proc. Natl. Acad. Sci. U. S. A.* **2005,** *102* (29), 10105-10110.

30. Robin, J. C.; Ambrus, J. L., Studies on osteoporosis VI. Effect of human and salmon calcitonin on experimental osteoporosis. *Res. Commun. Chem. Pathol. Pharmacol.* **1982,** *35* (3), 491-498.

31. Ye, H.; Zhou, J.; Li, H.; Gao, Z., Heme prevents highly amyloidogenic human calcitonin (hCT) aggregation: A potential new strategy for the clinical reuse of hCT. *J. Inorg. Biochem.* **2019,** *196*, 110686.

32. Visser, E. J., A review of calcitonin and its use in the treatment of acute pain. *Acute Pain* **2005,** *7*, 185-189.

33. Avidan-Shpalter, C.; Gazit, E., The early stages of amyloid formation: biophysical and structural characterization of human calcitonin pre-fibrillar assemblies. *Amyloid* **2006,** *13* (4), 216-225.

34. Yamamoto, Y.; Nakamuta, H.; Koida, M.; Seyler, J. K.; Orlowski, R. C., Calcitonin-induced anorexia in rats: a structure-activity study by intraventricular injections. *Jpn. J. Pharmacol.* **1982,** *32* (6), 1013-1017.

35. Levy, F.; Muff, R.; Dotti-Sigrist, S.; Dambacher, M. A.; Fischer, J. A., Formation of neutralizing antibodies during intranasal synthetic salmon calcitonin treatment of Paget's disease. *J. Clin. Endocrinol. Metab.* **1988,** *67* (3), 541-545.

36. Muff, R.; Dambacher, M. A.; Fischer, J. A., Formation of neutralizing antibodies during intranasal synthetic salmon calcitonin treatment of postmenopausal osteoporosis. *Osteoporos. Int.* **1991,** *1* (2), 72-75.

37. Rambaran, R. N.; Serpell, L. C., Amyloid fibrils: abnormal protein assembly. *Prion* **2008,** *2* (3), 112-117.

38. Eanes, E. D.; Glenner, G. G., X-ray diffraction studies on amyloid filaments. *J. Histochem. Cytochem.* **1968,** *16* (11), 673-677.

39. Powers, E. T.; Powers, D. L., Mechanisms of protein fibril formation: nucleated polymerization with competing off-pathway aggregation. *Biophys. J.* **2008,** *94* (2), 379-391.

40. Chatani, E.; Yamamoto, N., Recent progress on understanding the mechanisms of amyloid nucleation. *Biophys Rev* **2018,** *10* (2), 527-534.

41. Lomakin, A.; Chung, D. S.; Benedek, G. B.; Kirschner, D. A.; Teplow, D. B., On the nucleation and growth of amyloid beta-protein fibrils: detection of nuclei and

quantitation of rate constants. *Proc. Natl. Acad. Sci. U. S. A.* **1996,** *93* (3), 1125-1129.

42. Harper, J. D.; Lansbury, P. T., Jr., Models of amyloid seeding in Alzheimer's disease and scrapie: mechanistic truths and physiological consequences of the time-dependent solubility of amyloid proteins. *Annu. Rev. Biochem.* **1997,** *66*, 385-407.

43. Hong, L.; Qi, X.; Zhang, Y., Dissecting the kinetic process of amyloid fiber formation through asymptotic analysis. *J. Phys. Chem. B* **2012,** *116* (23), 6611-6617.

44. Arosio, P.; Knowles, T. P.; Linse, S., On the lag phase in amyloid fibril formation. *Phys. Chem. Chem. Phys.* **2015,** *17* (12), 7606-7618.

45. Kanaori, K.; Nosaka, A. Y., Study of human calcitonin fibrillation by proton nuclear magnetic resonance spectroscopy. *Biochemistry* **1995,** *34* (38), 12138-12143.

46. Kamihira, M.; Naito, A.; Tuzi, S.; Nosaka, A. Y.; Saito, H., Conformational transitions and fibrillation mechanism of human calcitonin as studied by high-resolution solid-state 13C NMR. *Protein Sci.* **2000,** *9* (5), 867-877.

47. Naito, A.; Kamihira, M.; Inoue, R.; Saito, H., Structural diversity of amyloid fibril formed in human calcitonin as revealed by site-directed 13C solid-state NMR spectroscopy. *Magn. Reson. Chem.* **2004,** *42* (2), 247-257.

48. Huang, R.; Vivekanandan, S.; Brender, J. R.; Abe, Y.; Naito, A.; Ramamoorthy, A., NMR characterization of monomeric and oligomeric conformations of human calcitonin and its interaction with EGCG. *J. Mol. Biol.* **2012,** *416* (1), 108-120.

49. Lakshmanan, A.; Cheong, D. W.; Accardo, A.; Di Fabrizio, E.; Riekel, C.; Hauser, C. A., Aliphatic peptides show similar self-assembly to amyloid core sequences, challenging the importance of aromatic interactions in amyloidosis. *Proc. Natl. Acad. Sci. U. S. A.* **2013,** *110* (2), 519-524.

50. Kamihira, M.; Oshiro, Y.; Tuzi, S.; Nosaka, A. Y.; Saito, H.; Naito, A., Effect of electrostatic interaction on fibril formation of human calcitonin as studied by high resolution solid state 13C NMR. *J. Biol. Chem.* **2003,** *278* (5), 2859-2865.

51. Naito, A.; Kawamura, I., Solid-state NMR as a method to reveal structure and membrane-interaction of amyloidogenic proteins and peptides. *Biochim. Biophys. Acta* **2007,** *1768* (8), 1900-1912.

52. Itoh-Watanabe, H.; Kamihira-Ishijima, M.; Javkhlantugs, N.; Inoue, R.; Itoh, Y.; Endo, H.; Tuzi, S.; Saito, H.; Ueda, K.; Naito, A., Role of aromatic residues in amyloid fibril formation of human calcitonin by solid-state 13C NMR and molecular dynamics simulation. *Phys. Chem. Chem. Phys.* **2013,** *15* (23), 8890-8901.

53. Andreotti, G.; Vitale, R. M.; Avidan-Shpalter, C.; Amodeo, P.; Gazit, E.; Motta, A., Converting the highly amyloidogenic human calcitonin into a powerful fibril inhibitor by three-dimensional structure homology with a non-amyloidogenic analogue. *J. Biol. Chem.* **2011,** *286* (4), 2707-2718.

54. Scherzer-Attali, R.; Shaltiel-Karyo, R.; Adalist, Y. H.; Segal, D.; Gazit, E., Generic inhibition of amyloidogenic proteins by two naphthoquinone-tryptophan hybrid molecules. *Proteins* **2012,** *80* (8), 1962-1973.

55. Epand, R. M.; Stahl, G. L.; Orlowski, R. C., Conformational and biological properties of partial sequences of salmon calcitonin. *Int. J. Pept. Protein Res.* **1986,** *27* (5), 501-507.

56. Malchiodi-Albedi, F.; Contrusciere, V.; Raggi, C.; Fecchi, K.; Rainaldi, G.; Paradisi, S.; Matteucci, A.; Santini, M. T.; Sargiacomo, M.; Frank, C.; Gaudiano, M. C.; Diociaiuti, M., Lipid raft disruption protects mature neurons against amyloid oligomer toxicity. *Biochim. Biophys. Acta* **2010,** *1802* (4), 406-415.

57. Diociaiuti, M.; Giordani, C.; Kamel, G. S.; Brasili, F.; Sennato, S.; Bombelli, C.; Meneses, K. Y.; Giraldo, M. A.; Bordi, F., Monosialoganglioside-GM1 triggers binding of the amyloid-protein salmon calcitonin to a Langmuir membrane model mimicking the occurrence of lipid-rafts. *Biochem. Biophys. Rep.* **2016,** *8*, 365-375.

58. Lantz, R.; Busbee, B.; Wojcikiewicz, E. P.; Du, D., Effects of disulfide bond and cholesterol derivatives on human calcitonin amyloid formation. *Biopolymers* **2020,** *111*, e23343.

59. Meleleo, D.; Sblano, C., Influence of cholesterol on human calcitonin channel formation. Possible role of sterol as molecular chaperone. *Aims Biophysics* **2019,** *6* (1), 23-38.

60. Simons, K.; Toomre, D., Lipid rafts and signal transduction. *Nat. Rev. Mol. Cell Biol.* **2000,** *1* (1), 31-39.

61. Grouleff, J.; Irudayam, S. J.; Skeby, K. K.; Schiott, B., The influence of cholesterol on membrane protein structure, function, and dynamics studied by molecular dynamics simulations. *Biochim. Biophys. Acta* **2015,** *1848* (9), 1783-1795.

62. Diociaiuti, M.; Polzi, L. Z.; Valvo, L.; Malchiodi-Albedi, F.; Bombelli, C.; Gaudiano, M. C., Calcitonin forms oligomeric pore-like structures in lipid membranes. *Biophys. J.* **2006,** *91* (6), 2275-2281.

63. Sheynis, T.; Jelinek, R., Lipid-induced calcitonin fibrillation blocks membrane interactions of a peptide antibiotic. *J. Phys. Chem. B* **2010,** *114* (47), 15530-15535.

64. Belfiore, M.; Cariati, I.; Matteucci, A.; Gaddini, L.; Macchia, G.; Fioravanti, R.; Frank, C.; Tancredi, V.; D'Arcangelo, G.; Diociaiuti, M., Calcitonin native prefibrillar oligomers but not monomers induce membrane damage that triggers NMDA-mediated Ca(2+)-influx, LTP impairment and neurotoxicity. *Sci. Rep.* **2019,** *9* (1), 5144.

65. Ledeen, R. W.; Wu, G., The multi-tasked life of GM1 ganglioside, a true factotum of nature. *Trends Biochem. Sci.* **2015,** *40* (7), 407-418.

66. Stipani, V.; Gallucci, E.; Micelli, S.; Picciarelli, V.; Benz, R., Channel formation by salmon and human calcitonin in black lipid membranes. *Biophys. J.* **2001,** *81* (6), 3332-3338.

67. Chiti, F.; Dobson, C. M., Protein misfolding, amyloid formation, and human disease: A summary of progress over the last decade. *Annu. Rev. Biochem.* **2017,** *86*, 27-68.

68. Caughey, B.; Lansbury, P. T., Protofibrils, pores, fibrils, and neurodegeneration: separating the responsible protein aggregates from the innocent bystanders. *Annu. Rev. Neurosci.* **2003,** *26*, 267-298.

69. Lashuel, H. A.; Hartley, D.; Petre, B. M.; Walz, T.; Lansbury, P. T., Jr., Neurodegenerative disease: amyloid pores from pathogenic mutations. *Nature* **2002,** *418* (6895), 291-292.

70. Kagan, B. L.; Azimov, R.; Azimova, R., Amyloid peptide channels. *J. Membr. Biol.* **2004,** *202* (1), 1-10.

71. Grauer, A.; Reinel, H. H.; Ziegler, R.; Raue, F., Neutralizing antibodies against calcitonin. *Horm. Metab. Res.* **1993,** *25* (9), 486-488.

72. Chen, Y. T.; Hu, K. W.; Huang, B. J.; Lai, C. H.; Tu, L. H., Inhibiting human halcitonin fibril formation with its most relevant aggregation-resistant analog. *J. Phys. Chem. B* **2019,** *123* (48), 10171-10180.

73. Andreotti, G.; Motta, A., Modulating calcitonin fibrillogenesis: an antiparallel alpha-helical dimer inhibits fibrillation of salmon calcitonin. *J. Biol. Chem.* **2004,** *279* (8), 6364-6370.

74. Frydman-Marom, A.; Shaltiel-Karyo, R.; Moshe, S.; Gazit, E., The generic amyloid formation inhibition effect of a designed small aromatic beta-breaking peptide. *Amyloid* **2011,** *18* (3), 119-127.

75. Reches, M.; Porat, Y.; Gazit, E., Amyloid fibril formation by pentapeptide and tetrapeptide fragments of human calcitonin. *J. Biol. Chem.* **2002,** *277* (38), 35475-35480.

76. Gazit, E., A possible role for pi-stacking in the self-assembly of amyloid fibrils. *FASEB J.* **2002,** *16* (1), 77-83.

77. Lee, H. H.; Choi, T. S.; Lee, S. J.; Lee, J. W.; Park, J.; Ko, Y. H.; Kim, W. J.; Kim, K.; Kim, H. I., Supramolecular inhibition of amyloid fibrillation by cucurbit[7]uril. *Angew. Chem. Int. Ed. Engl.* **2014,** *53* (29), 7461-7465.

78. Shang, H.; Zhou, A.; Jiang, J.; Liu, Y.; Xie, J.; Li, S.; Chen, Y.; Zhu, X.; Tan, H.; Li, J., Inhibition of the fibrillation of highly amyloidogenic human calcitonin by cucurbit[7]uril with improved bioactivity. *Acta Biomater.* **2018,** *78*, 178-188.

79. Zhu, M.; Rajamani, S.; Kaylor, J.; Han, S.; Zhou, F.; Fink, A. L., The flavonoid baicalein inhibits fibrillation of alpha-synuclein and disaggregates existing fibrils. *J. Biol. Chem.* **2004,** *279* (26), 26846-26857.

80. Dragicevic, N.; Smith, A.; Lin, X.; Yuan, F.; Copes, N.; Delic, V.; Tan, J.; Cao, C.; Shytle, R. D.; Bradshaw, P. C., Green tea epigallocatechin-3-gallate (EGCG) and other flavonoids reduce Alzheimer's amyloid-induced mitochondrial dysfunction. *J. Alzheimers Dis.* **2011,** *26* (3), 507-521.

81. Pallas, M.; Porquet, D.; Vicente, A.; Sanfeliu, C., Resveratrol: new avenues for a natural compound in neuroprotection. *Curr. Pharm. Des.* **2013,** *19* (38), 6726-6731.

82. Wei, L.; Jiang, P.; Xu, W.; Li, H.; Zhang, H.; Yan, L.; Chan-Park, M. B.; Liu, X. W.; Tang, K.; Mu, Y.; Pervushin, K., The molecular basis of distinct aggregation pathways of islet amyloid polypeptide. *J. Biol. Chem.* **2011,** *286* (8), 6291-6300.

83. Hase, T.; Shishido, S.; Yamamoto, S.; Yamashita, R.; Nukima, H.; Taira, S.; Toyoda, T.; Abe, K.; Hamaguchi, T.; Ono, K.; Noguchi-Shinohara, M.; Yamada, M.; Kobayashi, S., Rosmarinic acid suppresses Alzheimer's disease development by reducing amyloid beta aggregation by increasing monoamine secretion. *Sci. Rep.* **2019,** *9* (1), 8711.

84. Sun, G. J., and Shigemori H., Inhibitory activity on amyloid aggregation of rosmarinic acid and its substructures from isodon japonicus. *Nat. Prod. Commun.* **2019,** *14*, 1-5.

85. Guo, C.; Ma, L.; Zhao, Y.; Peng, A.; Cheng, B.; Zhou, Q.; Zheng, L.; Huang, K., Inhibitory effects of magnolol and honokiol on human calcitonin aggregation. *Sci. Rep.* **2015,** *5*, 13556.

86. Ehrnhoefer, D. E.; Bieschke, J.; Boeddrich, A.; Herbst, M.; Masino, L.; Lurz, R.; Engemann, S.; Pastore, A.; Wanker, E. E., EGCG redirects amyloidogenic polypeptides into unstructured, off-pathway oligomers. *Nat. Struct. Mol. Biol.* **2008,** *15* (6), 558-566.

87. Meng, X.; Munishkina, L. A.; Fink, A. L.; Uversky, V. N., Molecular mechanisms underlying the flavonoid-induced inhibition of alpha-synuclein fibrillation. *Biochemistry* **2009,** *48* (34), 8206-8224.

88. Ishii, T.; Mori, T.; Tanaka, T.; Mizuno, D.; Yamaji, R.; Kumazawa, S.; Nakayama, T.; Akagawa, M., Covalent modification of proteins by green tea polyphenol (-)-epigallocatechin-3-gallate through autoxidation. *Free Radic. Biol. Med.* **2008,** *45* (10), 1384-1394.

89. Popovych, N.; Brender, J. R.; Soong, R.; Vivekanandan, S.; Hartman, K.; Basrur, V.; Macdonald, P. M.; Ramamoorthy, A., Site specific interaction of the polyphenol EGCG with the SEVI amyloid precursor peptide PAP(248-286). *J. Phys. Chem. B* **2012,** *116* (11), 3650-3658.

90. Cao, P.; Raleigh, D. P., Analysis of the inhibition and remodeling of islet amyloid polypeptide amyloid fibers by flavanols. *Biochemistry* **2012,** *51* (13), 2670-2683.

91. Wang, S. H.; Dong, X. Y.; Sun, Y., Thermodynamic analysis of the molecular interactions between amyloid beta-protein fragments and (-)-epigallocatechin-3-gallate. *J. Phys. Chem. B* **2012,** *116* (20), 5803-5809.

92. Jameson, L. P.; Smith, N. W.; Dzyuba, S. V., Dye-binding assays for evaluation of the effects of small molecule inhibitors on amyloid (abeta) self-assembly. *ACS Chem. Neurosci.* **2012,** *3* (11), 807-819.

93. Hawe, A.; Sutter, M.; Jiskoot, W., Extrinsic fluorescent dyes as tools for protein characterization. *Pharm. Res.* **2008,** *25* (7), 1487-1499.

94. Stsiapura, V. I.; Maskevich, A. A.; Kuzmitsky, V. A.; Turoverov, K. K.; Kuznetsova, I. M., Computational study of thioflavin T torsional relaxation in the excited state. *J. Phys. Chem. A* **2007,** *111* (22), 4829-4835.

95. Biancalana, M.; Koide, S., Molecular mechanism of Thioflavin-T binding to amyloid fibrils. *Biochim. Biophys. Acta* **2010,** *1804* (7), 1405-1412.

96. Kelly, S. M.; Jess, T. J.; Price, N. C., How to study proteins by circular dichroism. *Biochim. Biophys. Acta* **2005,** *1751* (2), 119-139.

97. Liu, H.; Lantz, R.; Cosme, P.; Rivera, N.; Andino, C.; Gonzalez, W. G.; Terentis, A. C.; Wojcikiewicz, E. P.; Oyola, R.; Miksovska, J.; Du, D., Site-specific dynamics of amyloid formation and fibrillar configuration of Abeta(1-23) using an unnatural amino acid. *Chem. Commun.* **2015,** *51* (32), 7000-7003.

98. Juszczyk, P.; Kolodziejczyk, A. S.; Grzonka, Z., Circular dichroism and aggregation studies of amyloid beta (11-8) fragment and its variants. *Acta Biochim. Pol.* **2005,** *52* (2), 425-431.

99. Kawashima, H.; Katayama, M.; Yoshida, R.; Akaji, K.; Asano, A.; Doi, M., A dimer model of human calcitonin13-32 forms an alpha-helical structure and robustly aggregates in 50% aqueous 2,2,2-trifluoroethanol solution. *J. Pept. Sci.* **2016,** *22* (7), 480-484.

100. Jozef Adamcik, R. M., Study of amyloid fibrils via atomic force microscopy. *Curr. Opin. Colloid Interface Sci.* **2012,** *17*, 369-376.

101. Anderson, M.; Bocharova, O. V.; Makarava, N.; Breydo, L.; Salnikov, V. V.; Baskakov, I. V., Polymorphism and ultrastructural organization of prion protein amyloid fibrils: an insight from high resolution atomic force microscopy. *J. Mol. Biol.* **2006,** *358* (2), 580-596.

102. Maurstad, G.; Prass, M.; Serpell, L. C.; Sikorski, P., Dehydration stability of amyloid fibrils studied by AFM. *Eur. Biophys. J.* **2009,** *38* (8), 1135-1140.

103. Vahabi, S.; Nazemi Salman, B.; Javanmard, A., Atomic force microscopy application in biological research: a review study. *Iran J. Med. Sci.* **2013,** *38* (2), 76-83.

104. Mastrangelo, I. A.; Ahmed, M.; Sato, T.; Liu, W.; Wang, C.; Hough, P.; Smith, S. O., High-resolution atomic force microscopy of soluble Abeta42 oligomers. *J. Mol. Biol.* **2006,** *358* (1), 106-119.

105. Liu, Z.; Li, Z.; Zhou, H.; Wei, G.; Song, Y.; Wang, L., Observation of the mica surface by atomic force microscopy. *Micron* **2005,** *36* (6), 525-531.

106. Carvalho, P. M.; Felicio, M. R.; Santos, N. C.; Goncalves, S.; Domingues, M. M., Application of light scattering techniques to nanoparticle characterization and development. *Front. Chem.* **2018,** *6*, 237.

107. Streets, A. M.; Sourigues, Y.; Kopito, R. R.; Melki, R.; Quake, S. R., Simultaneous measurement of amyloid fibril formation by dynamic light scattering and fluorescence reveals complex aggregation kinetics. *PLoS One* **2013,** *8* (1), e54541.

108. Terakawa, M. S.; Yagi, H.; Adachi, M.; Lee, Y. H.; Goto, Y., Small liposomes accelerate the fibrillation of amyloid beta (1-40). *J. Biol. Chem.* **2015,** *290* (2), 815-826.

109. Byard, R. W.; Thorner, P. S.; Chan, H. S.; Griffiths, A. M.; Cutz, E., Pathological features of multiple endocrine neoplasia type IIb in childhood. *Pediatric pathology* **1990,** *10* (4), 581-592.

110. Greenland, P.; Bowley, N. L.; Meiklejohn, B.; Doane, K. L.; Sparks, C. E., Blood cholesterol concentration: fingerstick plasma vs venous serum sampling. *Clin. Chem.* **1990,** *36* (4), 628-630.

111. Strott, C. A.; Higashi, Y., Cholesterol sulfate in human physiology: what's it all about? *J. Lipid Res.* **2003,** *44* (7), 1268-1278.

112. Huang, Y. S.; Eid, K.; Davignon, J., Cholesteryl sulfate: measurement with beta-sitosteryl sulfate as an internal standard. *Can. J. Biochem.* **1981,** *59* (8), 602-605.

113. Serizawa, S.; Nagai, T.; Ito, M.; Sato, Y., Simplified determination of serum cholesterol sulfate by gas-liquid chromatography combined with cyclohexylsilane-bonded phase column purification. *Arch. Dermatol. Res.* **1989,** *281* (6), 411-416.

114. Body, J. J.; Demeester-Mirkine, N.; Borkowski, A.; Suciu, S.; Corvilain, J., Calcitonin deficiency in primary hypothyroidism. *J. Clin. Endocrinol. Metab.* **1986,** *62* (4), 700-703.

115. Elbassal, E. A.; Liu, H.; Morris, C.; Wojcikiewicz, E. P.; Du, D., Effects of charged cholesterol derivatives on Abeta40 amyloid formation. *J. Phys. Chem. B* **2016,** *120* (1), 59-68.

116. Chen, M.; Deng, Q.; Li, X. R.; Liu, Y., The hypocalcemia effect of salmon calcitonin ultra-flexible liposomes after intranasal administration in rats. *Yao Xue Xue Bao* **2007,** *42* (6), 681-686.

117. Fantini, J.; Yahi, N.; Garmy, N., Cholesterol accelerates the binding of Alzheimer's beta-amyloid peptide to ganglioside GM1 through a universal hydrogen-bond-dependent sterol tuning of glycolipid conformation. *Front. Physiol.* **2013,** *4*, 120.

118. Kanaori, K.; Nosaka, A. Y., Characterization of human calcitonin fibrillation in aqueous urea solution by 1H NMR spectroscopy. *Biochemistry* **1996,** *35* (39), 12671-12676.

119. Ellman, G. L., A colorimetric method for determining low concentrations of mercaptans. *Arch. Biochem. Biophys.* **1958,** *74* (2), 443-450.

120. Epand, R. M.; Epand, R. F.; Orlowski, R. C.; Schlueter, R. J.; Boni, L. T.; Hui, S. W., Amphipathic helix and its relationship to the interaction of calcitonin with phospholipids. *Biochemistry* **1983,** *22* (22), 5074-5084.

121. Steiner, A. M.; Bulaj, G., Optimization of oxidative folding methods for cysteine-rich peptides: a study of conotoxins containing three disulfide bridges. *J. Pept. Sci.* **2011,** *17* (1), 1-7.

122. Winther, J. R.; Thorpe, C., Quantification of thiols and disulfides. *Biochim. Biophys. Acta* **2014,** *1840* (2), 838-846.

123. Groenning, M., Binding mode of Thioflavin T and other molecular probes in the context of amyloid fibrils-current status. *J. Chem. Biol.* **2010,** *3* (1), 1-18.

124. LeVine, H., 3rd, Quantification of beta-sheet amyloid fibril structures with thioflavin T. *Methods Enzymol.* **1999,** *309*, 274-84.

125. Getz, E. B.; Xiao, M.; Chakrabarty, T.; Cooke, R.; Selvin, P. R., A comparison between the sulfhydryl reductants tris(2-carboxyethyl)phosphine and dithiothreitol for use in protein biochemistry. *Anal. Biochem.* **1999,** *273* (1), 73-80.

126. LeVine, H., 3rd, Thioflavine T interaction with synthetic Alzheimer's disease beta-amyloid peptides: detection of amyloid aggregation in solution. *Protein Sci.* **1993,** *2* (3), 404-410.

127. Haberland, M. E.; Reynolds, J. A., Self-association of cholesterol in aqueous solution. *Proc. Natl. Acad. Sci. U. S. A.* **1973,** *70* (8), 2313-2316.

128. Choo-Smith, L. P.; Garzon-Rodriguez, W.; Glabe, C. G.; Surewicz, W. K., Acceleration of amyloid fibril formation by specific binding of Abeta-(1-40) peptide to ganglioside-containing membrane vesicles. *J. Biol. Chem.* **1997,** *272* (37), 22987-22990.

129. Wakabayashi, M.; Okada, T.; Kozutsumi, Y.; Matsuzaki, K., GM1 ganglioside-mediated accumulation of amyloid beta-protein on cell membranes. *Biochem. Biophys. Res. Commun.* **2005,** *328* (4), 1019-1023.

130. Wang, S. S.; Rymer, D. L.; Good, T. A., Reduction in cholesterol and sialic acid content protects cells from the toxic effects of beta-amyloid peptides. *J. Biol. Chem.* **2001,** *276* (45), 42027-42034.

131. Herbig, M. E.; Fromm, U.; Leuenberger, J.; Krauss, U.; Beck-Sickinger, A. G.; Merkle, H. P., Bilayer interaction and localization of cell penetrating peptides with model membranes: a comparative study of a human calcitonin (hCT)-derived peptide with pVEC and pAntp(43-58). *Biochim. Biophys. Acta* **2005,** *1712* (2), 197-211.

132. Micelli, S.; Meleleo, D.; Picciarelli, V.; Gallucci, E., Effect of pH-variation on insertion and ion channel formation of human calcitonin into planar lipid bilayers. *Front. Biosci.* **2006,** *11*, 2035-2044.

133. Kremer, J. J.; Murphy, R. M., Kinetics of adsorption of beta-amyloid peptide Abeta(1-40) to lipid bilayers. *J. Biochem. Biophys. Methods* **2003,** *57* (2), 159-169.

134. Pozzi, D.; Marchini, C.; Cardarelli, F.; Salomone, F.; Coppola, S.; Montani, M.; Zabaleta, M. E.; Digman, M. A.; Gratton, E.; Colapicchioni, V.; Caracciolo, G., Mechanistic evaluation of the transfection barriers involved in lipid-mediated gene delivery: interplay between nanostructure and composition. *Biochim. Biophys. Acta* **2014,** *1838* (3), 957-967.

135. Gordon, D. J.; Meredith, S. C., Probing the role of backbone hydrogen bonding in beta-amyloid fibrils with inhibitor peptides containing ester bonds at alternate positions. *Biochemistry* **2003,** *42* (2), 475-485.

136. Davis, A. P.; Draper, S. M.; Dunne, G.; Ashton, P., The N-carbamoyl squaramide dimer: a compact, strongly associated H-bonding motif. *Chem. Commun. (Cambridge, U. K.)* **1999,** (22), 2265-2266.

137. Rzepecki, P.; Nagel-Steger, L.; Feuerstein, S.; Linne, U.; Molt, O.; Zadmard, R.; Aschermann, K.; Wehner, M.; Schrader, T.; Riesner, D., Prevention of Alzheimer's

disease-associated Abeta aggregation by rationally designed nonpeptidic beta-sheet ligands. *J. Biol. Chem.* **2004,** *279* (46), 47497-47505.

138. Kroth, H.; Ansaloni, A.; Varisco, Y.; Jan, A.; Sreenivasachary, N.; Rezaei-Ghaleh, N.; Giriens, V.; Lohmann, S.; Lopez-Deber, M. P.; Adolfsson, O.; Pihlgren, M.; Paganetti, P.; Froestl, W.; Nagel-Steger, L.; Willbold, D.; Schrader, T.; Zweckstetter, M.; Pfeifer, A.; Lashuel, H. A.; Muhs, A., Discovery and structure activity relationship of small molecule inhibitors of toxic beta-amyloid-42 fibril formation. *J. Biol. Chem.* **2012,** *287* (41), 34786-34800.

139. Smith, P. E.; Brender, J. R.; Ramamoorthy, A., Induction of negative curvature as a mechanism of cell toxicity by amyloidogenic peptides: the case of islet amyloid polypeptide. *J. Am. Chem. Soc.* **2009,** *131* (12), 4470-4478.

140. Cudd, A.; Arvinte, T.; Das, R. E.; Chinni, C.; MacIntyre, I., Enhanced potency of human calcitonin when fibrillation is avoided. *J. Pharm. Sci.* **1995,** *84* (6), 717-719.

141. Sacchettini, J. C.; Kelly, J. W., Therapeutic strategies for human amyloid diseases. *Nat. Rev. Drug Discovery* **2002,** *1* (4), 267-275.

142. Pithadia, A. S.; Bhunia, A.; Sribalan, R.; Padmini, V.; Fierke, C. A.; Ramamoorthy, A., Influence of a curcumin derivative on hIAPP aggregation in the absence and presence of lipid membranes. *Chem. Commun. (Camb)* **2016,** *52* (5), 942-945.

143. Pithadia, A.; Brender, J. R.; Fierke, C. A.; Ramamoorthy, A., Inhibition of IAPP aggregation and toxicity by natural products and derivatives. *J. Diabetes Res.* **2016,** *2016*, 2046327.

144. Giorgetti, S.; Greco, C.; Tortora, P.; Aprile, F. A., Targeting amyloid aggregation: an overview of strategies and mechanisms. *Int. J. Mol. Sci.* **2018,** *19* (9).

145. Porat, Y.; Abramowitz, A.; Gazit, E., Inhibition of amyloid fibril formation by polyphenols: structural similarity and aromatic interactions as a common inhibition mechanism. *Chem. Biol. Drug Des.* **2006,** *67* (1), 27-37.

146. Sarah J. Cox, D. C. R. C., Young-Ho Lee, Magdalena I. Ivanova, Vediappen Padmini, Bernd Reif, Ayyalusamy Ramamoorthy, Small molecule induced toxic human-IAPP species characterized by NMR. *bioRxiv* **2019**.

147. Khan, N.; Afaq, F.; Saleem, M.; Ahmad, N.; Mukhtar, H., Targeting multiple signaling pathways by green tea polyphenol (-)-epigallocatechin-3-gallate. *Cancer Res.* **2006,** *66* (5), 2500-2505.

148. Attar, A.; Rahimi, F.; Bitan, G., Modulators of amyloid protein aggregation and toxicity: EGCG and CLR01. *Trans. Neurosci.* **2013,** *4* (4), 385-409.

149. Palhano, F. L.; Lee, J.; Grimster, N. P.; Kelly, J. W., Toward the molecular mechanism(s) by which EGCG treatment remodels mature amyloid fibrils. *J. Am. Chem. Soc.* **2013,** *135* (20), 7503-7510.

150. Bolton, J. L.; Dunlap, T., Formation and biological targets of quinones: cytotoxic versus cytoprotective effects. *Chem. Res. Toxicol.* **2017,** *30* (1), 13-37.

151. Feng, S.; Song, X.-H.; Zeng, C.-M., Inhibition of amyloid fibrillation of lysozyme by phenolic compounds involves quinoprotein formation. *FEBS Lett.* **2012,** *586* (22), 3951-3955.

152. Sang, S.; Lee, M. J.; Hou, Z.; Ho, C. T.; Yang, C. S., Stability of tea polyphenol (-)-epigallocatechin-3-gallate and formation of dimers and epimers under common experimental conditions. *J. Agric. Food Chem.* **2005,** *53* (24), 9478-9484.

153. An T.; Feng, S.; Zenga, C., Oxidized epigallocatechin gallate inhibited lysozyme fibrillation more strongly than the native form. *Redox Biology* **2017,** *11*, 315-321.

154. Bittner, S., When quinones meet amino acids: chemical, physical and biological consequences. *Amino Acids* **2006,** *30* (3), 205-224.

155. Shira Shaham-Niv, P. R., Dor Zaguri, Aviad Levin, Lihi Adler-Abramovich, Lela Vuković,; Gazit, P. K. E., Differential inhibition of metabolite amyloid formation by generic fibrillation-modifying polyphenols. *Communications Chemistry* **2018,** *1*, 1-25.

156. Bieschke, J.; Russ, J.; Friedrich, R. P.; Ehrnhoefer, D. E.; Wobst, H.; Neugebauer, K.; Wanker, E. E., EGCG remodels mature alpha-synuclein and amyloid-beta fibrils and reduces cellular toxicity. *Proc. Natl. Acad. Sci. U. S. A.* **2010,** *107* (17), 7710-7715.

157. Manach, C.; Scalbert, A.; Morand, C.; Remesy, C.; Jimenez, L., Polyphenols: food sources and bioavailability. *Am. J. Clin. Nutr.* **2004,** *79* (5), 727-747.

158. Cordes, E. H.; Jenck J. P., On the mechanism of schiff base formation and hydrolysis. *J. Am. Chem. Soc.* **1962,** *84*, 832-837.

159. Malisauskas, R.; Botyriute, A.; Cannon, J. G.; Smirnovas, V., Flavone derivatives as inhibitors of insulin amyloid-like fibril formation. *PLoS One* **2015,** *10* (3), e0121231.

160. Velander, P.; Wu, L.; Ray, W. K.; Helm, R. F.; Xu, B., Amylin amyloid inhibition by flavonoid baicalein: key roles of its vicinal dihydroxyl groups of the catechol moiety. *Biochemistry* **2016,** *55* (31), 4255-4258.

161. Shimoi, K.; Okada, H.; Furugori, M.; Goda, T.; Takase, S.; Suzuki, M.; Hara, Y.; Yamamoto, H.; Kinae, N., Intestinal absorption of luteolin and luteolin 7-O-beta-glucoside in rats and humans. *FEBS Lett.* **1998,** *438* (3), 220-224.

162. Lopez-Lazaro, M., Distribution and biological activities of the flavonoid luteolin. *Mini-Rev. Med. Chem.* **2009,** *9* (1), 31-59.

163. Ravishankar, D.; Watson, K. A.; Boateng, S. Y.; Green, R. J.; Greco, F.; Osborn, H. M., Exploring quercetin and luteolin derivatives as antiangiogenic agents. *Eur. J. Med. Chem.* **2015,** *97*, 259-274.

164. Li, Y.; Yao, J.; Han, C.; Yang, J.; Chaudhry, M. T.; Wang, S.; Liu, H.; Yin, Y., Quercetin, Inflammation and Immunity. *Nutrients* **2016,** *8* (3), 167.

165. Wang, J. B.; Wang, Y. M.; Zeng, C. M., Quercetin inhibits amyloid fibrillation of bovine insulin and destabilizes preformed fibrils. *Biochem. Biophys. Res. Commun.* **2011,** *415* (4), 675-679.

166. Akaishi, T.; Morimoto, T.; Shibao, M.; Watanabe, S.; Sakai-Kato, K.; Utsunomiya-Tate, N.; Abe, K., Structural requirements for the flavonoid fisetin in inhibiting fibril formation of amyloid beta protein. *Neurosci. Lett.* **2008,** *444* (3), 280-285.

167. Cao, D.; Zhang, Y.; Zhang, H.; Zhong, L.; Qian, X., Systematic characterization of the covalent interactions between (-)-epigallocatechin gallate and peptides under physiological conditions by mass spectrometry. *Rapid Commun. Mass Spectrom.* **2009,** *23* (8), 1147-1157.

168. Hirohata, M.; Hasegawa, K.; Tsutsumi-Yasuhara, S.; Ohhashi, Y.; Ookoshi, T.; Ono, K.; Yamada, M.; Naiki, H., The anti-amyloidogenic effect is exerted against

Alzheimer's beta-amyloid fibrils in vitro by preferential and reversible binding of flavonoids to the amyloid fibril structure. *Biochemistry* **2007,** *46* (7), 1888-1899.

169. Caruana, M.; Hogen, T.; Levin, J.; Hillmer, A.; Giese, A.; Vassallo, N., Inhibition and disaggregation of alpha-synuclein oligomers by natural polyphenolic compounds. *FEBS Lett.* **2011,** *585* (8), 1113-1120.

170. Phan, H. T. T.; Samarat, K.; Takamura, Y.; Azo-Oussou, A. F.; Nakazono, Y.; Vestergaard, M. C., Polyphenols modulate alzheimer's amyloid beta aggregation in a structure-dependent manner. *Nutrients* **2019,** *11* (4), 756-770.

171. Li, B. Q.; Fu, T.; Gong, W. H.; Dunlop, N.; Kung, H.; Yan, Y.; Kang, J.; Wang, J. M., The flavonoid baicalin exhibits anti-inflammatory activity by binding to chemokines. *Immunopharmacology* **2000,** *49* (3), 295-306.

172. Wu, J. A.; Attele, A. S.; Zhang, L.; Yuan, C. S., Anti-HIV activity of medicinal herbs: usage and potential development. *Am. J. Chin. Med.* **2001,** *29* (1), 69-81.

173. Ikezoe, T.; Chen, S. S.; Heber, D.; Taguchi, H.; Koeffler, H. P., Baicalin is a major component of PC-SPES which inhibits the proliferation of human cancer cells via apoptosis and cell cycle arrest. *Prostate* **2001,** *49* (4), 285-292.

174. Gao, Z.; Huang, K.; Xu, H., Protective effects of flavonoids in the roots of Scutellaria baicalensis Georgi against hydrogen peroxide-induced oxidative stress in HS-SY5Y cells. *Pharmacol. Res.* **2001,** *43* (2), 173-178.

175. Shieh, D. E.; Liu, L. T.; Lin, C. C., Antioxidant and free radical scavenging effects of baicalein, baicalin and wogonin. *Anticancer Res.* **2000,** *20* (5A), 2861-2865.

176. Choi, S. M.; Kim, B. C.; Cho, Y. H.; Choi, K. H.; Chang, J.; Park, M. S.; Kim, M. K.; Cho, K. H.; Kim, J. K., Effects of flavonoid compounds on beta-amyloid-

peptide-induced neuronal death in cultured mouse cortical neurons. *Chonnam. Med. J.* **2014,** *50* (2), 45-51.

177. Hong, D. P.; Fink, A. L.; Uversky, V. N., Structural characteristics of alpha-synuclein oligomers stabilized by the flavonoid baicalein. *J. Mol. Biol.* **2008,** *383* (1), 214-223.

178. Meng, X.; Munishkina, L. A.; Fink, A. L.; Uversky, V. N., Effects of various flavonoids on the alpha-synuclein fibrillation process. *Parkinsons Dis.* **2010,** *2010*, 650794.

179. Choi, J. S.; Braymer, J. J.; Nanga, R. P.; Ramamoorthy, A.; Lim, M. H., Design of small molecules that target metal-Abeta species and regulate metal-induced A{beta} aggregation and neurotoxicity. *Proc. Natl. Acad. Sci. U. S. A.* **2010,** *107* (51), 21990-21995.

180. Hindo, S. S.; Mancino, A. M.; Braymer, J. J.; Liu, Y.; Vivekanandan, S.; Ramamoorthy, A.; Lim, M. H., Small molecule modulators of copper-induced Abeta aggregation. *J. Am. Chem. Soc.* **2009,** *131* (46), 16663-16665.

181. Ramamoorthy, A.; Lim, M. H., Structural characterization and inhibition of toxic amyloid-beta oligomeric intermediates. *Biophys. J.* **2013,** *105* (2), 287-288.

182. Singh, N. A.; Mandal, A. K.; Khan, Z. A., Potential neuroprotective properties of epigallocatechin-3-gallate (EGCG). *Nutr. J.* **2016,** *15* (1), 60.

183. Lorenzen, N.; Nielsen, S. B.; Yoshimura, Y.; Vad, B. S.; Andersen, C. B.; Betzer, C.; Kaspersen, J. D.; Christiansen, G.; Pedersen, J. S.; Jensen, P. H.; Mulder, F. A.; Otzen, D. E., How epigallocatechin gallate can inhibit alpha-synuclein oligomer toxicity in vitro. *J. Biol. Chem.* **2014,** *289* (31), 21299-21310.

184. Engel, M. F.; vandenAkker, C. C.; Schleeger, M.; Velikov, K. P.; Koenderink, G. H.; Bonn, M., The polyphenol EGCG inhibits amyloid formation less efficiently at phospholipid interfaces than in bulk solution. *J. Am. Chem. Soc.* **2012,** *134* (36), 14781-14788.

185. Manach, C.; Donovan, J. L., Pharmacokinetics and metabolism of dietary flavonoids in humans. *Free Radic. Res.* **2004,** *38* (8), 771-785.

186. Visentin, C.; Pellistri, F.; Natalello, A.; Vertemara, J.; Bonanomi, M.; Gatta, E.; Penco, A.; Relini, A.; De Gioia, L.; Airoldi, C.; Regonesi, M. E.; Tortora, P., Epigallocatechin-3-gallate and related phenol compounds redirect the amyloidogenic aggregation pathway of ataxin-3 towards non-toxic aggregates and prevent toxicity in neural cells and Caenorhabditis elegans animal model. *Hum. Mol. Genet.* **2017,** *26* (17), 3271-3284.

187. Cabrera, C.; Artacho, R.; Giménez, R., Beneficial effects of green tea—a review. *Journal of the American College of Nutrition* **2006,** *25* (2), 79-99.

188. Nicholson, G. C.; Moseley, J. M.; Sexton, P. M.; Mendelsohn, F. A.; Martin, T. J., Abundant calcitonin receptors in isolated rat osteoclasts. Biochemical and autoradiographic characterization. *J. Clin. Invest.* **1986,** *78* (2), 355-360.

189. Kamgar-Parsi, K.; Hong, L.; Naito, A.; Brooks, C. L., 3rd; Ramamoorthy, A., Growth-incompetent monomers of human calcitonin lead to a noncanonical direct relationship between peptide concentration and aggregation lag time. *J. Biol. Chem.* **2017,** *292* (36), 14963-14976.

190. Motta, A.; Andreotti, G.; Amodeo, P.; Strazzullo, G.; Castiglione Morelli, M. A., Solution structure of human calcitonin in membrane-mimetic environment: the role of the amphipathic helix. *Proteins* **1998,** *32* (3), 314-323.

191. Rideau, E.; Dimova, R.; Schwille, P.; Wurm, F. R.; Landfester, K., Liposomes and polymersomes: a comparative review towards cell mimicking. *Chem. Soc. Rev.* **2018,** *47* (23), 8572-8610.

192. Bulbake, U.; Doppalapudi, S.; Kommineni, N.; Khan, W., Liposomal formulations in clinical use: an updated review. *Pharmaceutics* **2017,** *9* (2), 1-33.

193. HORIBA, L. Particle size analysis of liposomes using dynamic light scattering. https://www.horiba.com/scientific/products/particlecharacterization/applications/pharmaceuticals/liposomes/ (accessed 3/19/2020).

194. Micelli, S.; Meleleo, D.; Picciarelli, V.; Stoico, M. G.; Gallucci, E., Effect of nanomolar concentrations of sodium dodecyl sulfate, a catalytic inductor of alpha-helices, on human calcitonin incorporation and channel formation in planar lipid membranes. *Biophys. J.* **2004,** *87* (2), 1065-1075.

195. Schubert, D.; Behl, C.; Lesley, R.; Brack, A.; Dargusch, R.; Sagara, Y.; Kimura, H., Amyloid peptides are toxic via a common oxidative mechanism. *Proc. Natl. Acad. Sci. U. S. A.* **1995,** *92* (6), 1989-1993.

196. Mizuno, N.; Varkey, J.; Kegulian, N. C.; Hegde, B. G.; Cheng, N.; Langen, R.; Steven, A. C., Remodeling of lipid vesicles into cylindrical micelles by alpha-synuclein in an extended alpha-helical conformation. *J. Biol. Chem.* **2012,** *287* (35), 29301-29311.

197. Jiang, Z.; de Messieres, M.; Lee, J. C., Membrane remodeling by alpha-synuclein and effects on amyloid formation. *J. Am. Chem. Soc.* **2013,** *135* (43), 15970-15973.

198. Zhu, T. F.; Budin, I.; Szostak, J. W., Preparation of fatty acid or phospholipid vesicles by thin-film rehydration. *Methods Enzymol.* **2013,** *533*, 267-74.

199. Zhu, T. F.; Budin, I.; Szostak, J. W., Vesicle extrusion through polycarbonate track-etched membranes using a hand-held mini-extruder. *Methods Enzymol.* **2013,** *533*, 275-282.

200. Davidson, W. S.; Jonas, A.; Clayton, D. F.; George, J. M., Stabilization of alpha-synuclein secondary structure upon binding to synthetic membranes. *J. Biol. Chem.* **1998,** *273* (16), 9443-9449.

201. Ong, S. G.; Chitneni, M.; Lee, K. S.; Ming, L. C.; Yuen, K. H., Evaluation of extrusion technique for nanosizing liposomes. *Pharmaceutics* **2016,** *8* (4).

202. Lesieur, S.; Grabielle-Madelmont, C.; Paternostre, M. T.; Ollivon, M., Size analysis and stability study of lipid vesicles by high-performance gel exclusion chromatography, turbidity, and dynamic light scattering. *Anal. Biochem.* **1991,** *192* (2), 334-343.

203. Olson, F.; Hunt, C. A.; Szoka, F. C.; Vail, W. J.; Papahadjopoulos, D., Preparation of liposomes of defined size distribution by extrusion through polycarbonate membranes. *Biochim. Biophys. Acta* **1979,** *557* (1), 9-23.

204. Gaudiano, M. C.; Colone, M.; Bombelli, C.; Chistolini, P.; Valvo, L.; Diociaiuti, M., Early stages of salmon calcitonin aggregation: effect induced by ageing and oxidation processes in water and in the presence of model membranes. *Biochim. Biophys. Acta* **2005,** *1750* (2), 134-145.

205. Wagner, K.; Beck-Sickinger, A. G.; Huster, D., Structural investigations of a human calcitonin-derived carrier peptide in a membrane environment by solid-state NMR. *Biochemistry* **2004,** *43* (39), 12459-12468.

206. Bradshaw, J. P., Phosphatydylglycerol promotes bilayer insertion of salmon calcitonin. *Biophys. J.* **1997,** *72* (5), 2180-2186.

207. Campelo, F.; McMahon, H. T.; Kozlov, M. M., The hydrophobic insertion mechanism of membrane curvature generation by proteins. *Biophys. J.* **2008,** *95* (5), 2325-2339.

208. Varkey, J.; Isas, J. M.; Mizuno, N.; Jensen, M. B.; Bhatia, V. K.; Jao, C. C.; Petrlova, J.; Voss, J. C.; Stamou, D. G.; Steven, A. C.; Langen, R., Membrane curvature induction and tubulation are common features of synucleins and apolipoproteins. *J. Biol. Chem.* **2010,** *285* (42), 32486-32493.

209. Carmona, P. and Rodriguez M. L., Hydrogen bonding between phosphate and amino acid side chains. *J. Mol. Struct.* **1986,** *143*, 365-368.